Bayesian Analysis of Rotating Machines

A statistical approach to estimate and track the fundamental frequency

Thorkild Find Pedersen
EF 812

IMM-PHD-2003-117

2003

ATV, Danish Academy of Technical Sciences,
Brüel & Kjær Sound & Vibration Measurement A/S,
and
Informatics and Mathematical Modelling, Technical University of Denmark.

Preface

This thesis has been prepared at Informatics and Mathematical Modelling (IMM), at the Technical University of Denmark. The work has been carried out in cooperation with Brüel & Kjær Sound & Vibration Measurement A/S (B&K). It is a partial fulfillment of the requirements for the degree of Ph.D. in electrical engineering, and as a part of the Danish Industrial Ph.D. programme administered by the Danish Academy of Technical Sciences (ATV). This work has been partly sponsored by ATV.

Acknowledgments.

This thesis could not have been written without the encouragement and support by many people.

First of all I would like to express my gratitude to the management of Brüel & Kjær Sound & Vibration Measurement A/S, for allowing me the privilege to pursue what four years ago seemed a wild idea. To present and former colleagues at Brüel & Kjær I also express my sincerest thanks, in particular to Otto Vinter who challenged me to pursue the idea in the first place, and to the Innovation group for always being understanding and supportive.

My supervisors also deserve my sincerest gratitude: to Henrik Herlufsen and Ole Roth at B&K for sharing their invaluable practical experience with noise and vibration analysis and for always being supportive. To Klaus Gram Hansen, Gram&Juhl Aps, for participating in the project. To John Aasted Sørensen and Per Chr. Hansen who played an important role in getting the project started. To Jan Larsen and Lars Kai Hansen, who willingly took over when John left and for subsequently introducing me to the world of Bayesian estimation theory.

Finally, I express my deepest gratitude to my family. Thank you for your support and encouragement over the past 3 years.

Copenhagen, March 2003
Thorkild Find Pedersen

Abstract

Rotating and reciprocating mechanical machines emit acoustic noise and vibrations when they operate. Typically, the noise and vibrations are concentrated in narrow frequency bands related to the running speed of the machine. The frequency of the running speed is referred to as the *fundamental frequency* and the related frequencies as *orders* of the fundamental frequency. When analyzing rotating or reciprocating machines it is important to know the running speed. Usually this requires direct access to the rotating parts in order to mount a dedicated tachometer probe.

In this thesis different frequency estimation techniques are considered for predicting the true fundamental frequency from measured acoustic noise or vibration signal. Among the methods are auto-correlation based methods, subspace methods, interpolated Fourier transform methods, and adaptive filters. A modified version of an adaptive comb filter is derived for tracking non-stationary signals.

The estimation problem is then rephrased in terms of the Bayesian statistical framework. In the Bayesian framework both parameters and observations are considered stochastic processes. The result of the estimation is an expression for the probability density function (PDF) of the parameters conditioned on observation. Considering the fundamental frequency as a parameter and the acoustic and vibration signals as observations, a novel Bayesian frequency estimator is developed. With simulations the new estimator is shown to be superior to any of the previously considered estimation techniques.

Within the Bayesian framework, two schemes for tracking the fundamental frequency are proposed. For both schemes the tracking capability is defined as a PDF of the next frequency estimate conditioned on the previous estimate(s). The first scheme works in real-time and is not guaranteed to find the optimal track, i.e., the track with highest probability. The second scheme is retrospective and requires all observation to be available, but it is guaranteed to find the optimal track.

The Bayesian estimator can also estimate the amplitude of non-stationary frequencies. An example of this is given, where the amplitudes of the orders of the fundamental frequency are estimated. The result is found comparable with existing amplitude order tracking methods.

Nomenclature

Symbols and Abbreviations Unless explicity stated otherwise, the symbols and abbreviations listed below are used throughout the report.

Symbols and Notations

$\arg\max f(x)$	The value of x which maximizes $f(x)$
$\lvert \cdot \rvert$	Absolute value of real values and magnitude for complex values
$\star$	The convolution operator, i.e $f(t) \star g(t) = \int_{-\infty}^{+\infty} f(\tau)g(t-\tau)\,d\tau$
$(\cdot)^\top$	Matrix transpose operator
$\overline{(\cdot)}$	Complex conjugate operator
$(\cdot)^H$	Matrix hermitan operator, i.e complex conjugated transpose
$E\{\cdot\}$	The expectation (mean value) of $(\cdot)$.
F_f	The fundamental frequency of a harmonic signal.
$\mathcal{F}$	Fourier transform.
$\mathcal{F}^{-1}$	Inverse Fourier transform.
$\mathcal{L}(\theta; \mathbf{d})$	The likelihood function for the observations $\mathbf{d}$ being modelled by the parameterset θ.
$\mathbf{v}$	Bold lower-case letters denotes a vector.
$\mathbf{M}$	Bold upper-case letters denotes a matrix. In some cases the dimension are indicated with subscript notation.
$x \sim \mathcal{N}(\mu, \sigma^2)$	Indicates that scalar x is normally distributed with mean value, μ, and the variance, σ^2.

Abbreviations

ACF	Adaptive Comb Filter.
ALE	Adaptive Line Enhance
ANF	Adaptive Notch Filter.
AR	Auto-Regressive.
ARMA	Auto-Regressive Moving Average.
BSS	Blind Source Separation
BT	Band-width Time
BW	Band-width
CRLB	The Cramér Rao Lower Bound for unbiased estimators.
DFT	Discrete Fourier Transform.
EKF	Extended Kalman Filter.
FFT	Fast Fourier Transform.
FIR	Finite Impulse Response.
FRF	Frequency Response Function.
DFT	Discrete Fourier Transform.
DOA	Direction of Arrival.
i.i.d.	Independent identically distributed.
IIR	Infinite Impulse Response.
LPC	Linear Predictor Coefficients.
MAP	Maximum a Posteriori.
ML	Maximum Likelihood.
PDF	Probability Density Function.
RMS	Root of the Mean Squared.
RMSE	Root of the Mean Squared Error.
SDOF	Single Degree Of Freedom.
SIFT	Simplified Inverse Filtering.
SNR	Signal to Noise Ratio.
Std.dev	Standard deviation.
w.r.t.	With respect to

Contents

Chapter 1

Introduction

This thesis deals with the detection and tracking of the fundamental frequency of rotating machines based on indirect measurements, e.g., in form of acoustic noise or of mechanical vibrations.

Driving in a passenger car most people will have an impression of the running speed of the engine by merely listening to it. Typically, the sound heard is not a pure sinusoidal wave but is comprised of multiple harmonic tones related to the fundamental frequency in the presence of noise.

In the literature great attention has been paid to the detection and tracking of harmonic signals, and it is used in many different application areas, e.g. *pitch detection* in speech processing, *direction of arrival (DOA) estimation* in radar processing.

The methods for estimating frequencies are numerous and each method has its own strengths and limitations. Some methods operate in real-time, i.e. they update the frequency estimate for each new input data and some operate in batches of input samples (batch-mode). The best known and most used method is probably the fast Fourier transform (FFT).

1.1 Motivation

When analyzing rotating machines, it is of interest to investigate how higher orders of the fundamental frequency behave as the running speed changes. Causes for changes in the running speed are numerous, e.g. changes in operational load or changes in control parameters.

The most common frequency analysis methods are based on equidistant sampled data values, e.g. in the time domain for traditional frequency spectrum analysis. To

analyze the harmonic orders of some fundamental frequency, the data values needs to be sampled equidistantly in the angular domain instead of time domain.

Most data acquisition systems provide data sampled equidistantly in the time domain, it is thus necessary to transform the measured data from the time domain to the angular domain. This operation is called resampling.

The resampling process depends on an accurate angular reference signal. This reference is typically labeled the tacho-signal and is measured with a tachometer. Tachometers often require direct access to revolving parts of the machine. In practice this can be difficult to obtain, especially for small and compact machines.

Different resampling techniques are examined in [13]. They stress the importance of the accuracy of the tacho signal.

1.2 Problem Definition

The purpose of the study has been to evaluate and if possible improve existing methods for estimating and tracking the fundamental frequency of vibro- acoustic signals generated by rotating machinery.

1.3 Thesis Outline

Chapter two deals with the characteristics and statistics of vibro- acoustic signals. These are illustrated by the analysis of a set of experimental data, based on which a simple model is derived and tested.

Chapter three presents a summary of existing frequency estimation methods. The methods are primarily used in speech processing and in radar applications.

In *Chapter four* the frequency estimation problem of vibro acoustic signals is formulated in a Bayesian context. This has previously not been documented. The new approach presents obvious advantages since the Bayesian framework easily incorporates prior knowledge of the signal. For the given case, this prior knowledge concerns the harmonic structure of the signal.

Chapter five extends the Bayesian model derived in chapter four with the ability to track the fundamental frequency. This is accomplished by including additional prior knowledge of the fundamental frequency's variation over time, e.g. as the outcome of a Markov Chain Process.

In *Chapter six*, the theories have been applied to two cases to illustrate the applicability of the new concepts. The first case is rather simple. It concerns a race car passing a microphone. The strength of the new method is its ability to give a high-resolution estimate of the Doppler shifted frequency. The second case is more complicated. It illustrates that besides the fundamental frequency it is possible to estimate the amplitude of different harmonic orders of the fundamental frequency. The results show very good agreement with estimates obtained using conventional methods relying on a measured tacho reference. Often such a reference requires di-

rect access to the rotating parts. In this respect the proposed method is non-invasive due to the elimination of a tacho reference.

Chapter seven concludes the investigations and outlines areas for futher research.

Chapter 2

Signal Characteristics

This chapter investigates the properties of vibro-acoustic signals. For this purpose experimental data is acquired from an automobile. The data is described in section 2.2 in terms of its time-domain and frequency domain characteristics.

The statistical properties are investigated in section 2.3 using both traditional descriptive statistics and the theory α-stable distributions (αSD). The reason for considering αSD is their ability to describe impulsive distributions and the fact that vibration signals often show impulsive characteristics.

In the last part of the chapter a simplified model is developed based on the experimental data and the observed statistical properties. The model is used in later chapters to analyze the performance of various frequency estimation algorithms.

2.1 Noise and Vibration Signals

References to measuring and analyzing noise and vibration signals can be found in the literature e.g. [2,26,47]. However, the topic of most of the references is condition monitoring. In short, the goal of condition monitoring is to identify and extract features from the signals that reveal the health condition of the machine.

Traditional methods for conditioning monitoring as described in [2] are often based on Fourier analyses, hence limited to stationary or quasi-stationary signals. Thus the frequency spectra of the vibrations are measured under stationary conditions, i.e while the the machine is running at a constant speed. Faults are then observed if the level changes over time in selected frequency bands.

For rotating machines important information can be found in signals from run-up

or run-down measurements [17]. These signals are non-stationary and reveal speed-dependent information.

For non-stationary signals, time-frequency methods are more appropriate [14, 17, 27]. The advantage of time-frequency methods over the Fourier transform is increased temporal resolution.

Recent methods being applied to condition monitoring are taken from the field of *Machine Learning*. Blind source separation (BSS) is one of the methods. Given that the original sources are statistically independent, BSS separates the sources from observations which are assumed to be unknown linear mixtures of the sources. Machine Learning in condition monitoring is the topic of [69].

Indicators of faults in rotating machines are often small impulses, caused by impacting of mechanical components, e.g. tooth meshing in gear-boxes. The small impulses are difficult to measure in high levels of background noise.

2.2 Experimental Data

The purpose of this study is to estimate and track the fundamental frequency of rotating machines from easily accessible signals such as emitted sound or measured vibrations. In the following focus will be on signals generated by a combustion engine, and to investigate the properties of this type of signals, experimental data has been acquired from an automobile.

The data consists of three signals: the first is the tacho reference measured optically from the cam-shaft of the engine, the second is accelerations in the vertical direction of the engine block measured with an accelerometer, and the third signal is the acoustic sound pressure measured with a microphone approximately 1m above the engine block.

During the experiment the car is in neutral and is accelerated manually from idle at 670 RPM to 3600 RPM over a 40 second period after which the accelerator is released and the speed decreases to idle within 5 seconds. The profile of the fundamental frequency as measured with the tacho-probe is shown in Figure 2.1.

The vibration and acoustic signals are sampled at a rate of 8192 samples per second. Both signals are normalized, i.e. the mean is subtracted and the amplitude is scaled to unit variance, $\hat{x}_t = (x_t - \overline{x})/\sqrt{\mathrm{Var}(x)}$. The acquired time signals are shown in Figure 2.2 where the large graph is the entire signal and the smaller graphs are excerpts comprising 4 full cycles of the fundamental frequency at T=2.5s and T=45s respectively. The top figures 2.2(a) and 2.2(b) show the vibration and acoustic time signals at full measurement bandwidth; It is noted that when idle (T=2.5s) the acoustic signal is dominated by a harmonic component at 2.5 times the fundamental frequency. Since the engine has 5 cylinders this frequency corresponds to the firing frequency of the cylinders. Both signals are oversampled with respect to the fundamental frequency shown in Fig. 2.1. Therefore the two lower figures 2.2(c) and 2.2(d) show the same vibration and acoustic signals, but with the sample rate reduced to 1024 samples per second equivalent to a measurement bandwidth of 400 Hz. Sub-

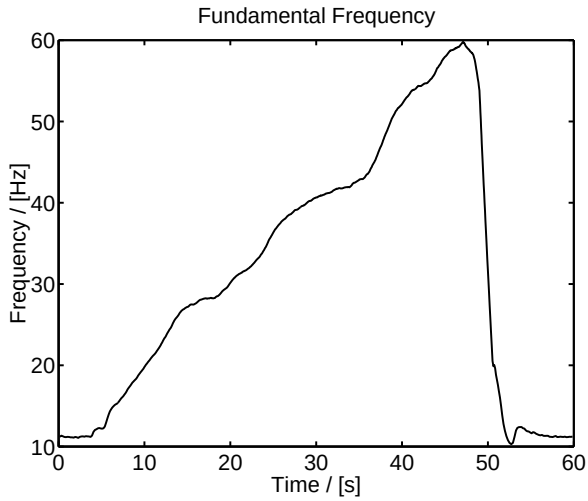

Figure 2.1: Profile of the fundamental frequency for the experimental data from the passenger car. The engine is accelerated manually from idle to 3600 RPM when the accelerator is released.

jective comparison of the upper and lower graphs, suggests that the vibration signal is more impulsive than the acoustic signal at the high sample rate but the difference is less pronounced at the low sample rate.

The frequency contents of the experimental data is shown in Figure 2.3 in the form of spectrograms. The harmonic orders stand out more clearly for the vibration signal than the acoustic signal, and at 400 Hz bandwidth (Fig. 2.3(c)) the 2*nd* order of the fundamental frequency is easily identified.

For both signals the harmonic structure is seen to be complex, containing a large number of fractional orders of the fundamental frequency. At the high measurement bandwidth it is almost impossible to distinguish the orders from each other and thus makes it more difficult to detect the fundamental frequency. This is in part caused by the *smearing* of the amplitude estimates that occur if the frequencies are non-stationary during the measurement interval.

Structural properties pose another problem. This is seen in Fig. 2.3(a) where a bright band is observed in the frequency range from 1100 Hz to 1500 Hz. The structural properties will cause certain frequencies to be damped and others amplified depending on where the vibrations are measured. Figure 2.4 shows the frequency response function (FRF) at the mounting point of the accelerometer measuring the engine vibrations. The FRF is obtained as the average of 10 hits with a hammer on top of the engine block. It is seen that the frequency response in the range from 1100 Hz to 1600 Hz is elevated almost 20 dB compared than the lower frequencies.

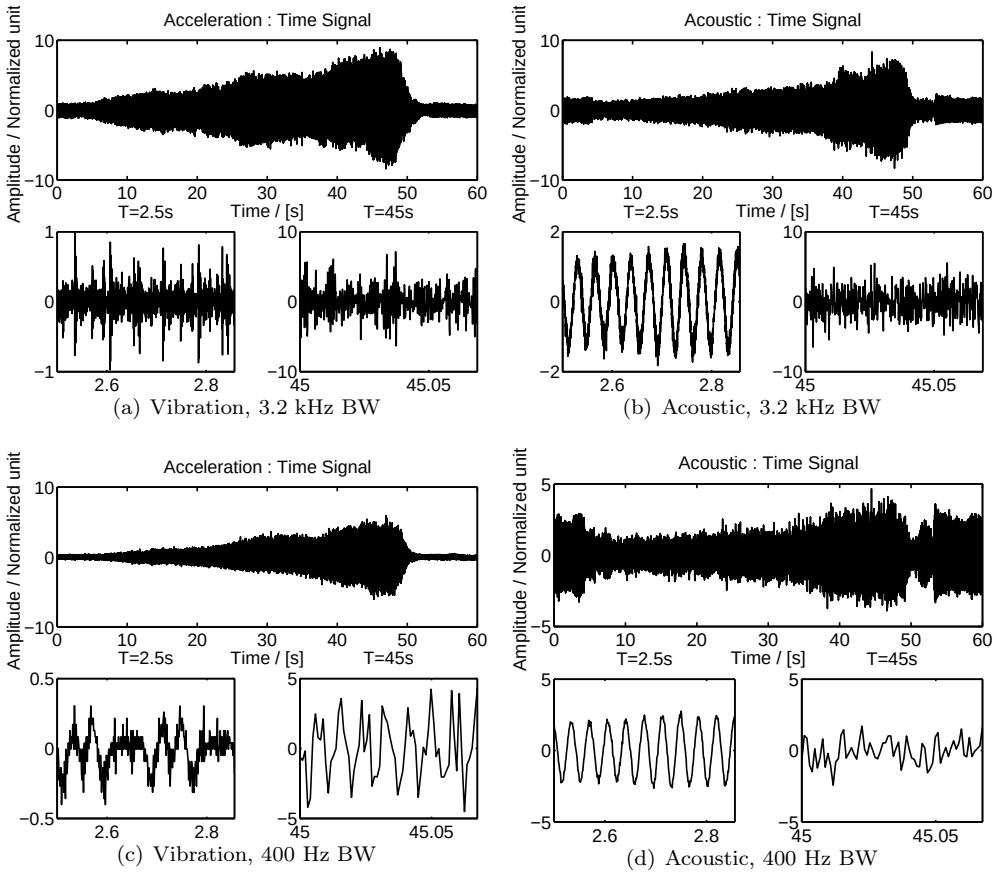

(a) Vibration, 3.2 kHz BW (b) Acoustic, 3.2 kHz BW

(c) Vibration, 400 Hz BW (d) Acoustic, 400 Hz BW

Figure 2.2: Vibro-Acoustic signals in the time domain. (a) Engine vibration with a bandwidth of 3.2 kHz. (b) Engine noise with a bandwidth of 3.2 kHz. (c) Low-pass filtered engine vibration (BW=400 Hz). (d) Low-pass filtered engine noise (BW=400 Hz). The large graphs show the entire signal and the smaller graphs are excerpts comprising 4 full cycles of the fundamental frequency at T=2.5s and T=45s.

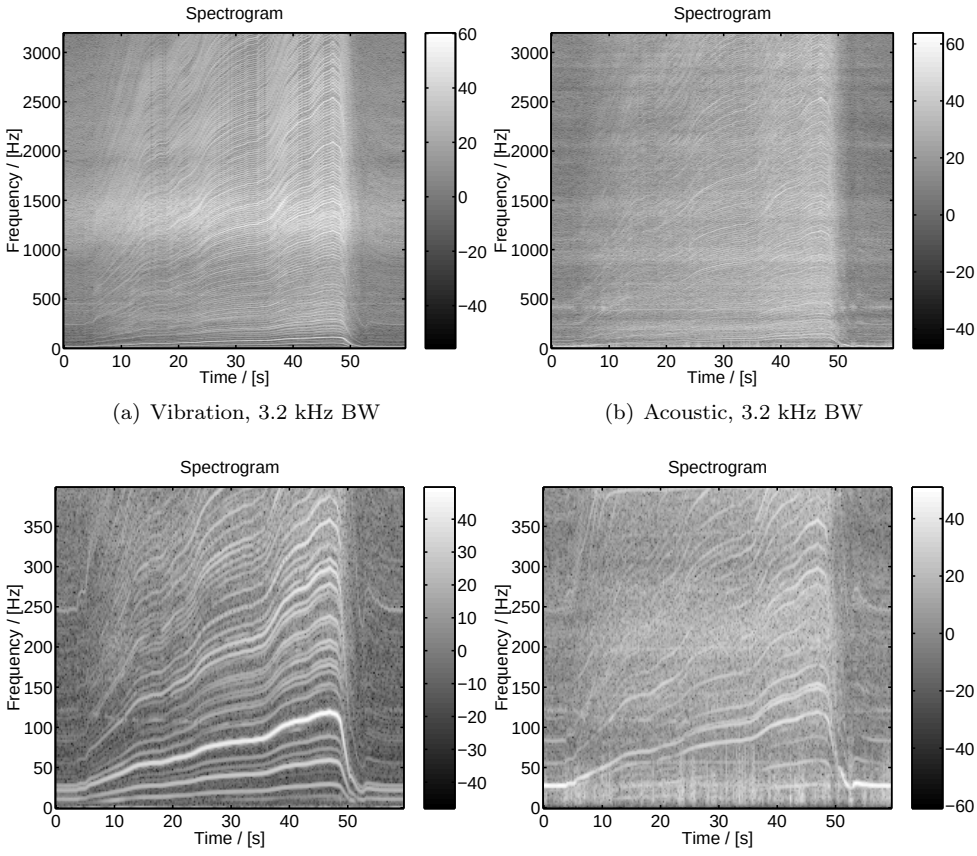

(a) Vibration, 3.2 kHz BW

(b) Acoustic, 3.2 kHz BW

(c) Vibration, 400 Hz BW

(d) Acoustic, 400 Hz BW

Figure 2.3: Frequency contents of the experimental data. Top row shows the spectrograms for signals for the 3.2 kHz measurement bandwidth, and bottom row for the 400 Hz bandwidth. For both bandwidths the signals are segmented into records of 1/2 s with 50% overlap equivalent to a frequency resolution of $\Delta F = 2$ Hz. In the left column is shown the spectrograms of vibration signal and in the right column of the acoustic signal. The noise in the vibration spectra is most prominent for higher orders of the fundamental frequency and allows visible identification of the 2nd harmonic (c). For the acoustic signal the noise seems more white making a clear identification of the harmonics difficult.

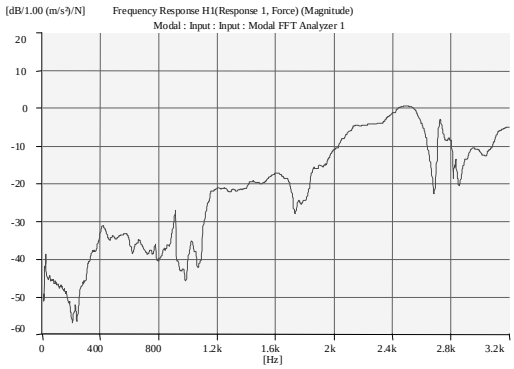

Figure 2.4: Measured Frequency Response Function on top of an engine block mounted in a passenger car.

2.3 Statistical Properties

It is often assumed that the noise contribution in a signal is normally distributed. In case of the noise being a sum of many independent identically distributed (i.i.d.) variables, this assumption is supported by the central limit theorem.

The conditions under which vibro-acoustic signals are generated may vary - not only from one experiment to another - but also within one experiment by itself, e.g. during a run-up or run-down experiment of a car engine. To gain fundamental understanding of how the signals are effected it is of interest to examine the statistical properties of the vibro-acoustic signals.

In this section two different statistical methods are applied to the vibro-acoustic signals. The first method is to compute the traditional parameters from descriptive statistics: mean($\overline{x}$), standard deviation(σ), skewness(τ) and kurtosis(κ). The second method assumes the signals to be α-stable distributions, and estimates the four parameters for stable laws: characteristic exponent (α), location (μ), index of symmetry (β), and dispersion (γ).

Distributions for random variable are described by their probability density functions (PDF's). Figure 2.5 shows the PDF's for two well-known distributions: the normally distributed Gaussian and the Cauchy distribution. The PDF of a randomly sampled sinusoid is also shown in the figure.

2.3.1 Descriptive Statistics

The definitions of the traditional descriptive parameters are given in Table 2.1. The descriptive parameters are estimated in blocks of 1 second for the vibration and acoustic signals. The parameters are computed at the measurement bandwidths of 3200 Hz and 400 Hz yielding the four graphs shown in Figure 2.6. The graphs in the figure show that the vibration signal at high bandwidth has heavier tails (κ>3) than

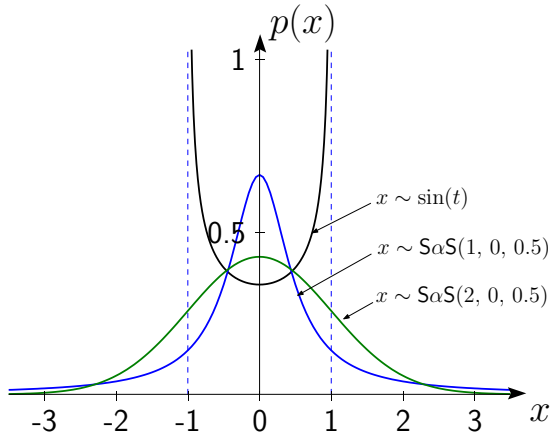

Figure 2.5: Probability Density Functions: i) a sinusoid, $x \sim \sin(t)$; ii) the normally distributed Gaussian with unit variance ($\sigma^2 = 2\gamma$), $x \sim \mathrm{S}\alpha\mathrm{S}(2, 0, 0.5)$; and iii) the Cauchy distribution with $\gamma = 0.5$. $x \sim \mathrm{S}\alpha\mathrm{S}(1, 0, 0.5)$.

the acoustic signal which is close to Gaussian ($\kappa \approx 3$). As the fundamental frequency increases the skewness for the vibration signal increases whereas the acoustic noise remains symmetrical. At the low bandwidth the distribution of vibration signal becomes more flat ($\kappa < 3$). The PDF of a sinusoid has no tails (see e.g. appendix A.1). This could indicate that the vibration noise is located at the higher frequencies and that at the low frequency range the signal is dominated by the pure harmonics of the fundamental frequency. The spectrograms in Figure 2.3 supports this observation.

Parameter	Symbol	Equation
Mean	$\overline{x}$	$\frac{1}{N}\sum_{i=1}^{N} x_i$
Standard deviation	σ	$\sqrt{\frac{\sum_{i=1}^{N}(x-\overline{x})^2}{N-1}}$
Skewness	τ	$\frac{\sum_{i=1}^{N}(x-\overline{x})^3}{(N-1)\sigma^3}$
Kurtosis	κ	$\frac{\sum_{i=1}^{N}(x-\overline{x})^4}{(N-1)\sigma^4}$

Table 2.1: Descriptive Parameters

2.3.2 The α-Stable Distribution

Stable distributions are a flexible modeling tool for heavy tailed distributions as they have a controlling parameter α that describe how thick the tail should be. α is called the characteristic exponent and this class of distributions is often called α-stable

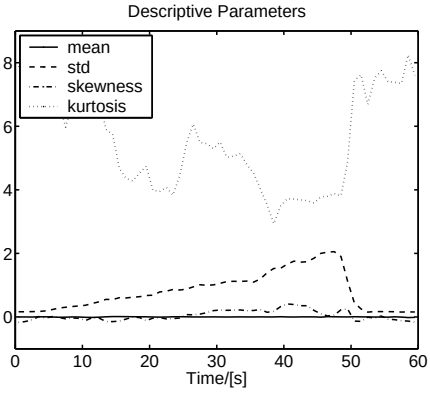

(a) Vibration, 3.2 kHz BW

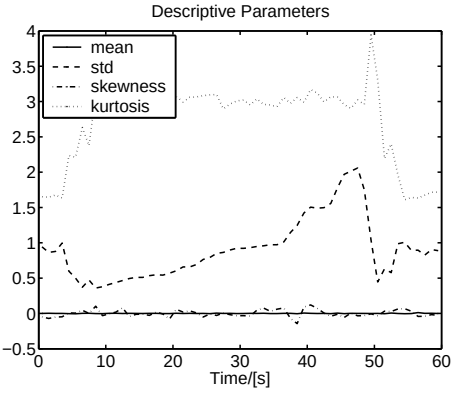

(b) Acoustic, 3.2 kHz BW

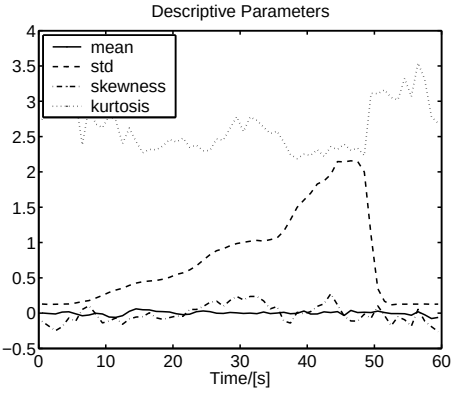

(c) Vibration, 400 Hz BW

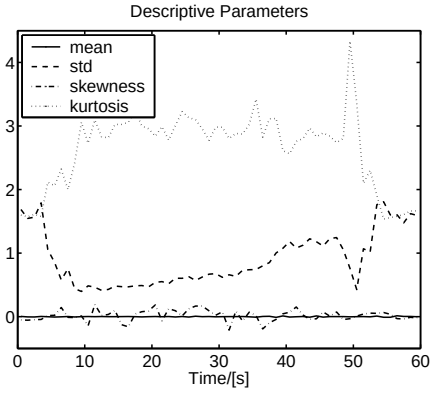

(d) Acoustic, 400 Hz BW

Figure 2.6: Descriptive Parameters. This figure shows the estimated statistical parameters for the experimental data. Most variation is observed in the kurtosis parameter. For a standard normally distribution the kurtosis is 3; values below indicate a flatter distribution and value above distributions with heavier tails. The acoustic signal exhibits almost normality for both bandwidths, whereas the vibration signal is heavy tailed for the high BW and flat for the low BW.

distributions. In fact, the α-stable distributions contain the Gaussian distribution as a limiting case when $\alpha = 2$. The Cauchy distribution is also included in this class of distributions with $\alpha = 1$ (e.g. recall Figure 2.5).

There exists no closed-form expression for the probability density function of an α-stable distribution, but the characteristic function, $\psi(t)$, which is the Fourier transform of the probability density function is defined by

$$\psi(t) = \exp\left(i\mu t - \gamma|t|^{\alpha}\left[1 + i\beta \text{sign}(t)\omega(t,\alpha)\right]\right) \tag{2.1}$$

where

$$\omega(t,\alpha) = \begin{cases} \tan\frac{\alpha\pi}{2}, & \text{if } \alpha \neq 1 \\ \frac{2}{\pi}\log|t|, & \text{if } \alpha = 1 \end{cases} \tag{2.2}$$

The parameters in Eq. (2.1) are α, β, γ and μ.

- α is the *characteristic exponent*. It satisfies $0 < \alpha \leq 2$. It controls how heavy the tails are. The lower α is the heavier they are and hence the distribution is more impulsive.
- β is the *index of symmetry* ($-1 \leq \beta \leq 1$). When $\beta = 0$, the distribution is symmetrically around the location parameter.
- γ is the *dispersion parameter* ($\gamma > 0$), which determines the spread of the density around its location parameter. It behaves similar as the variance of the Gaussian density, and when $\alpha = 2$ it equals the half of the variance.
- μ is the *location parameter* ($-\infty < \mu < \infty$). It corresponds to the mean for $1 < \alpha \leq 2$ and the median for $0 < \alpha \leq 1$.

When $\beta = 0$ the distribution is symmetric. Such distributions are called Symmetrically α Stable distributions or SαS for short. SαS distributions do not have a finite second (or higher) order moments. In fact, only moments for $0 \leq \delta < \alpha$ are defined, where δ is called the *fractional lower order moment*. If X is an α-stable random variable then with $E\{X\}$ denoting the expectation of X the following apply [33]:

$$\begin{aligned} E\{|X|^{\delta}\} &= \infty, \quad \text{if } \delta \geq \alpha \\ E\{|X|^{\delta}\} &< \infty, \quad \text{if } 0 \leq \delta < \alpha \\ E\{|X|^{\delta}\} &< \infty, \quad \text{if } \alpha = 2 \text{ and } \delta \geq 0 \end{aligned}$$

The implications of this is that SαS distributions have no variance and that two processes generated by an SαS distribution do not have any covariance (cross-correlation).

The estimated αS parameters for the accelerometer and microphone signals are plotted in Figure 2.7. The parameters are estimated in blocks of 1 second using the regression method of Koutrouvelis [23].

The two upper figures, Fig. 2.7(a) and Fig. 2.7(b) show the estimated parameters for stable distributions for the vibration and acoustic signal at the high sample rate.

The characteristic exponent, α, is very close to 2 for the acoustic signal and varies between 1.6 and 2.0 for the vibration signal. This indicates that distribution of the vibration signal has heavier tails (i.e. is spikier) than the acoustic signal which is almost Gaussian. Looking at the small graphs in figures, Fig. 2.2(a) and Fig. 2.2(b) this is also seen to be the case. Since the signals are normalized the location parameter, μ, is zero as expected for both signals. The symmetry parameter, β, indicates that the acoustic signal is more symmetrical than the vibration signal since it is negatively biased for the vibration signal. The scale parameter, γ, increases with the fundamental frequency. In the two lower figures, Fig. 2.7(c) and Fig. 2.7(d) the estimated αS parameters are shown for the signals at the reduced bandwidth of 400 Hz. Apparently, the removal of the higher frequencies from the vibration signal makes α very close to 2.0. and supports the observations regarding the small time segments of Figure 2.2, that the impulsive nature of vibration signal is less pronounced at the low bandwidth.

2.3.3 Discussion

The examination of the experimental data using both descriptive statistics and α-stable distributions, lead to similar conclusions: Firstly, with a bandwidth of 3.2 kHz the distribution of the vibration signal is confirmed by both methods to be heavy tailed ($\kappa > 3$ and $\alpha < 2$). However, the heavy tails disappear when the bandwidth is reduced to 400 Hz ($\kappa < 3$ and $\alpha = 2$). The fact that $\kappa < 3$ indicates a flat distribution and it is probable that this is caused by the sine waves corresponding to the orders of the fundamental frequency. Secondly, both σ and γ increase with the fundamental frequency. The energy in the vibration and acoustic signals thus increases with the speed of the engine.

For the purpose of determining the fundamental frequency in the experimental data it is sufficient with a measurement bandwidth of 400 Hz. In this range neither the vibration or acoustical signal exhibit impulsive characteristics. Had this not been the case, one could resort to using Heavy-tailed models as described in [24, 33].

2.4 Modeling Noise and Vibration Signals

When evaluating methods for estimating and tracking the fundamental frequency it is desirable to have a model of the source signals. In order for the model to be useful it must capture the essential properties of the real signals.

As an example of such models, two different models are described briefly in the following.

In [27] Lee and White proposes an adaptive line enhancer (ALE) which enhances the impulses in the signal and then uses time-frequency analysis to relate the impulses to the angle of the crank-shaft. They propose the following model for vibration signal in condition monitoring applications

$$x(t) = s_h(t) + s_i(t) + i(t) + n(t) \tag{2.3}$$

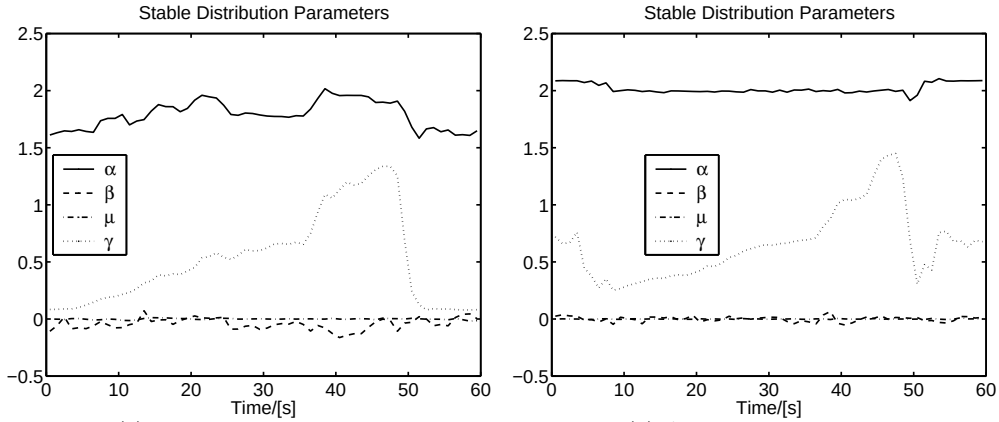

(a) Vibration, 3.2 kHz BW

(b) Acoustic, 3.2 kHz BW

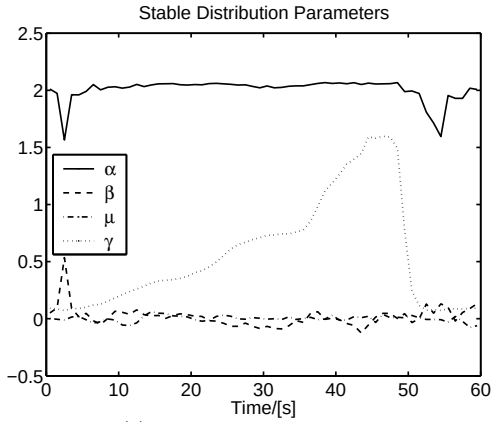

(c) Vibration, 400 Hz BW

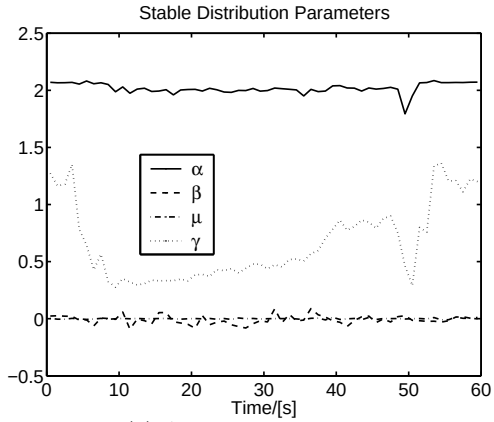

(d) Acoustic, 400 Hz BW

Figure 2.7: Estimated αS Parameters. The low-pass filter removes much of the noise from the vibration signal. This is reflected in the increase of the characteristic exponent from (a) to (c) . No noticeable difference is observed for the acoustic signal. In the regions where the signals are almost periodic, the estimates of the characteristic exponent are noted to be invalid ($\alpha > 2$).

where $s_h(t)$ represents all harmonic signals related to the fundamental frequency, $s_i(t)$ are the incommensurated harmonic signal (i.e. *not* related to the fundamental frequency) , $i(t)$ is the impulsive part of the signal and finally $n(t)$ is broadband random noise.

A more complete linear model is found in [69],

$$x_j(t,\theta) = \sum_{i=1}^{NF} h_{ij}^F(t,\theta) \star F_i(t,\theta) + \sum_{i=1}^{NI} h_{ij}^I(t,\theta) \star I_i(t,\theta) + h_j^S(t,\theta) \star m(t,\theta) + n_j(t,\theta) \quad (2.4)$$

where $x_j(t,\theta)$ is the vibration signal measured at the sensor position j. The model operates with two time scales, t being the normal time in seconds and θ being a slow time-scale corresponding to the life-cycle of the machine. The model separates the data into fault related sources $F_i(t,\theta)$, interfering machinery components $I_i(t,\theta)$, and the modal machine response $m(t,\theta)$. All sources have separate transfer paths from their origin to the sensor. This is indicated with the $\star$ operator denoting convolution of the sources with the impulse responses, $h_{ij}^F(t,\theta)$, $h_{ij}^I(t,\theta)$ and $h_j^S(t,\theta)$, corresponding to the filtering by the machine casing from the source to the sensor. The measured signal $x_j(t,\theta)$ is called a *convolutive mixture* and methods exist which can solve it, but it is more difficult than for the linear mixtures.

2.4.1 Harmonic Modeling

The model proposed here is a special case of the above models. It is tailored to model periodic signals with changing fundamental frequency as encountered in rotating machines under run-up/down operation.

Assuming that the experimental data is representative for signals where the fundamental frequency is to be estimated, then the essential properties to be captured by the model are: i) The *harmonic structure* of the signal. The structure is specified by a number of orders of the fundamental frequency. The number of orders can be large. ii) The frequency of the orders, which need not be integer multiplicands of the fundamental frequency. iii) The amplitudes of the orders, which may depend on the fundamental frequency.

The model is shown in Figure 2.8. It consists of three parts. The first part is a harmonic signal generator. The generator is driven by a fundamental frequency and produces a sequence of sinusoids with predefined phases, amplitudes and frequencies being constant orders of the fundamental frequency. The equation for the output of the generator is shown in Eq.(2.5), where $x(t)$ is the output of the generator; $\omega(t)$ is the fundamental frequency of the periodic signal, $\Omega(t)$ is the phase angle of the fundamental, and η_n is the order number.

$$\begin{aligned} x(t) &= \sum_{n=1}^{N} a_n \cos(\eta_n \Omega(t)) + b_n \sin(\eta_n \Omega(t)) \\ \Omega(t) &= \int_0^t \omega(\tau)\, d\tau \end{aligned} \quad (2.5)$$

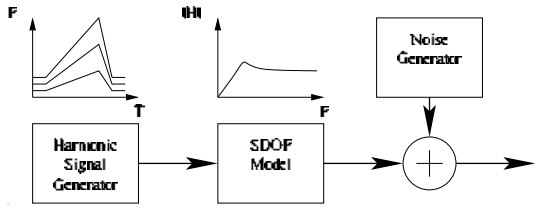

Figure 2.8: Signal Generation. Simulating the response of a mechanical system using a digital filter. The digital filter is designed to have response similar to that of a simple second order mechanical system with a single degree of freedom. The excitation of the system is modeled with the harmonic signal generator that generates a predetermined harmonic sequence. Gaussian noise is added after the filtering to simulate measurement noise.

The a_n and b_n parameters determine the amplitude and phase of the nth harmonic component through the relation

$$a_n \cos(\eta_n \Omega(t)) + b_n \sin(\eta_n \Omega(t)) = A_n \cos(\eta_n \Omega(t) + \phi_n)$$

where

$$\tan(\phi_n) = -b_n/a_n, \quad A_n = \sqrt{a_n^2 + b_n^2}$$

Amplitude dependency of the fundamental frequency is accomplished by the second part of the model. This part models the transfer path from the source to the transducer as a simple 2nd order mechanical system with a single degree of freedom (SDOF). The equation of motion for the system is governed by

$$m\,\ddot{x}(t) + c\,\dot{x}(t) + k\,x(t) = F(t) \tag{2.6}$$

where m is the mass, c is the damping, k is the spring forcing and F is the external forcing on the mass. $\dot{(\cdot)}$ and $\ddot{(\cdot)}$ indicates single and double differentiation in time. $x(t)$ is the displacement of the mass. The frequency response for displacement, velocity and acceleration of the system is shown in Figure 2.9 together with the system. The mechanical system is simulated with a digital filter, which can be derived from the Laplace transform of the transfer function $X(s)/F(s)$ from Eq.(2.6) using the bilinear transformation. The Laplace transform of Eq. (2.6) is shown in Table 2.2 together with the transfer functions for the velocity and acceleration. The last part of the model is to add white Gaussian noise with a specified variance. The noise variance controls the signal to noise ration (SNR) of the signal. When the noise variance is kept constant and the fundamental frequency is stationary, then the SNR will also be constant. But, when the fundamental frequency changes, the amplitudes of the harmonic components and hence also the SNR changes because of response of the SDOF system.

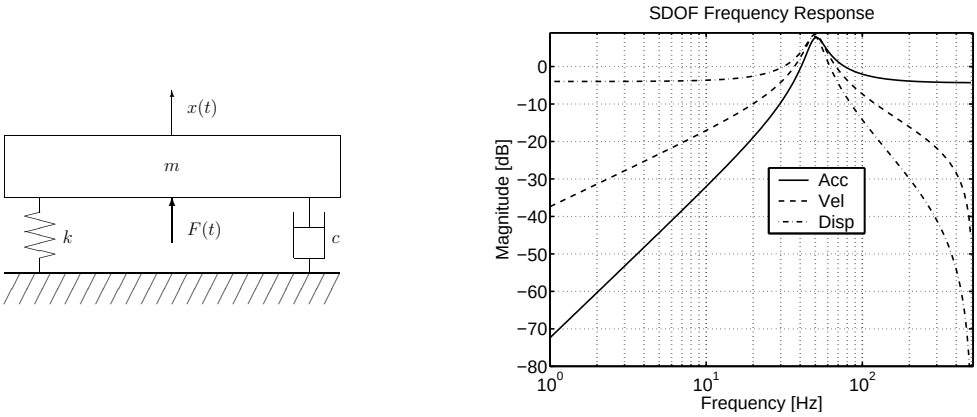

(a) Mechanical System (b) Frequency Response

Figure 2.9: a) Mechanical system (see text) with a single degree of freedom. b) Frequency responses of the second order filters simulating the mechanical system when specified by the damping ratio, $\zeta = 1/8$, and the damped natural frequency $\omega_d = 0.307$ rad/s.

Displacement:	$H_D(s) = \frac{1}{ms^2+cs+k}$	(Compliance)
Velocity:	$H_V(s) = \frac{s}{ms^2+cs+k}$	(Mobility)
Acceleration:	$H_A(s) = \frac{s^2}{ms^2+cs+k}$	(Accelerance)

Table 2.2: SDOF system Transfer Functions. The transfer functions defined as the system response over the excitation. They are also referred to as frequency response functions under the names of compliance, mobility and accelerance

Example

To illustrate the properties of the model, the harmonic signal generator is configured to generate a harmonic signal composed of the first three harmonics of the fundamental frequency as shown in Eq.(2.7). The amplitudes of the harmonic components are selected to be inversely proportional to the order of the component.

$$x(t) = A\sum_{k=1}^{3}\frac{1}{k}\cos(k\Omega(t)), \quad \Omega(t) = \int_0^t \omega_F(\tau)d\tau \tag{2.7}$$

Figure 2.10 shows how the relative amplitudes of the orders change as ω_F changes and the orders pass through the resonance of the system. The top graph shows the profile of the harmonic orders of ω_F. The lower graph shows the RMS acceleration amplitudes of the harmonic orders[1].

[1]The units are arbitrary and have no physical interpretation.

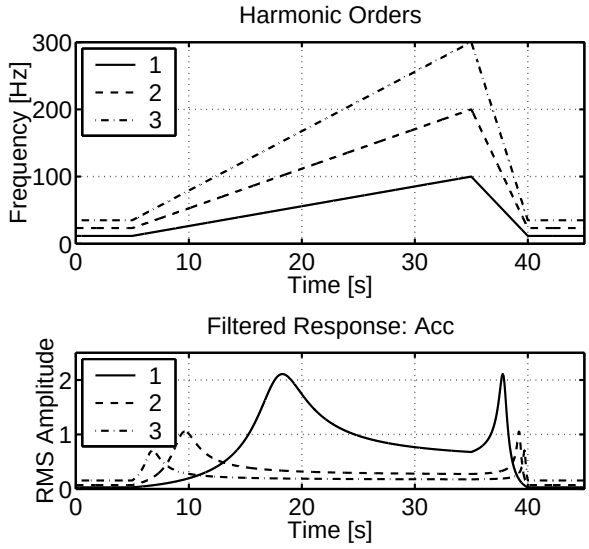

Figure 2.10: Harmonic orders of the periodic signal. *Top graph*: the three curves show the frequency profiles of the three harmonic components in the driving force of the mechanical system. The harmonic orders decrease 6 dB per octave. *Bottom graph*: RMS amplitudes of the acceleration response of the driving force. The relative amplitudes of the harmonic components change with the fundamental frequency; it starts at the low frequency with the 3^{rd} order dominating, then as the frequency increases the 2^{nd} order and then the 1^{st} order dominate.

White Gaussian noise with variance, σ_N^2, is added to the simulated response of the mechanical system. The simulated response thus becomes

$$\begin{aligned} y(t) &= h(t) \star x(t) \\ d(t) &= yt) + e(t), \quad e(t) \sim \mathcal{N}(0, \sigma_N^2) \end{aligned} \tag{2.8}$$

where $\star$ denotes convolution, $h(t)$ is the impulse response of the mechanical system, $x(t)$ is the generator signal, $y(t)$ is the simulated response, and $d(t)$ is the observed response with the additive noise, $e(t)$. The noise variance is determined from an average signal to noise ratio (SNR) level defined as $SNR_{dB} = 10\log(\text{Var}(y(t))/\sigma_N^2)$. Since $y(t)$ varies over time, so will the actual SNR level which is also observed in practice. Figure 2.11 shows the variation in SNR for the three responses, acceleration, velocity and displacement, when the average SNR is 10 dB.

Cramér Rao Lower bound

The Cramér Rao Lower bound (CRLB) is a lower bound on the covariance of the parameter errors of unbiased estimators. For estimation problems such as finding the

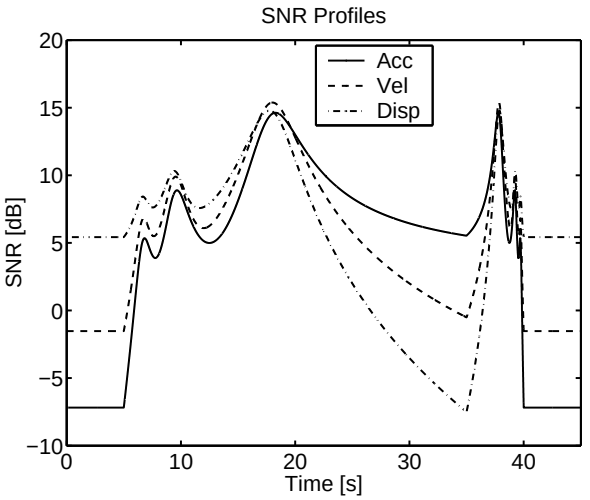

Figure 2.11: Variation in SNR. This figure shows the non-stationary behavior of the signal to noise ratio when the fundamental frequency and harmonic orders changes as shown in Figure 2.10. The noise variance is set for each of the three responses , such that an average SNR of 10 dB is achieved.

fundamental frequency, the amplitudes and the phases of the signal $d(t)$ in Eq. (2.8), the CRLB gives the minimum variance of the parameters.

The CRLB for the parameter estimates of harmonic signals in noise, such as Eq. (2.8) is derived in [31]. For the fundamental frequency, $\hat{\omega_F}$, and the amplitudes, $\hat{A}_k$ the lower bounds are,

$$\mathrm{Var}(\hat{\omega_F}) \geq 2\sigma_N^2 \frac{12}{\gamma N^3}, \quad \mathrm{Var}(\hat{A}_k) \geq \frac{2\sigma_N^2}{N}, \quad \gamma = \sum_{k=1}^{K} k^2 A_k^2 \tag{2.9}$$

N is the number of observations, σ_N^2 is the variance of the additive Gaussian noise, and K is the number of harmonic components.

Though the CRLB is only valid for unbiased estimates, it is here used to indicate the expected limits of an optimal unbiased estimator.

2.5 Summary

The properties of vibro-acoustic signals have been investigated in this chapter, with the focus on determining the fundamental frequency of rotating machines. Experimental data from a passenger car was examined and the results were used to design a simple model for synthesizing vibro-acoustic signals.

Chapter 3

Frequency Estimation and Tracking

Estimating periodic signals is a well established field in the literature of signal processing. It is not the intention to give a detailed account of all methods, but rather to present a summary of the different approaches used in following two application areas:

Speech Processing In coding of voiced speech signals two parameters are estimated. The first is the fundamental frequency of the vocal cords, called the pitch frequency. The second, is the auto-regressive (AR) coefficients which models the influence of the vocal tract.

Radar Applications Estimating and tracking the direction of arrival (DOA) is the primary focus in many radar applications. It is accomplished by finding harmonic structures in the correlation matrix corresponding to the array of detectors.

3.1 Pitch Detection

In principle the problem of determining the pitch frequency in speech signals is similar to the problem of determining the fundamental frequency of a rotating mechanical system.

The pitch frequency of speech is controlled by the vibration of the vocal cords, which opens and closes for streaming air from the lungs. It varies with the speakers, ranging from 40 Hz for low-pitched males to 800 Hz for high-pitched females and

children [44, 63]. In the creation of speech, the vocal cords are followed by the vocal tract which is perceivable as a resonance chamber of varying size and shape. For speech the resonance chamber has 3 to 4 dominant resonance frequencies. In the speech processing literature these are called formants. A characteristic section of a voiced speech signal is shown in Figure 3.1.

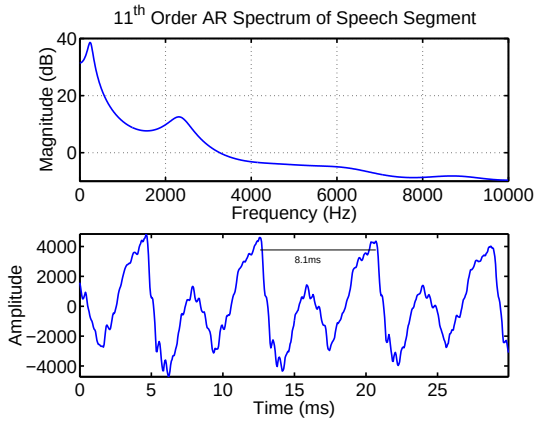

Figure 3.1: The lower graph shows the time signal of a 30 ms segment of speech taken form the Keel Pitch Data base [39], the pitch period of 8.1 ms is clearly visible. The top graph shows the corresponding 11^{th} order AR spectrum signal with two characteristic formants at 240 Hz and 2310 Hz.

With both the pitch frequency and the detailed structure of the sound signal changing rapidly, it is difficult to measure an accurate pitch frequency. This resembles the problem of determining the running speed of rotating machines. Equivalent to the vocal tract, the resonances in the mechanical structure alters the signature of the fundamental frequency and its higher orders as the running speed changes. Although the running speed under normal operations is fairly stationary, rapid changes do occur (e.g. a gear shift in car) where it is important not to loose track of the fundamental frequency.

It must be mentioned however, there are important differences in the nature of the two types of signals. If vibrations are caused by imbalance, the driving force is a harmonic wave form opposed to a periodic pulse train. Depending on the application, the fundamental frequency range of mechanical system is much wider than in speech applications. The fundamental frequency of rotating mechanical systems varies with the application, from below 1 Hz for large generators to 1.5 kHz for centrifuges separating nuclear particles. When focusing on combustion engines for automobiles the fundamental frequency is typically in the range from 5 Hz to 100 Hz (300 RPM to 6000 RPM).

3.1.1 Methods and Algorithms

Digital processing of speech is a well established research area and numerous methods and algorithms have been proposed for pitch detection. In [46] Rabiner *et al.* provides a comparative study of seven different methods, three of which will be described shortly. Most of the algorithms estimate the pitch period in segments of constant length (30-50ms) of the speech signal but do not track the change across segments. The resolution is limited by the sample rate because the pitch period is estimated instead of the pitch frequency, therefore the frequency resolution will be higher at low frequencies than at higher frequencies. It is possible to use interpolation techniques to increase the pitch period resolution beyond the sample interval as is shown in e.g. [25, 30, 63] and the references therein.

Modified Autocorrelation Analysis

The motivation to use short-time autocorrelation analysis to extract the pitch period is evident looking at the short speech segment of Figure 3.1. Due to the periodic nature in the signal the autocorrelation function is expected to have a peak at the lag equivalent to the pitch period. First defining the short-time cross correlation function, $\hat{R}$, of the two segments $x(k)$ and $y(l)$ as

$$\hat{R}_{x(k)y(l)}(m) = \frac{1}{N} \sum_{n=0}^{N-m-1} \left(x(n+k)w(n)\right)\left(y(n+l+m)w(n+m)\right) \tag{3.1}$$

where $w(n)$ is a window function, then the estimate of the short-time autocorrelation function is

$$\hat{R}_{x(l)}(m) \equiv \hat{R}_{x(l)x(l)}(m) \tag{3.2}$$

In [44] variants of autocorrelation based pitch analysis as shown in Figure 3.2 are examined. Firstly, the effect of higher formats are eliminated by low-pass filtering the signal above 900 Hz. Secondly, the peak in the autocorrelation function is enhanced by center clipping the amplitude of $x(n)$ when it exceeds a certain threshold level C_L. The non-linear clipping functions are shown in Eq. (3.3); $\mathrm{clp}(x)$ is a simple center clipper, $\mathrm{clc}(x)$ is a compressed center clipper and $\mathrm{sgn}(x)$ is a combination of the two.

$$\mathrm{clp}(x) = \begin{cases} x, & |x| \geq C_L \\ 0, & |x| < C_L \end{cases}, \quad \mathrm{clc}(x) = \begin{cases} x - C_L, & x \geq C_L \\ 0, & |x| < C_L \\ x + C_L, & x \leq -C_L \end{cases}, \quad \mathrm{sgn}(x) = \begin{cases} +1, & x \geq C_L \\ 0, & |x| < C_L \\ -1, & x \leq -C_L \end{cases} \tag{3.3}$$

The clipping level is determined for each frame as fixed percentage of the lesser of the absolute maxima of the first 1/3 and last 1/3 of the frame (Eq. (3.4)).

$$C_L = 0.68 \ \min\left[\max_{0 \leq i < N/3} |x(i)|, \max_{2N/3 \leq j < N} |x(j)|\right] \tag{3.4}$$

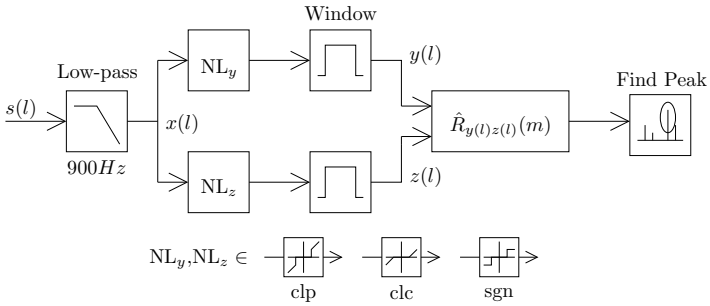

Figure 3.2: Modified Autocorrelation Analysis for Pitch Estimation. NL_x and NL_y are the non-linear clipping functions a (see text)

By clipping $x(n)$ its impulsiveness is enhanced. In the frequency domain this results in spectral flattening and thus the effect of the format structure is reduced.

A problem in autocorrelation based pitch analysis is to select the frame length. Setting the frame too short may result in pitch doubling whereby a higher order of the pitch frequency is detected. Similarly, a too long a frame may result in detection of a lower fractional of the true pitch frequency. To the extend these problems can be solved by tracking the pitch over multiple frames and thus detecting when pitch doubles or halves. In [44] this is accomplished by slowly adapting the frame length to three times the average pitch period. Another approach is to compare the pitch estimate computed using multiple window lengths as in [63].

Simplified Inverse Filter Technique (SIFT)

The SIFT is similar to the modified autocorrelation method except for the use of a more complex spectral flattening. The principle is shown in Figure 3.3. For each segment the spectral content is estimated by modeling it as the output of a 12^{th} order auto regressive(AR) process,

$$x(n) = -\sum_{i=1}^{12} a_i x(n-i) + e(n), \quad e \sim \mathcal{N}(0, \sigma^2)$$

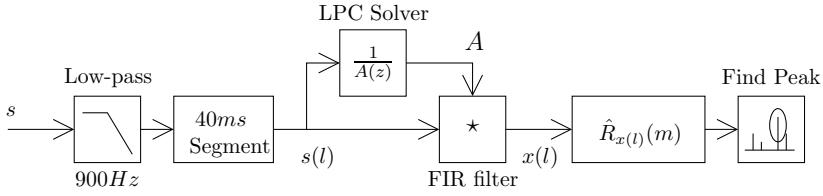

Figure 3.3: Simplified Inverse Filtering Technique

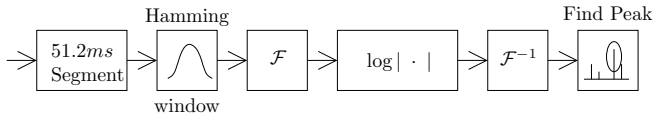

Figure 3.4: Block diagram of the cepstral based pitch estimation

where the noise e is assumed to be normally distributed noise. The coefficients, $a_i, \ldots, a_N$, are called the linear prediction coefficients (LPC). AR-modeling is often used in applied signal processing, and there are many approaches to compute them, e.g. using the Yule-Walker estimate or Levinson-Durbin algorithm (see e.g. [40, chapt. 6] for more on the subject). Once the LPC's have been found, they are used as coefficients in a finite impulse response (FIR) filter which then gives the inverse filtered signal.

Cepstral Analysis

Cepstrum analysis is a technique suited to detect periodic structures in the spectrum of a signal. The complex cepstrum, $C_x(\tau)$ of the signal $x(t)$ is defined as the inverse Fourier transform of the logarithm of the spectrum, $X(f) = \mathcal{F}\{x(t)\} = |X(f)|\, e^{j\phi(f)}$, i.e.

$$C_x(\tau) = \mathcal{F}^{-1}\{\log X(f)\} = \mathcal{F}^{-1}\{\log|X(f)|\} + \mathcal{F}^{-1}\{j\phi(f)\} \tag{3.5}$$

when $\mathcal{F}$ and $\mathcal{F}^{-1}$ symbolize the Fourier transform and its inverse. In most speech processing applications only the amplitude of the spectra is used. As the contribution of the angular term in Eq.(3.5) is ignored, the expression is called the real or power cepstrum. Besides speech processing the cepstrum is also used in machine diagnostics. More information on properties and applications of the cepstrum are found in [47, chapt.8]. Figure 3.4 shows the block diagram of the cepstral based pitch detector as described in [46] and [63]. The most noticeable differences between the two pitch applications is that the latter implements spectral flattening of frequencies above 1.5 kHz prior to the inverse Fourier transform.

3.2 Subspace Methods

Direction of arrival (DOA) estimation is the term used to describe the problem of determining the incoming angle of objects (e.g. aircrafts) using sensor arrays. The objects are seen as far-field narrow-band sources. The plane wave signals emanating from the sources are observed by the sensor array and depending on the angle of an incoming wave and the geometry of the array, the wavefront is detected by the different sensors at different times. This is illustrated in Figure 3.5 for a uniform linear array with an incoming angle, θ, of the plane wave and the first sensor, $s_0(t)$ is chosen as the reference sensor. From the geometry of the array, the propagation

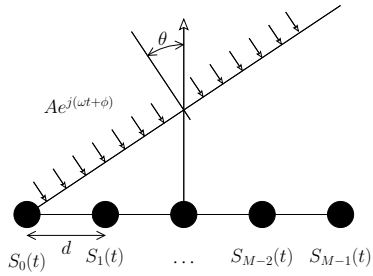

Figure 3.5: Sensor array

delay between two sensors is

$$\tau(\theta) = d \sin\theta / c$$

where c is the speed of propagation for the wave. The detected signal at the other sensors thus becomes

$$s_m(t) = s_0(t - m\tau(\theta)) = Ae^{j(\omega t + \phi - md\sin\theta/c)}$$

In the case with K plane waves impinging from K different directions on the array with M sensors, the vector $\mathbf{s}$ becomes,

$$\begin{aligned}
\mathbf{s} &= \mathbf{A}\mathbf{f} + \mathbf{n} \\
\mathbf{A} &= \begin{bmatrix} 1 & \cdots & 1 \\ e^{-j\omega_1 d\sin\theta_1/c} & \cdots & e^{-j\omega_K d\sin\theta_K/c} \\ \vdots & & \vdots \\ e^{-j(M-1)\omega_1 d\sin\theta_1/c} & \cdots & e^{-j(M-1)\omega_K d\sin\theta_K/c} \end{bmatrix} \\
\mathbf{f} &= \begin{bmatrix} A_1 e^{j(\omega_1 t+\phi_1)} \\ \vdots \\ A_K e^{j(\omega_K t+\phi_K)} \end{bmatrix}
\end{aligned}$$

where $\mathbf{n}$ is the noise vector. The covariance matrix of the sensors is

$$\mathbf{R_{ss}} = E\{\mathbf{s}\,\mathbf{s}^H\} = \mathbf{A}\; E\{\mathbf{f}\,\mathbf{f}^H\}\,\mathbf{A}^H + \sigma^2\mathbf{I}$$

which has rank K in the noiseless case ($\sigma^2 = 0$). When $K < M$ and $\sigma^2 > 0$, then the covariance matrix can be separated into a signal subspace and a noise subspace from which the K incoming angles can be determined.

The link between DOA and frequency estimation is that each of the K impinging wavefronts results in a sinusoidal wave across the sensors. To estimate the frequencies in a signal, $x(t)$, the sensor signals, $s_m(t)$ are simply replaced by time-shifted versions of $x(t)$, i.e., $s_m(t) = x(t + \Delta T)$, where ΔT is the sample interval.

3.2.1 Estimation Methods

In the following the MUSIC and ESPRIT algorithms are explained. Both methods are based on the eigen decomposition of the auto covariance function of the signal. These two algorithms are among the most popular of the so called high-resolution subspace methods which also includes the Pisarenko algorithm [32, sec 8.3], [40, sec 9.7], [42, sec 12.5]

The methods are only considered for complex sinusoids, but they are easily applied to real valued signals since real valued sinusoids can be expressed as the sum of two complex sinusoids through Eulers identities.

First a complex signal is defined containing K complex sinusoids. The signal is corrupted by additive white Gaussian noise with variance σ^2 and results in the observed complex signal $x(n)$ in (3.6).

$$x(n) = \sum_{k=1}^{K} A_k e^{j(\omega_k n+\phi_k)} + w(n), \quad w \sim \mathcal{N}(0,\sigma^2) \tag{3.6}$$

A vector containing M consecutive observed samples,

$$\mathbf{x}(n) = \begin{bmatrix} x(n), & x(n+1), & \dots, & x(n+M-1) \end{bmatrix}^\top \tag{3.7}$$

can be written using matrix notation

$$\mathbf{x}(n) = \mathbf{S}\mathbf{a}(n) + \mathbf{w}(n) \tag{3.8}$$

$$\mathbf{S} = \begin{bmatrix} 1 & \cdots & 1 \\ e^{j\omega_1} & \dots & e^{j\omega_K} \\ \vdots & & \vdots \\ e^{j(M-1)\omega_1} & \dots & e^{j(M-1)\omega_K} \end{bmatrix} \tag{3.9}$$

$$\mathbf{a}(n) = \begin{bmatrix} A_1 e^{j\theta_1(n)}, & \dots, & A_K e^{j\theta_K(n)} \end{bmatrix}^\top \tag{3.10}$$

$$\theta_i(n) = \omega_i n + \phi_i \tag{3.11}$$

The auto covariance matrix is defined as the expectation

$$\mathbf{R_{xx}} = E\{\mathbf{x}(n)\mathbf{x}(n)^H\} \tag{3.12}$$

$$= E\{(\mathbf{S}\mathbf{a}(n) + \mathbf{w}(n))(\mathbf{w}(n)^H + \mathbf{a}(n)^H\mathbf{S}^H)\} \tag{3.13}$$

$$= \mathbf{S}\, E\{\mathbf{a}(n)\,\mathbf{a}(n)^H\}\,\mathbf{S}^H + \sigma^2\mathbf{I} \tag{3.14}$$

$$= \mathbf{S}\mathbf{A}\mathbf{S}^H + \sigma^2\mathbf{I} \tag{3.15}$$

where $\mathbf{A} = \mathrm{diag}[{A_1}^2, \dots, {A_K}^2]$. It is seen that$\mathbf{R_{xx}}$ has full rank, but the first term in (3.15) contributed by the signal only has rank K.

MUSIC

The MUSIC (*multiple signal classification*) algorithm due to Schmidt [54] separates the auto covariance matrix into a signal subspace and a noise subspace. This is

accomplished through eigen decomposition of $\mathbf{R_{xx}}$ by solving (3.16) for $\{(\mathbf{v}_i, \lambda_i), 1 \leq i \leq M\}$.

$$\mathbf{R_{xx}}\mathbf{v}_i = \lambda_i \mathbf{v}_i \tag{3.16}$$

Assuming the eigenvectors are normalized then $\mathbf{R_{xx}}$ can be rewritten as

$$\mathbf{R_{xx}} = \sum_{i=1}^{K} \lambda_i \mathbf{v}_i \mathbf{v}_i{}^H + \sigma^2 \sum_{j=1}^{M} \mathbf{v}_j \mathbf{v}_j{}^H \tag{3.17}$$

$$= \sum_{i=1}^{K} (\lambda_i + \sigma^2) \mathbf{v}_i \mathbf{v}_i{}^H + \sigma^2 \sum_{j=K+1}^{M} \mathbf{v}_j \mathbf{v}_j{}^H \tag{3.18}$$

where the first summation is the signal subspace and the last summation is the noise subspace. The MUSIC algorithm defines the spectral estimate,

$$P_{MUSIC}(\omega) = \frac{1}{\sum_{i=K+1}^{M} |\mathbf{s}(\omega)^H \mathbf{v}_i|^2} \tag{3.19}$$

$$\mathbf{s}(\omega) = [1, e^{j\omega}, \ldots, e^{j(M-1)\omega}] \tag{3.20}$$

Since all the eigenvectors, $\mathbf{v}_i$, are orthogonal, the projection of any frequency vector, $\mathbf{s}(\omega)$, onto the noise subspace, results in a sharp peak in the P_{MUSIC} spectrum when ω is close to the true frequencies in the signal subspace.

The problem still remains to find the frequencies. For this purpose the *Root-MUSIC* algorithm exists. It avoids the nonlinear maximization of P_{MUSIC} otherwise required to find the frequencies of the signal subspace (see e.g [40, sec.9.7]).

ESPRIT

The ESPRIT (*estimation of signal parameters via rotational invariance techniques*) algorithm due to Roy *et al.* [53] also estimates the frequencies using eigen value decomposition. The idea of ESPRIT is to divide the sensor array into two displaced sub-arrays and use the spatial covariance matrix and cross-covariance matrix between the two sub-arrays.

For the detection of sinusoids in the measured signal, the sub-arrays are equivalent to two vectors of the signal, displaced one sample. The signal is modeled by

$$x(n) = \sum_{k=1}^{K} A_k e^{j(\omega_k n + \phi_k)} + w(n), \quad w \sim \mathcal{N}(0, \sigma^2) \tag{3.21}$$

from which the two sub arrays are formed,

$$\mathbf{x}(n) = \left[\, x(n), \quad x(n+1), \quad \ldots, \quad x(n+m-1) \,\right]^\top \tag{3.22}$$

$$\mathbf{y}(n) = \left[\, x(n+1), \quad x(n+2), \quad \ldots, \quad x(n+m) \,\right]^\top \tag{3.23}$$

$$\mathbf{w}(n) = \left[\, w(n), \quad w(n+1), \quad \ldots, \quad w(n+m-1) \,\right]^\top \tag{3.24}$$

By use of (3.21), $\mathbf{x}(n)$ can be written as

$$\mathbf{x}(n) = \mathbf{S}\mathbf{a}(n) + \mathbf{w}(n) \tag{3.25}$$

$$\mathbf{y}(n) = \mathbf{S}\Phi\mathbf{a}(n) + \mathbf{w}(n+1) \tag{3.26}$$

where

$$\mathbf{S} = \begin{bmatrix} 1 & \cdots & 1 \\ e^{j\omega_1} & \cdots & e^{j\omega_K} \\ \vdots & & \vdots \\ e^{j(m-1)\omega_1} & \cdots & e^{j(m-1)\omega_K} \end{bmatrix} \tag{3.27}$$

$$\mathbf{a}(n) = \begin{bmatrix} A_1 e^{j\theta_1(n)}, & \ldots, & A_K e^{j\theta_K(n)} \end{bmatrix} \tag{3.28}$$

$$\theta_i(n) = \omega_i n + \phi_i \tag{3.29}$$

$$\mathbf{\Phi} = \mathrm{diag}[e^{j\omega_1}, e^{j\omega_2}, \ldots, e^{j\omega_K}] \tag{3.30}$$

The spatial covariance matrix of $\mathbf{x}$ and the cross covariance matrix of $\mathbf{x}$ and $\mathbf{y}$ are

$$\mathbf{R_{xx}} = E\{\mathbf{x}(n)\mathbf{x}(n)^H\} = \mathbf{S}\mathbf{A}\mathbf{S}^H + \sigma^2\mathbf{I}_{\mathrm{m}\times\mathrm{m}} \tag{3.31}$$

$$\mathbf{R_{xy}} = E\{\mathbf{x}(n)\mathbf{y}(n)^H\} = \mathbf{S}\mathbf{A}\Phi\mathbf{S}^H + \sigma^2 \begin{bmatrix} \mathbf{0}_{1\times\mathrm{m}\text{-}1} & 0 \\ \mathbf{I}_{\mathrm{m}\text{-}1\times\mathrm{m}\text{-}1} & 0 \end{bmatrix} \tag{3.32}$$

$$\mathbf{A} = \mathrm{diag}[{A_1}^2, {A_2}^2, \ldots, {A_K}^2] \tag{3.33}$$

Now, since the noise is white Gaussian the variance, σ^2 is found as the smallest eigenvalues of $\mathbf{R_{xx}}$. Hence, by first estimating $\mathbf{R_{xx}}$ and $\mathbf{R_{xy}}$, the noise contribution can be removed,

$$\mathbf{C_{xx}} = \mathbf{R_{xx}} - \sigma^2\mathbf{I}_{\mathrm{m}\times\mathrm{m}} = \mathbf{S}\mathbf{A}\mathbf{S}^H \tag{3.34}$$

$$\mathbf{C_{xy}} = \mathbf{R_{xy}} - \sigma^2 \begin{bmatrix} \mathbf{0}_{1\times\mathrm{m}\text{-}1} & 0 \\ \mathbf{I}_{\mathrm{m}\text{-}1\times\mathrm{m}\text{-}1} & 0 \end{bmatrix} = \mathbf{S}\mathbf{A}\Phi\mathbf{S}^H \tag{3.35}$$

The frequencies, $\omega_i, 1 \leq i \leq K$, are now found as K generalized eigen values of the matrix pair $(\mathbf{C_{xx}}, \mathbf{C_{xy}})$ that lie on the unit circle, i.e. $\mathbf{C_{xx}} - \lambda\mathbf{C_{xy}} = \mathbf{S}\mathbf{A}\left(\mathbf{I} - \lambda\mathbf{\Phi}\right)\mathbf{S}^H$

Discussion

The statistical properties of MUSIC and ESPRIT are compared in [57] which concludes that both methods have similar asymptotic variance. The estimates are shown to improve with increasing M, unfortuneately complexity in the algorithm also increases with M^3. In general for frequency estimation ESPRIT should be prefered over MUSIC, since it has a slightly lower variance and is also computational less demanding. This is also the conclusion of [48] in which the performance of Root-MUSIC is investigated.

A common problem for all subspace methods, is the computational complexity of determining the eigen values of the covariance matrix. Instead of re-estimating the covariance matrix and its eigen values for each new observation, adaptive, iterative or recursive update methods can be used [7, 11, 61, 62]. An overview of such methods is provided in [11].

3.2.2 Tracking Methods

Tracking the objects between observations is of great interest in radar applications and has been studied intensively. When the aforementioned subspace methods are used for the detection, then the adaptive update methods in themselves serves as trackers. But a remaining problem is when the signal to noise level is low to be able to discriminate between true and false detections. The analogy to the topic of this thesis is obvious, I.e. the problem of determining which of the detected frequencies can be linked to some rotating part and which can not.

In the literature about target tracking (see e.g. [3, 58]), a common solution is to use state-space models of the targets and then use the observations to update the target states. When the state space models are linear the Kalman filter [3] provide the optimal solution. The state space model for a target moving with constant velocity in one dimensional space is

$$\begin{aligned} \mathbf{x} &= \begin{bmatrix} x & \dot{x} \end{bmatrix}^\top \\ \mathbf{F} &= \begin{bmatrix} 1 & T \\ 0 & 1 \end{bmatrix} \\ \mathbf{x}_{n+1} &= \mathbf{F}\,\mathbf{x}_n + \mathbf{v},\ \mathbf{v} \sim \mathcal{N}(\mathbf{0}, \mathbf{\Lambda_v}) \\ y_n &= \begin{bmatrix} 1 & 0 \end{bmatrix} \mathbf{x}_n + u,\ u \sim \mathcal{N}(0, {\sigma_u}^2) \end{aligned}$$

The vector $\mathbf{x}$ is called the state vector and describes the state of the target in full. For a target moving with constant speed in one dimensional space this amounts to the current position x and the current velocity $\dot{x}$. $\mathbf{F}$ is the state transition matrix which relates the current state, $\mathbf{x}_n$, to the next state, $\mathbf{x}_{n+1}$. $\mathbf{v}$ is the state noise vector which is white Gaussian with zero mean and covariance matrix, $\mathbf{\Lambda_v}$. The observation is modeled by y, which in this simple example is identical to the position. u is called the measurement noise and is also Gaussian distributed with zero mean and variance, ${\sigma_u}^2$

For nonlinear systems the general state-space model is written [3]:

$$\begin{aligned} \mathbf{x}_{n+1} &= \mathbf{f}(n,\, \mathbf{x}_n,\, \mathbf{v}) \\ \mathbf{y}_n &= \mathbf{h}(n,\, \mathbf{x}_n,\, \mathbf{u}) \end{aligned} \tag{3.36}$$

where $\mathbf{x}_n$ is the state vector at time n, $\mathbf{y}_n$ is the observation vector related to state $\mathbf{x}_n$. The state- and measurement noise are represented by the vectors $\mathbf{v}$ and $\mathbf{u}$ respectively. The state transition matrix is replaced by the nonlinear function $\mathbf{f}(\cdot)$ and the output is computed by the function $\mathbf{h}(\cdot)$. The state vector can be estimated with the Extended Kalman Filter (EKF) which essentially is the linear Kalman filter applied by linearizing $\mathbf{f}(\cdot)$ and $\mathbf{h}(\cdot)$. An example using the EKF for frequency estimation is given in [37], where the fundamental frequency of a periodic signal along with the amplitudes and phases of the orders of the fundamental frequency are estimated directly from the observed signal.

Since the model adaption enters through the state- and measurement noise, the critical part of using Kalman filters is to determine the correct noise variances and

initial state estimates. When tracking multiple targets the state of each target is tracked separately. But since the observations are made without any prior knowledge of the targets, the interesting data association problem of assigning targets to the observations must be solved for each measurement. This leads to the following traditional steps in a tracking application:

1. *Detection*: Estimate possible positions of target.
2. *Data Association*: Assign the observed positions to targets.
3. *Update States*: Update the target states according to the observations.

The increase of computer power has allowed the development of more advanced tracking algorithms founded on probabilistic methods such as Bayesian statistics [5, 18, 35, 60, 67]. These approaches result in the three steps above being less distinct.

3.3 Fourier Transform Interpolation Methods

The Fast Fourier Transform (FFT) is a computationally efficient way to estimate the frequency contents of sampled signals. Unfortunately there are two disadvantages of using the FFT: Firstly the frequency resolution is inversely proportional to the length (in seconds) of the measured signal. Secondly, the energy from the main lobe leaks into the side-lobes.

To illustrate this, a harmonic signal with the frequency F_x is defined as

$$x(t) = A\sin(2\pi F_x t)$$

The signal is sampled uniformly at a rate of F_s samples per second, which gives the interval $\Delta T = 1/F_s$ between samples. It is assumed that $F_x < F_s/2$. For easier notation the sampled signal is denoted $x_n \equiv x(n\Delta T)$ where the subscript $_n$ indicates the sample number. The discrete Fourier Transform (DFT) of x_n is defined as

$$G(f_m) = \sum_{n=0}^{N-1} x_n e^{-j2\pi f_m n} \tag{3.37}$$

where $f_m = mF_s/N$. This shows that the N point DFT will give N equidistant frequency estimates with the distance $\Delta F = Fs/N = 1/T$ where T is duration of x_n in time. The subscript $_m$ is used to identify the frequency line and allows the shorter notation, $G_m \equiv G(f_m)$. The leakage effect is caused by the finite record length of the signal. The procedure of extracting the time record can be perceived as a multiplication of the continuous signal, $x(t)$, with a rectangular pulse $w_R(t)$, i.e.

$$w_R(t) = \begin{cases} 1, & 0 \le t < T \\ 0, & \text{otherwise} \end{cases} \quad \xrightarrow{\mathcal{F}} \quad W_R(f) = \frac{\sin(\pi T f)}{\pi T f}$$

The effect of the multiplication in the time-domain is equivalent to a convolution in the frequency domain. Figure 3.6 shows the DFT of x_n for $F_x = f_m + \delta\Delta F$ when $\delta = 0.33$ frequency lines. The dashed vertical line is the true location of the frequency

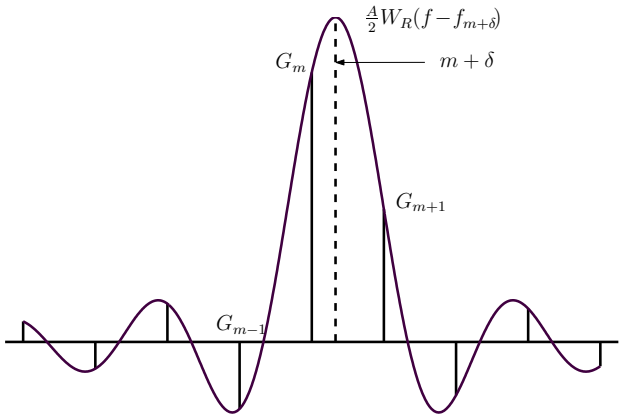

Figure 3.6: Rectangular Window

F_x and the solid lines are the amplitude of the Fourier coefficients, G_i. The solid curve is the window function for the rectangular window and it shows clearly the poor attenuation in the side lobes.

The Fourier transform interpolation methods have been developed to provide better frequency and amplitude estimates by examining the leakage into the side lobes. As has just been shown the leakage depends on the window function applied to the signal, hence different algorithms exist for different windows. In [43] Quinn proposes some algorithms for interpolation using the rectangular window, and shows that although the estimators do not achieve the asymptotic CRLB, the asymptotic variances are not far from the asymptotic CRLB. The algorithms are based on 3 complex Fourier coefficients. Quinn's FTI3 algorithm [43, pp.198] is listed in Table 3.1. It can

1.	$\hat{m}$	$=$	$\max_m \lvert G_m \rvert,\ 0 < m < \frac{N-1}{2}$
2.	α_{-1}	$=$	$\mathrm{Re}\left\{\frac{G_{\hat{m}-1}}{G_{\hat{m}}}\right\}$
	α_{+1}	$=$	$\mathrm{Re}\left\{\frac{G_{\hat{m}+1}}{G_{\hat{m}}}\right\}$
3.	$\hat{\delta}_{-1}$	$=$	$\frac{-\alpha_{-1}}{\alpha_{-1}-1}$
	$\hat{\delta}_{+1}$	$=$	$\frac{\alpha_{+1}}{\alpha_{+1}-1}$
4.	$\tilde{\delta}$	$=$	$\begin{cases} \hat{\delta}_{+1}, & \delta_{-1} > 0 \wedge \delta_{+1} > 0 \\ \hat{\delta}_{-1}, & \text{otherwise} \end{cases}$
5.	$\hat{\delta}$	$=$	$\frac{\hat{\delta}_{+1}+\hat{\delta}_{-1}}{2} + (\hat{\delta}_{+1} - \hat{\delta}_{-1})\frac{3\tilde{\delta}^3+2\tilde{\delta}}{3\tilde{\delta}^4+6\tilde{\delta}^2+1}$
6.	$\hat{f}$	$=$	$f_{\hat{m}} + \hat{\delta}\Delta F$

Table 3.1: FTI3 algorithm

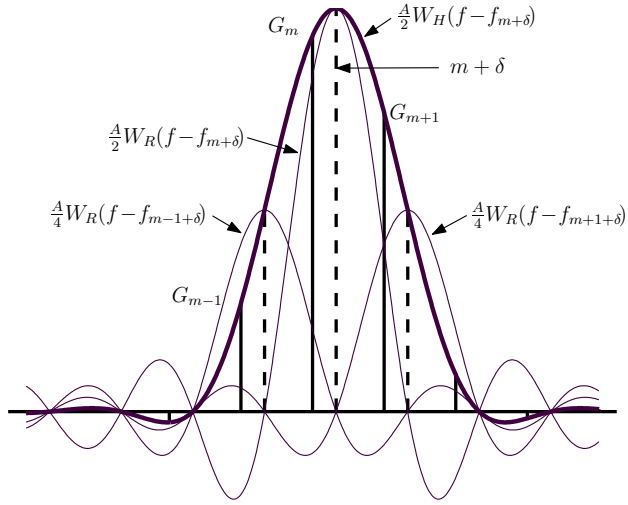

Figure 3.7: Hanning Window

be argued that the requirement for complex coefficients is disadvantage of the FTI3 algorithm since complex spectra requires twice the storage capacity and prevents use of averaged spectra. For low SNR levels averaging the moduli of multiple DFT spectra improves the spectral estimates. In this case the it is possible to apply the class of *Rife-Vincent* windows and interpolators [52]. The Hanning window belongs to this class of windows. In the time-domain the Hanning window is

$$w_H(t) = \begin{cases} 1-\cos^2(2\pi t/T), & 0 \le t < T \\ 0, & \text{otherwise} \end{cases}$$

which in the frequency domain becomes

$$W_H(f) = \frac{1}{2}W_R(f) + \frac{1}{4}\left(W_R(f+1/T) + W_R(f-1/T)\right) \tag{3.38}$$

The Hanning window is shown in Figure 3.7. When compared to Figure 3.6 it is seen that the Hanning window has a wider main lobe, but lower side lobes. The thin curves on the figure are individual rectangular windows that are summed in Eq. (3.38) to form the Hanning window (solid curve).

The interpolation algorithm for the Hanning window can be derived analytically from the expressions of $|G_m|$ and $|G_{m+1}|$ B.1 and is listed in Table 3.2.

When multiple harmonics are present it is obvious that the side lobes of the other harmonics will influence the estimate. In this case it is preferable to use Hanning window over the the rectangular window, since it has lower side lobes.

More information on the Fourier interpolation can be found in the literature, e.g. in [55] which is a comparative study of the rectangular, Hanning, and Rife-Vincent

1.	$\hat{m}$	$=$	$\max_m \lvert G_m \rvert,\ 0 < m < \frac{N-1}{2}$
2.	α	$=$	$\frac{\lvert G_{\hat{m}+1} \rvert}{\lvert G_{\hat{m}} \rvert}$
3.	$\hat{\delta}$	$=$	$\frac{2\alpha-1}{\alpha+1}$
4.	$\hat{f}$	$=$	$f_{\hat{m}} + \hat{\delta}\Delta F$

Table 3.2: Hanning Window Interpolation

windows. For the estimation of multiple sinusoids an iterative procedure is described in [49] which, provided sufficient frequency resolution to separate the sinusoids, gives highly accurate estimates of both frequencies, phases and amplitudes.

3.4 Adaptive Filter Based Methods

The fact that sinusoids are solutions to 2nd order difference equations has inspired the development of several frequency estimators. Three of these are described in the following. The first is the method of Prony which dates back to 1795 [22] and assumes there is no noise. The second method is a Auto-Regressive Moving Average (ARMA) which is similar to Prony's method but allows noise. The third method is an Adaptive Comb Filter (ACF) which in structure is similar to the ARMA model, but some of the known stability problems of adaptive ARMA models have been alleviated by adding constraints to the poles and zeros in the model.

3.4.1 Prony's Method

The essence in Prony's Method for frequency estimation is that a sum of sinusoids,

$$x(t) = \sum_{m=1}^{M} A_m \cos(\omega_m t + \phi_m) \tag{3.39}$$

can be expressed as the difference equation of order $2M$,

$$x(t) = -\sum_{k=1}^{2M} c_k x(t-k) \tag{3.40}$$

where the coefficients, c_k, are defined by the polynomial

$$C(z) = \prod_{m=1}^{M} (1 - 2\cos(\omega_m) z^{-1} + z^{-2}) = \sum_{k=0}^{2M} c_k z^{-k} \tag{3.41}$$

(The proof is summarized in appendix B.2). The interesting observation is that the complex roots of $C(z)$ are all located on the unit circle in the conjugate pairs,

$z = e^{\pm j\omega_m}$, I.e. the harmonic frequencies are found as the phase angles of the roots of $C(z)$. Since Eq. (3.40) is recognized as an AR model of order $2M$ then the coefficients of $C(z)$ are found directly from a sequence of $N \geq 4M$ samples of $y(t)$ or by the methods mentioned for the SIFT in section 3.1.1.

3.4.2 Auto-Regressive Moving-Average Modeling

When noise is added to the right hand side of Eq. (3.39) the accuracy of Prony's method deteriorates. The noise will enter the model as a moving average (MA) process which also needs to be modeled. To show this, we define an observed signal with one sinusoid, $d(t)$, and additive noise, $e(t)$

$$d(t) = A\cos(\omega t + \phi) + e(t), \quad e \sim \mathcal{N}(0, \sigma^2) \tag{3.42}$$

From Eq. (3.40) and (3.41) we know that the harmonic part can be written as

$$u(t) = A\cos(\omega t + \phi) = 2\cos(\omega)u(t-1) - u(t-2)$$

By isolating the harmonic part of Eq. (3.42) and setting

$$u(t) = d(t) - e(t)$$

then the difference equation gives

$$d(t) - 2\cos(\omega)d(t-1) + d(t-2) = e(t) - 2\cos(\omega)e(t-1) + e(t-2) \tag{3.43}$$

which is recognized as an ARMA (2,2) process. For M sinusoids this extends to an ARMA ($2M$, $2M$) process. Since ARMA modeling has been treated extensively in the literature (see e.g. [28] and the references therein) it is here sufficient to mention that it is generally more difficult than the simple AR estimation. In appendix B.3 the Quinn & Fernandez method [43] is explained. It is an iterative procedure for estimating a single sinusoid in noise based on the model of Eq. (3.43).

3.4.3 Adaptive Comb Filter

A practical problem of fitting ARMA models is to ensure stability. If the poles are located outside the unit circle, then the model becomes unstable. Another problem is the increase in model complexity when the signal consists of multiple sinusoids and hence an increase in the number of parameters to estimate. Furthermore the general ARMA model does not take into consideration the possibility of the sinusoids being fixed orders of a common fundamental frequency.

The adaptive comb filter (ACF) described here was originally introduced by Nehorai and Porat in [31]. The method is based on the same relationship as the general ARMA model of a sum of sinusoids in noise, namely that a signal $d(t)$ which consist of a number of sinusoids in additive white noise, $\epsilon(t)$, satisfies the relationship

$$A(q^{-1})d(t) = A(q^{-1})\epsilon(t), \quad \epsilon \sim \mathcal{N}(0, \sigma^2) \tag{3.44}$$

(this is the generalization of Eq. (3.43)) where q^{-1} symbolizes the unit delay operator and $A(q^{-1})$ is given by

$$A(q^{-1}) = \prod_{m=1}^{M} (1 - 2\cos(\omega_m)q^{-1} + q^{-2}) = \sum_{k=0}^{2M} a_k q^{-k} \tag{3.45}$$

The idea is then to design a pre-whitening filter for $d(t)$, i.e.

$$e(t) = H(q^{-1})d(t)$$

such that the output, $e(t)$, is minimized. The pre-whitening filter devised by Nehorai and Porat is

$$H(q^{-1}) = \frac{A(q^{-1})}{A(\rho q^{-1})} \tag{3.46}$$

where

$$A(\rho q^{-1}) = \prod_{m=1}^{M} (1 - \rho 2\cos(\omega_m)q^{-1} + \rho^2 q^{-2})$$

The scalar $\rho, 0 < \rho < 1$ ensures all poles to be located inside the unit circle.

With Fourier series non-sinusoidal periodic signals can be resolved into a sum of sinusoidal components with frequencies that are integer multiples of the fundamental frequency. Therefore if the sinusoids in the signal indeed are caused by a periodic signal, then $H(q^{-1})$ in Eq. (3.46) can be simplified by imposing two constraints: The first constraint is to assume that the orders of frequencies with regard to the fundamental frequency are known a priori, i.e., given the fundamental frequency then the phase angles of the roots of all poles and zeros can be computed. The second constraint concerns the magnitude of the roots, namely that all zeros are to be located on the unit circle and all the poles are assigned the same magnitude $\rho < 1$. The imposed constraints are illustrated in Figure 3.8(a) where the poles are marked with $\times$ and the zeros with $\circ$.

The frequency response shown in Fig. 3.8(b), clearly exhibits the characteristics of a comb filter, with narrow notches located at the first 5 harmonics of the fundamental frequency which is $F_F = 85$Hz. $H(q^{-1})$ thus attempts to attenuate the specified harmonics in the signal and the optimization problem can be seen as that of minimizing the output $e(t)$ w.r.t. F_F. The bandwidth of the notches is determined by ρ according to

$$B_\pi = \pi(1 - \rho), \quad B_{Hz} = \frac{F_S}{2}(1 - \rho)$$

where B_π is the bandwidth in radians and B_{Hz} is the bandwidth in Hz given the sample rate F_S.

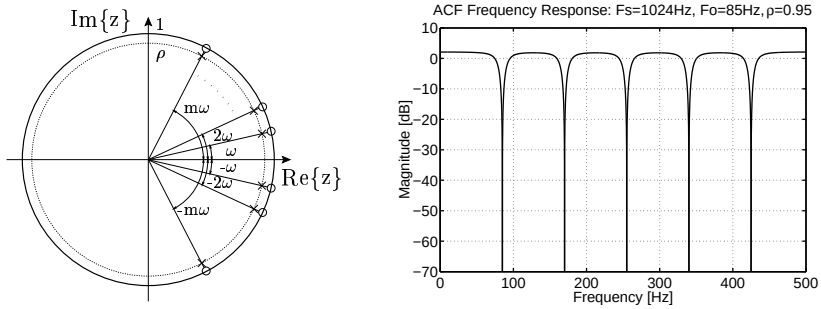

(a) Pole/Zero Constraints (b) Frequency Response

Figure 3.8: Adaptive Comb Filter

The algorithm given in [31] is general in the sense, that the sinusoids need not be pure harmonics of the fundamental frequency. It is a recursive prediction error algorithm [28] which uses the gradient of $e(t)$ for fast convergence.

Recursive prediction error algorithms have the form [28]

$$e(t) = d(t) - \hat{d}(t|\boldsymbol{\Theta}) \tag{3.47}$$

$$\hat{\boldsymbol{\Theta}}(t) = \hat{\boldsymbol{\Theta}}(t-1) + \gamma(t)\mathbf{R}^{-1}(t)\boldsymbol{\Psi}(t)e(t) \tag{3.48}$$

$$\mathbf{R}(t) = \mathbf{R}(t-1) + \gamma(t)\left[\boldsymbol{\Psi}(t)\boldsymbol{\Psi}^{\top}(t) - \mathbf{R}(t-1)\right] \tag{3.49}$$

where $\hat{d}(t|\boldsymbol{\Theta})$ is the predicted value of the observed signal $d(t)$, and $e(t)$ is called the prediction error. The model is represented by the vector $\hat{\boldsymbol{\Theta}}(t)$, and $\boldsymbol{\Psi}(t)$ is the gradient of the prediction error $e(t)$. $\mathbf{R}$ is an approximation of the Hessian of $e(t)$, i.e.

$$\boldsymbol{\Psi}(t) = \frac{\partial\, e(t)}{\partial \boldsymbol{\Theta}}, \quad \mathbf{R}(t) \approx \frac{\partial^2\, e(t)}{\partial \boldsymbol{\Theta}(t)\, \partial \boldsymbol{\Theta}^{\top}(t)}.$$

$\gamma(t)$ is update step size of the algorithm, also known as the gain of the algorithm. In [28] the *memory time constant* of the algorithm is defined as

$$T_0 = 1/\gamma(t) \tag{3.50}$$

for which observations older than T_0 will contribute in the algorithm with a weight of 36%. Using Eq. (3.50) prior knowledge about the time constant of the system can be used to choose a proper gain factor. The choice of Nehorai and Porat ([31]) is to slowly decrease the gain, thus increasing the weight on older samples and improving the estimates for the *stationary* signal.

A contribution from this study is the new variant of the adaptive comb filter, which is suitable for tracking dynamic signals. It distinguishes itself from [31] in two ways. First, the trigonometric functions have been eliminated from the algorithm. The trade-off for this is that all the harmonic frequencies must be integer

multiplicands of a common frequency. This gives a much simpler and more efficient algorithm. The reason is that the cosine terms in Eq. (3.45) can be replaced by polynomials in

$$b = -2\cos(\omega_F), \tag{3.51}$$

where ω_F is the common frequency. This simplifies computation of $A(q^{-1})$ in Eq. (3.45) as well as the gradient of $e(t)$ required for the adaption of the algorithm. Second, the focus in this study is estimation and tracking of non-stationary signals with large frequency variation. Motivated by the pitch detection algorithms where the record length is adjusted with the frequency, a similar approach is taken here. The relation in Eq. (3.50) allows the adjustment of the algorithm gain given the current frequency estimate,

$$\gamma(t+1) = \alpha\,\gamma(t) + (1-\alpha)\,\frac{\cos^{-1}(-0.5b(t))}{2\pi K} \tag{3.52}$$

where α serves as exponential averaging of the gain, $b(t)$ is the adaption parameter of the model, and K is a constant specifying the memory time constant of the algorithm in number of periods of ω_F.

The algorithm is derived in greater detail in appendix B.4, namely the computation of the gradient, $\mathbf{\Psi}(t)$.

3.5 Evaluation

The signal model described in Section 2.4 is used to evaluate the algorithms. The algorithms that are evaluated are

- Autocorrelation.
- Modified Autocorrelation with the center clipper and compressed clipper.
- Simplified Inverse Filter with a 5'th order LPC filter.
- ESPRIT .
- Interpolated FFT using Hanning window.
- Adaptive Comb Filter with 1, 3, and 5 notches.

For evaluation an acceleration signal with 5 orders of the fundamental frequency is generated. The amplitudes of the 5 harmonics are shown in Figure 3.9(a) where C_k is the amplitude of the k'th harmonic. The variance of the additive noise is varied to obtain an average SNR of 30 dB, 15 dB, and 0 dB. Figure 3.9(b) shows the actual variation in SNR as the fundamental frequency changes over time. Each algorithm is tested on 100 realizations of the acceleration signal where a new sequence of the noise is used for each realization. The phases are fixed. The signal is sampled 1024

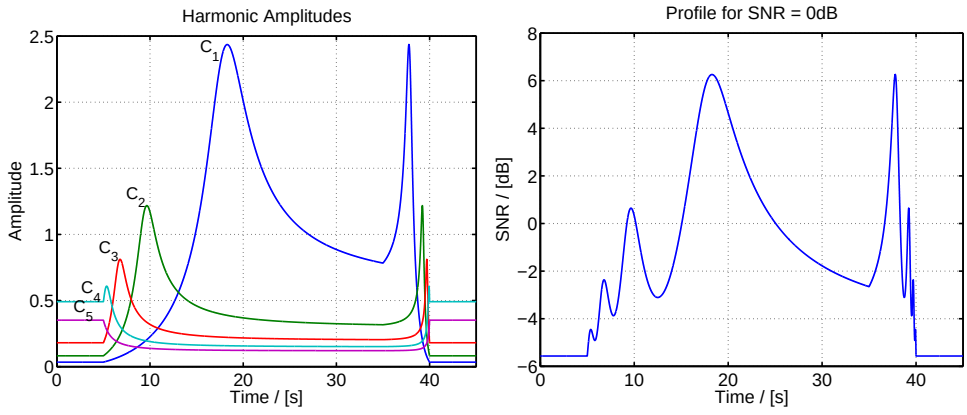

(a) (b)

Figure 3.9: Simulation Signal

times per second and segmented into records of 1/4 second overlapping 75% resulting in record lengths of 256 samples. For each record the algorithms provide an estimate of the fundamental frequency.

For the average SNR level of 15 dB the results are summarized in the Figures 3.10-3.11. The remaining figures for SNR = 30 dB and 0 dB are found in Appendix C as Figures C.2-C.7.

The results of the simulation are presented graphically with two graphs for each test: The left graph shows the distribution of the frequency estimates and the right graph shows the RMS error , the standard deviation of the error (σ), and the CRLB for the signal. The difference between the RMS error and σ is a measure of the bias in the estimate. The frequency distributions are useful for explaining the measured errors, e.g. in Fig. 3.10(c) there are visible signs of period doubling.

The results of the simulations are discussed briefly in the following.

3.5.1 Autocorr, Autoclip, and SIFT

Figure 3.10 shows the results for the autocorrelation based estimators. To increase the resolution, the correlation sequence is up-sampled 8 times to give a better resolution for choosing the peak.

For the simulated signal, it appears that of the three methods, the normal autocorrelation method performs best. But for all SNR values the RMS errors are observed to be an order of magnitude above the CRLB. At high SNR levels the standard deviation for some values tends towards zero, indicating strong bias. This is observed especially for high frequencies.

3.5.2 ESPRIT and Interpolated FFT

Both of theses algorithms estimate pure sinusoids and provides separate estimates for each of the 5 harmonics in the test signal. The approach taken to find the fundamental frequency is to estimate 5 frequencies and assume that the lowest frequency is the fundamental frequency. For ESPRIT the 5 frequencies are taken as those lying closest to the unit circle, and for the interpolated FFT the frequencies are chosen as the 5 largest peaks in the spectrum.

The ESPRIT algorithm (Fig. 3.11(a) and 3.11(b)) performs poorly on the simulated signals. The estimation errors are closely related to the SNR profile (Fig. 3.9(b)) and the lowest estimation error is achieved approximately at $t = 18$ seconds where the first harmonic peaks in amplitude.

The Interpolated FFT algorithm (Fig. 3.11(c) and 3.11(d))performs quite well. It has some problems when the SNR level is too low for the first harmonic at the low frequencies. But as the SNR increase so does the accuracy.

3.5.3 Adaptive Comb Filter

The adaptive comb filter is configured to either 1,3,or 5 notches. Its bandwidth is fixed to 10 Hz ($\rho = 0.98$). The test signal is not segmented in these tests.

The results for the filter with 3 notches[1] are shown in Fig. 3.11(e) and 3.11(f). Overall, the filter with 3 notches had the best performance for the given signal. The adaptive notch filter has the lowest variance of all the methods, but the RMS error is somewhat higher indicating biased estimates. For the chosen bandwidth the filter is capable of tracking the fundamental frequency on the relatively slow run-up, but it also manages to track the fast run-down until the SNR level becomes too low.

Initialization is important since the filter may lock to a wrong harmonic order of the signal. This is perfectly illustrated in Fig. C.5(a) where the one notch filter locks onto the 4'th harmonic which is the strongest at the time of initialization (Fig. 3.9(a)).

At the low SNR conditions, SNR = 0 dB, the figures in Appendix C show that ACF with 3 notches is significantly better than any of the other algorithms tested in this chapter.

3.6 Summary

This chapter has described different methods for frequency estimating. The methods were evaluated using a simulated periodic signal with varying amplitudes and SNR levels. Of the methods the interpolated Fourier transform and the adaptive comb filter were found perform quite well.

To the best of my knowledge, the variant of adaptive comb filter described in Section 3.4.3 is a new contribution of this work. It is able to track dynamic signals thanks to the feedback mechanism controlling the memory time constant. The derivation avoiding trigonometric functions is shown in Appendix. B.4.

[1] The results using the 1 or 5 notches are include in Appendix C

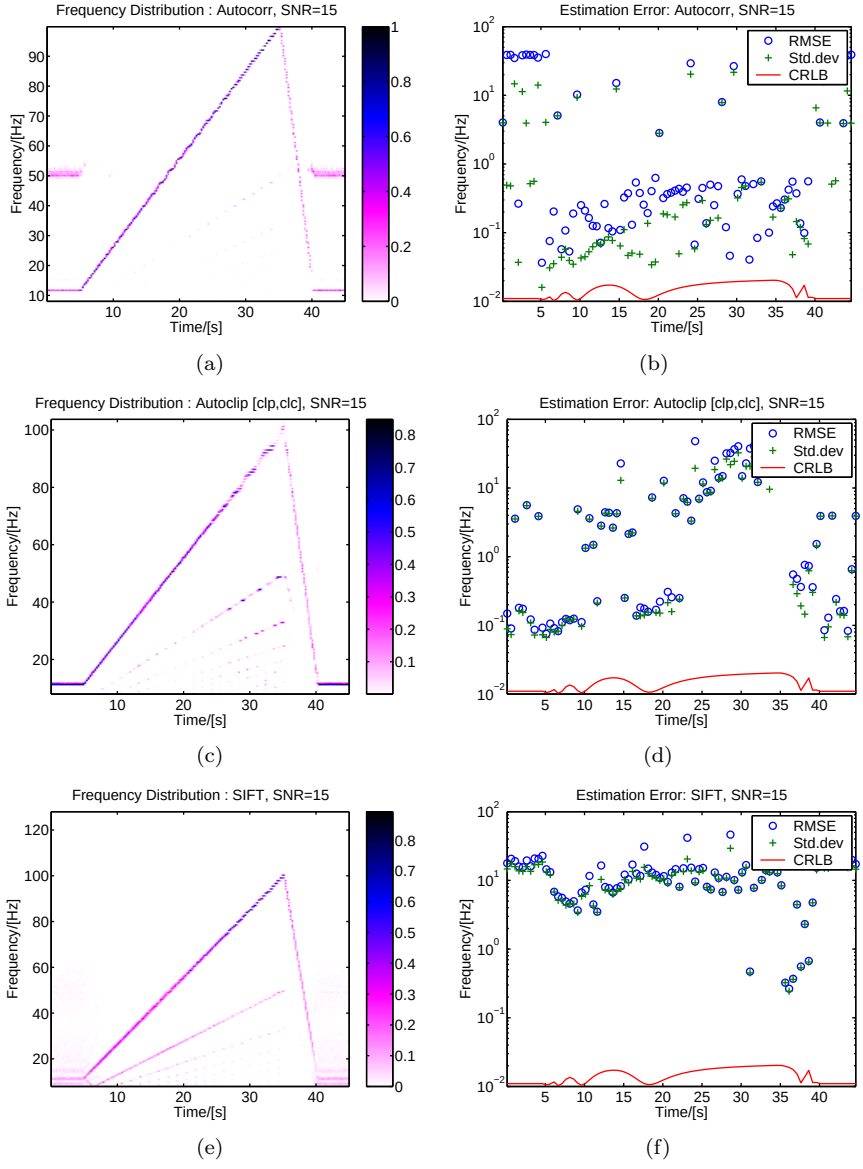

Figure 3.10: Simulation Results for Correlation Methods, SNR=15dB

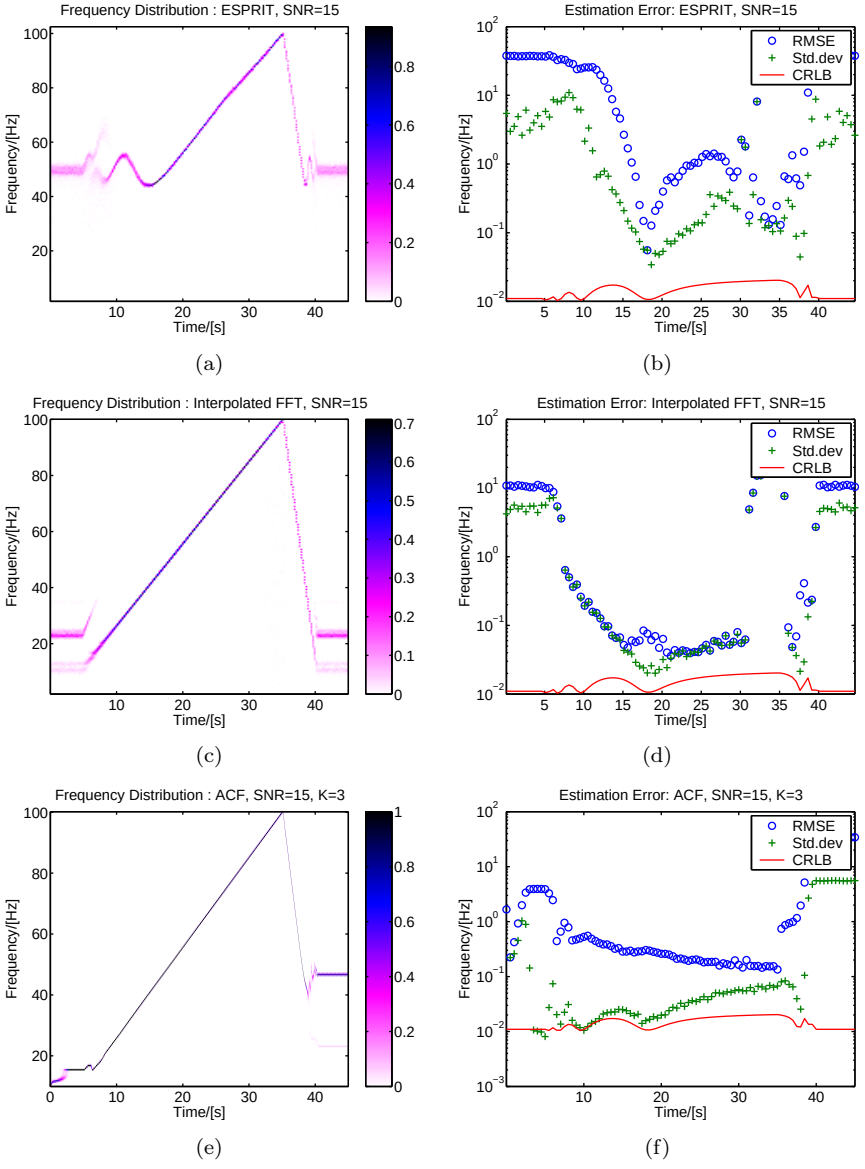

Figure 3.11: Simulation Results for ESPRIT, FFT, and ACF Methods, SNR=15dB

Chapter 4

Bayesian Estimation

Of the frequency estimation techniques mentioned in the previous chapter, the correlation methods and the ACF were the only methods that based their estimates on the harmonic structure. All of the traditional recognized high resolution estimation methods, Interpolated FFT, MUSIC or ESPRIT are all based on individual frequency estimates.

In this chapter a statistical approach is taken to derive a more robust estimation method that utilizes the harmonic structure to produce estimate closer to the CRLB.

The approach is based on Bayesian statistics. The application of Bayesian statistics to spectrum analysis was first introduced by Jaynes [19] and then treated more thoroughly by Bretthorst [6].

The chapter starts by introducing the Maximum Likelihood function in Sec. 4.1 as a prelude to the general Bayesian statistical framework described in Sec. 4.2. Here the frequency estimation problem is formulated in Bayesian terms to include a priori knowledge of the harmonic structure. In Sec 4.3 the Bayesian estimator is evaluated on the same simulated data used in Sec. 3.5 and the results are compared.

The Bayesian framework is very flexible. This is shown in section 4.4 where the model is expanded to estimate time-varying frequencies; in section 4.5 where it is shown how to model close frequencies; and in section 4.6 where it is shown how multiple channels can be combined to improve the estimate.

4.1 Maximum Likelihood

Maximum likelihood is a general estimation method. It can be applied whenever it is possible to formulate a *joint* probability density function of the observed data

sequence and the model parameters.

Recalling the harmonic model of Eq. (2.5) used to generate synthetic data, the observed data is modeled as a sum of K sinusoids with additive Gaussian noise. The model is shown in Eq. (4.1) for a data sequence with a constant frequency and an extra parameter A_0 that represents a constant level offset.

$$d(t) = A_0 + \sum_{k=1}^{K} \left(A_k \cos(\omega_k t) + B_k \sin(\omega_k t)\right) + e(t), \quad e(t) \sim \mathcal{N}(0, \sigma^2) \tag{4.1}$$

Assuming the harmonic sequence is known, i.e. $\omega_k = \eta_k \omega_F$, where η_k are the known orders of the fundamental frequency, ω_F, then the parameters to be estimated are

$$\theta \equiv \left\{A_0, A_1, \ldots, A_K, B_1, \ldots, B_K, \omega_F, \sigma^2\right\} \tag{4.2}$$

If the noise is isolated in Eq. (4.1) it becomes clear that *given* the parameters θ are known, *then* the observed data is distributed as the noise. The PDF of $d(t)$ given θ is therefore

$$p(d(t)|\theta) = \frac{1}{\sqrt{2\pi\sigma^2}} \exp\left\{-\frac{e^2(t)}{2\sigma^2}\right\} \tag{4.3}$$

For a sequence of N observations, $d(t_0), \ldots, d(t_{N-1})$ the maximum likelihood estimate of θ is the set of parameters that maximizes the joint PDF of *all* the observations given θ (Eq. (4.4)).

$$p(d(t_0), \ldots, d(t_{N-1})|\theta) = \prod_{n=0}^{N-1} p(d(t_n)|\theta) \tag{4.4}$$

When dealing with sequences of observations, then matrix notation is more convenient. The matrix notation below is therefore introduced where bold letters indicate matrices or vectors, and the subscript $_{N\times M}$ indicates the matrix dimension.

$$\begin{aligned}
\mathbf{t}_{\mathrm{N}\times 1} &= [t_0 \quad \ldots \quad t_{N-1}]^\top \\
\mathbf{d}_{\mathrm{N}\times 1} &= [d(t_0) \quad \ldots \quad d(t_{N-1})]^\top \\
\mathbf{b}_{2\mathrm{K}+1\times 1} &= [A_0 \quad A_1 \quad \ldots \quad A_K \quad B_1 \quad \ldots \quad B_K]^\top \\
\mathbf{e}_{\mathrm{N}\times 1} &= [e(t_0) \quad e(t_1) \quad \ldots \quad e(t_{N-1})]^\top \\
\mathbf{h}_{\mathrm{K}\times 1} &= [\eta_1 \quad \ldots \quad \eta_K]^\top \\
\mathbf{u}_{\mathrm{N}\times 1} &= [1 \quad \ldots \quad 1]^\top \\
\mathbf{G}_{\mathrm{N}\times 2\mathrm{K}+1} &= [\mathbf{u} \quad \cos(\omega_F\, \mathbf{t}\, \mathbf{h}^\top) \quad \sin(\omega_F\, \mathbf{t}\, \mathbf{h}^\top)]
\end{aligned} \tag{4.5}$$

Using the notation, a sequence of N observations (Eq. (4.1)) becomes:

$$\mathbf{d} = \mathbf{G}\,\mathbf{b} + \mathbf{e} \tag{4.6}$$

Eq. (4.6) is recognized as a $2K+1$ dimensional linear problem where $\mathbf{d}$ is the vector with the observations, $\mathbf{G}$ contains the $2K+1$ basis vectors and is defined by ω_F and

the known orders $\eta_{1\ldots K}$, $\mathbf{e}$ is the noise vector, and $\mathbf{b}$ is the vector with the amplitude parameters.

The *likelihood* of the observed data in $\mathbf{d}$ being modeled by θ is found by expanding Eq. (4.4) using Eq. (4.3):

$$\begin{aligned} p(\mathbf{d}|\theta) &= (2\pi\sigma^2)^{-N/2} \exp\left\{-\frac{\mathbf{e}^\top \mathbf{e}}{2\sigma^2}\right\} \\ &= (2\pi\sigma^2)^{-N/2} \exp\left\{-\frac{(\mathbf{d}-\mathbf{G}\,\mathbf{b})^\top(\mathbf{d}-\mathbf{G}\,\mathbf{b})}{2\sigma^2}\right\} \\ &= (2\pi\sigma^2)^{-N/2} \exp\left\{-\frac{\mathbf{d}^\top\mathbf{d}+\mathbf{b}^\top\mathbf{G}^\top\mathbf{G}\,\mathbf{b}-2\mathbf{b}^\top\mathbf{G}^\top\mathbf{d}}{2\sigma^2}\right\} \end{aligned} \tag{4.7}$$

Maximizing Eq. (4.7) w.r.t. $\mathbf{b}$ gives the *maximum likelihood estimate*[1], $\hat{\mathbf{b}}$, of the amplitudes (Eq. (4.8)).

$$\hat{\mathbf{b}} = (\mathbf{G}^\top\mathbf{G})^{-1}\mathbf{G}^\top\mathbf{d} \tag{4.8}$$

The part of the observed signal which is captured by the model is reconstructed by substituting the true amplitudes for the estimated amplitudes in Eq. (4.6):

$$\mathbf{f} = \mathbf{G}\,\hat{\mathbf{b}} \tag{4.9}$$

Using Eq. (4.9) and Eq. (4.8) the likelihood (Eq. (4.7) can be rewritten:

$$p(\mathbf{d}|\theta) = (2\pi\sigma^2)^{-N/2} \exp\left\{-\frac{\mathbf{d}^\top\mathbf{d}-\mathbf{f}^\top\mathbf{f}}{2\sigma^2}\right\} \tag{4.10}$$

where the likelihood is expressed as a function of the difference in energy of the observed signal and that captured by the model.

4.1.1 Properties

The properties of the maximum likelihood (ML) method has been studied intensively in the literature for the estimation of both single and multiple frequencies [21, 29, 43, 50, 51, 56, 65, 66]. The ML estimator is consistent, hence it converges to the true parameters (no bias) as N increases. It is also asymptotically efficient, i.e., the variance of the estimate approached the CRLB with increasing N. However, the drawback of the ML method is the computational burden of searching the parameter space for the global maximum. To estimate the parameters for a signal with K independent sinusoids requires a K-dimensional search. Including the references above, much of the literature on ML frequency estimation therefore deals with efficient ways for searching the parameter space.

The ML method also has its limitations. When fitting models to observed data, we usually do not know which model functions fits the data best or how many parameters

[1] In this case the ML estimate also gives the least squared error estimate: $\arg\min_{\mathbf{b}}\{\mathbf{e}^\top\mathbf{e}\}$

are needed. It is a recognized limitation of the ML method that it tends to over-parameterize thus leading to more complex models than required. Another limitation is that the ML estimates solely depend on the observed data and do not incorporate any prior knowledge regarding the probability of the parameters. This can lead to incomprehensible parameters [10, 34]. The method lacks a measure for the belief in the estimates.

4.2 The Bayesian Statistical Framework

With Bayesian statistics it is possible to include prior knowledge through the use of Bayes' theorem[2]:

$$p(\theta|\mathbf{d}, I_K) = \frac{p(\mathbf{d}|\theta, I_K)p(\theta|I_K)}{p(\mathbf{d}|I_K)} \tag{4.11}$$

The additional conditional, I_K, represents the prior knowledge represented by the choice of model for both data and noise. In the Bayesian terminology the four probability densities have been named as listed in Table 4.1.

Density	Name	Description
$p(\theta\|\mathbf{d}, I_K)$	*Joint Posterior*	The PDF of the parameters after the data is observed. I.e. knowledge of how well the parameters fits the data.
$p(\mathbf{d}\|\theta, I_K)$	*Likelihood*	The PDF for the data being produced by the given parameter set and the chosen model structure.
$p(\mathbf{d}\|I_K)$	*Evidence*	Prior knowledge of the data sequence given the chosen model structure.

Table 4.1: Bayesian Terminology

Eq. (4.11) states that the *joint posterior* PDF of the parameters conditioned on the observations, is identical to the likelihood multiplied by the prior probability of the parameters divided by evidence of the the observed data. The evidence allows different models to be compared. When the model structure is fixed, the evidence serves only as a scaling factor and is often omitted. In that case, Eq. (4.11) is written:

$$p(\theta|\mathbf{d}, I_K) \propto p(\mathbf{d}|\theta, I_K)p(\theta|I_K) \tag{4.12}$$

4.2.1 Marginalization

A strength of Bayesian estimation theory is that the joint posterior PDF can be marginalized. By this is meant that uninteresting parameters, also termed *nuisance*

[2]This is easily seen from the conditional probability, $P(A, B) = P(A|B)P(B) = P(B|A)P(A)$

parameters, are integrated out of the joint PDF. Depending on the nature of prior PDF's of the nuisance parameters, this may be accomplished analytically, otherwise numerical methods can be applied.

When estimating the fundamental frequency using (4.5) and the linear model (4.6) the amplitudes $\mathbf{b}$ and the noise variance σ^2 are nuisance parameters. In order to integrate them out of the joint posterior PDF, appropriate priors must be chosen and assigned to $\mathbf{b}$ and σ that reflect whatever prior knowledge we may have. When only little or no knowledge is available a prior with a very broad or flat PDF can be chosen. These priors carry very little information and are called *non-informative* priors. For unbounded real-valued parameters[3] either a uniform PDF or a Gaussian PDF with a very large variance are often used. For *scale* parameters that are strictly positive a well-known non-informative prior is Jeffrey's prior which assumes the logarithm of the parameter to have a uniform PDF.

Following these guidelines, the uniform probability density is chosen for the amplitudes and Jeffrey's prior for the noise variance:

$$\begin{aligned} p(\mathbf{b}|I_K) &= k_b \\ p(\sigma|I_K) &= \frac{k_\sigma}{\sigma} \end{aligned} \tag{4.13}$$

The integral to be solved is shown in Eq. (4.14). The evidence, $p(\mathbf{d}|I_K)$, and the prior $p(\mathbf{b}|I_K)$ are constants. Therefore by substituting the equal sign for proportionality, they can be ignored:

$$\begin{aligned} p(\omega_F|\mathbf{d}, I_K) &= \int_0^\infty \int_{\Re^{2K}} \frac{p(\mathbf{d}|\omega, \sigma, \mathbf{b}, I_K) p(\mathbf{b}|I_K) p(\sigma|I_K)}{p(\mathbf{d}|I_K)} \, d\mathbf{b} \, d\sigma \\ &\propto \int_0^\infty \int_{\Re^{2K}} p(\mathbf{d}|\omega, \sigma, \mathbf{b}, I_K) \frac{1}{\sigma} \, d\mathbf{b} \, d\sigma \\ &\propto \int_0^\infty \int_{\Re^{2K}} (2\pi\sigma^2)^{-N/2} \\ &\qquad \times \exp\left\{ -\frac{\mathbf{d}^\top \mathbf{d} + \mathbf{b}^\top \mathbf{G}^\top \mathbf{G}\, \mathbf{b} - 2\mathbf{b}^\top \mathbf{G}^\top \mathbf{d}}{2\sigma^2} \right\} \frac{1}{\sigma} \, d\mathbf{b} \, d\sigma \end{aligned} \tag{4.14}$$

The analytical solution to the integral is found in [6] or [34]. The procedure is first to integrate out $\mathbf{b}$. This necessitates a diagonalization of $\mathbf{G}^\top \mathbf{G}$ due to the cross terms. The standard deviation of the noise, σ, is then integrated out using a gamma integral. The result is shown in Eq. (4.15).

$$\begin{aligned} p(\omega_F|\mathbf{d}, I_K) &\propto \frac{\left(\mathbf{d}^\top \mathbf{d} - \mathbf{d}^\top \mathbf{G} (\mathbf{G}^\top \mathbf{G})^{-1} \mathbf{G}^\top \mathbf{d}\right)^{\frac{-(N-2K)}{2}}}{\sqrt{\det(\mathbf{G}^\top \mathbf{G})}} \\ &\propto \frac{\left(\mathbf{d}^\top \mathbf{d} - \mathbf{f}^\top \mathbf{f}\right)^{\frac{-(N-2K)}{2}}}{\sqrt{\det(\mathbf{G}^\top \mathbf{G})}} \end{aligned} \tag{4.15}$$

[3] Also referred to as *location* parameters

The marginalized posterior density for ω_F is in the form of a student-t distribution with $N - 2K - 1$ degrees of freedom. When the degrees of freedom is large it is numerically more convenient to compute the logarithm of Eq. (4.15):

$$\log p(\omega_F|\mathbf{d}, I_K) = -\frac{1}{2}\det(\mathbf{G}^\top\mathbf{G}) - \frac{N-2K}{2}\log(\mathbf{d}^\top\mathbf{d} - \mathbf{f}^\top\mathbf{f}) \tag{4.16}$$

4.3 Evaluation

We are now ready to do the frequency estimation in a Bayesian context. The procedure is as follows:

1. Choose a priori the harmonic sequence, $\mathbf{h}$ to use for the estimation
2. Choose a priori the range of frequencies for which the posterior is to be evaluated
3. Form the observation vector $\mathbf{d}$
4. Compute the matrix $\mathbf{G}$ as defined in (4.5)
5. Compute the vector $\mathbf{f}$ as defined by Eq. (4.9) with the aid of Eq. (4.8)
6. Compute $\log p(\omega_F|\mathbf{d}, I_K)$ according to Eq. (4.16)
7. Repeat steps 4-6 for all frequencies defined in step 2 and find the maximum.

After the search for the maximizer for $p(\omega_F|\mathbf{d}, I_K)$ it is possible to improved the estimate by fitting a parabola to the peak of $\log p(\omega_F|\mathbf{d}, I_K)$. The maximum of the parabola is then taken as the maximum *a posteriori* (MAP) estimate for ω_F. This interpolation is motivated by the fact that the student-t distribution is approximately Gaussian when the number of degrees of freedom is large ($>$ 25-30, [20]).

4.3.1 Simulations

The Bayesian frequency estimator is evaluated similarly to the the Adaptive Comb Filter in Section 3.5. The test signal is replicated 100 times with identical amplitudes and phases but different noise realizations.

Three different harmonic sequences are evaluated. The first estimates using a single frequency ($\mathbf{h}_1$), the second estimates using the first 3 harmonics ($\mathbf{h}_3$), and the last estimates using all 5 harmonics in the test signal ($\mathbf{h}_5$).

$$\mathbf{h}_1 = [1]$$
$$\mathbf{h}_3 = [1 \quad 2 \quad 3]$$
$$\mathbf{h}_5 = [1 \quad 2 \quad 3 \quad 4 \quad 5]$$

The marginal PDF, $p(\omega_F|\mathbf{d}, I_K)$ is computed in segments of 1/4 second of the test signal overlapping 75%. This is identical to all the block based frequency estimators in Sec. 3.5.

The actual estimate of the fundamental frequency is obtained as maximizer of the marginal PDF

$$\max_{\omega_F=2\pi f} p(\omega_F|\mathbf{d}, I_K), \quad f \in \{8.0, 8.5, \ldots, 128.0\}$$

The result of the simulation is shown in Fig. 4.1 for a SNR level of 15 dB. The left graphs (a,c,e) show the distribution of the frequency estimates, and the right graphs (b,d,f) show the associated RMS errors.

The result in Fig. 4.1(a) is for the single frequency model ($\mathbf{h}_1$). It shows that the strongest harmonic is estimated (see e.g. Fig. 3.9(a)). It starts with the 4th harmonic, then as the frequency increases it jumps to the 3rd, 2nd and 1st. The low standard deviation of the estimates (Fig. 4.1(b)) indicates that the estimate is consistent. Comparing with the Interpolated FFT estimates (Fig. 3.11(d)) very similar RMS errors are observed when the first order is dominant.

Figure 4.1(c) shows the results for the model with 3 harmonics ($\mathbf{h}_3$). In the beginning and end of the signal where the first harmonic is significantly lower than the 4th harmonic (Fig. 3.9(a)) it estimates the second harmonic instead of the first. The explanation is that the harmonic sequence {2, 4, 6} carries more energy than {1, 2, 3}. The error curves in Fig. 4.1(d) show that the estimates are close to the optimal. Periodic fluctuations in both standard deviation and the RMS error are observed. This phenomena has not been studied closer.

Figures 4.1(e) and 4.1(f) show the results for the correct model with 5 harmonics ($\mathbf{h}_5$). The correct fundamental frequency is estimated for the entire length of the signal and with the lowest error of all methods. The periodic fluctuation in standard deviation and RPM error are observed as in the previous example. The fluctuation are almost identical and on the same scale. It is speculated that the phenomena may be caused by the non-stationarity of the signal, but it needs to be investigated further.

Further simulation results can be found in appendix C where the results are shown for simulations with SNR=30dB (Fig. C.8) and SNR=0dB (Fig. C.9).

From the simulations it is concluded the Bayesian frequency estimator is superior to the previous investigated methods.

4.4 Modeling Non-stationary Frequencies

To this point only stationary frequencies have been considered as basis vectors of $\mathbf{G}$. That is Eqs.(4.5,4.6):

$$\mathbf{G} = [\mathbf{u} \quad \mathrm{gc}_1(\mathbf{t}) \quad \ldots \quad \mathrm{gc}_K(\mathbf{t}) \quad \mathrm{gs}_1(\mathbf{t}) \quad \ldots \quad \mathrm{gs}_K(\mathbf{t})] \tag{4.17}$$

where the functions for computing the basis vectors are defined by

$$\mathrm{gc}_k(t) \equiv \cos(\eta_k \Omega_F(t)), \qquad \mathrm{gs}_k(t) \equiv \sin(\eta_k \Omega_F(t)) \tag{4.18}$$

$$\Omega_F(t) = \int_0^t \omega_F(\tau)\, d\tau \tag{4.19}$$

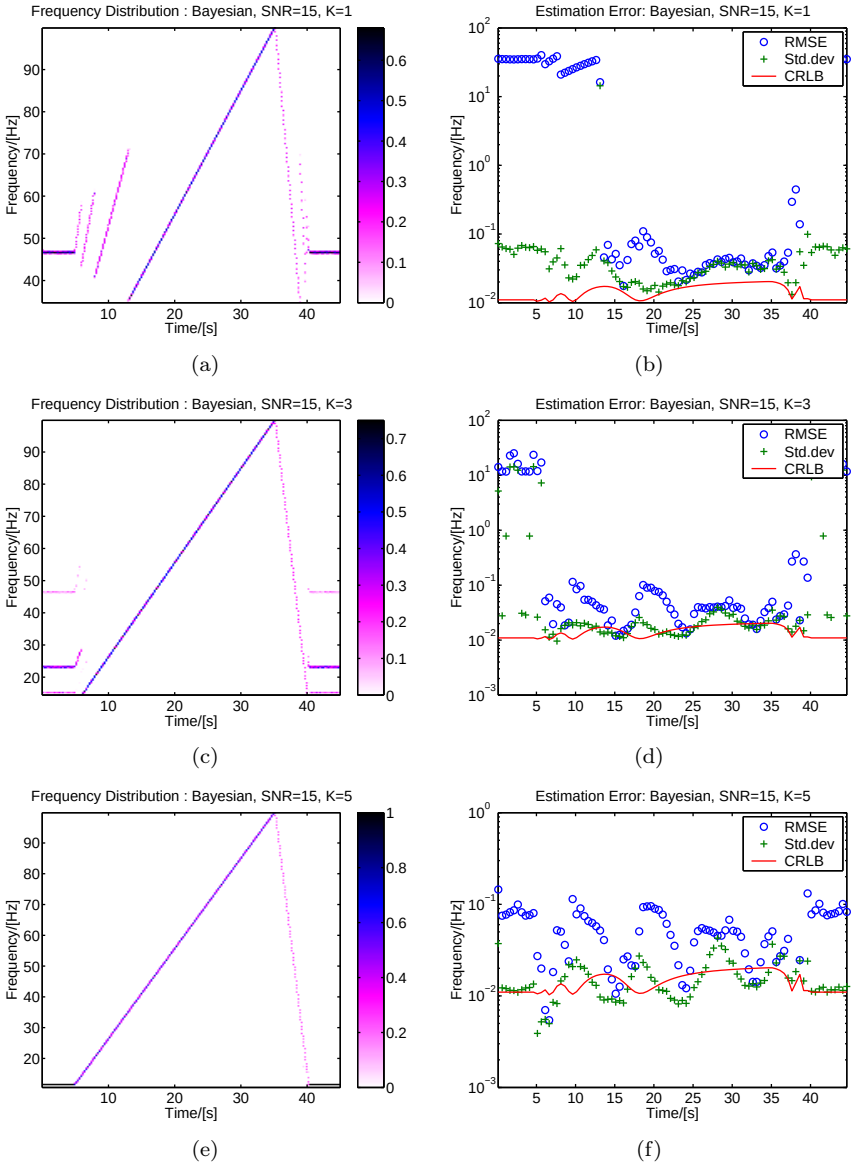

Figure 4.1: Simulation Results for Bayesian estimation, SNR=15dB. These figures show the performance of the Bayesian frequency estimator when assuming the signal has (a) one harmonic, (b) two harmonics, and (c) three harmonics. Compared to the results from the other frequency estimators shown in figures 3.10 and 3.11, the Bayesian frequency estimator is superior.

When the frequency is stationary, then $\omega_F(t)$ is constant and $\Omega_F(t) = \omega_F t$. It follows from Eq. (4.19) that when estimating a non-stationary frequency, the non-stationarity should be reflected in $\Omega_F(t)$. If we suppose that $\omega_F(t)$ is linearly increasing and the rate of change is to be estimated, then

$$\omega_F(t) = \omega_{F,0} + \alpha t \quad \Rightarrow \quad \Omega_F(t) = \omega_{F,0} t + \frac{1}{2}\alpha t^2 \tag{4.20}$$

θ is thus increased with the additional parameter α equivalent to the acceleration of fundamental frequency's phase angle. The new parameter affects only how the basis vectors in $\mathbf{G}$ are computed, the overall procedure therefore remains unchanged.

The effect of including the frequency change in the estimation is illustrated by an example. A signal with a single sine wave is constructed where the frequency increases linearly from 50 Hz to 150 Hz over a period of one second. The signal is defined by Eq. (4.21). The sine wave has unit RMS amplitude.

$$\begin{aligned} x(t) &= A\cos(\Omega_F(t)) + e(t), \quad \Omega_F(t) = \int_0^t 2\pi f(\tau)\, d\tau \\ A &= \sqrt{2}, \quad f(t) = 50 + 100t, \quad 0 \le t < 1 \end{aligned} \tag{4.21}$$

The signal is sampled at 1024 samples per second. A total of 100 simulations are carried out for each of the record lengths 32, 128, and 256 samples ($\sim 1/32$ s, $1/8$ s, and $1/4$ s), and at SNR levels of 0 dB and 25 dB. The marginalized posterior PDF for $\omega_{F,0}, \alpha$ is evaluated at each of the parameters in the range

$$\begin{aligned} \omega_{F,0}/2\pi &= \{10, 10.5, \ldots, 200\} \\ \alpha/2\pi &= \{0, 10, \ldots, 170\} \end{aligned}$$

The MAP estimate of $(\omega_{F,0}, \alpha)$, is located and used to compute the ML estimate of the amplitude. Table 4.2 contains the mean square errors of the frequency estimate, $\omega_{F,0}$, and the amplitude estimate, A. The frequency errors are given in Hz. The rows labeled $\alpha = 0$ are the estimate errors when the frequency change is not modeled.

SNR Level		Frequency MSE			Amplitude MSE		
		N=32	N=128	N=256	N=32	N=128	N=256
0 dB	$\alpha \neq 0$	5.9	0.42	0.14	0.034	0.0086	0.003
	$\alpha = 0$	5.9	0.48	4.3	0.034	0.011	0.2
25 dB	$\alpha \neq 0$	0.011	0.011	0.01	4.8e-008	3.1e-008	1e-007
	$\alpha = 0$	0.0096	0.085	4	3.4e-007	0.0043	0.24

Table 4.2: Estimation Errors

The table shows that at low SNR and when α is estimated, the long record length N=256, gives the best estimates of both frequency and amplitude. It is noted that for N=32 hardly anything is gained in accuracy by estimating α, for N=128 and SNR=0 the gain is limited. For N=256 and SNR=0 significant improvements are

observed. Regarding amplitude estimation the table indicates that longer record lengths give more accurate estimates, provided the frequency profile matches the observed signal. If α is not estimated the table reveals that the long record length gives the worst amplitude estimate! The effect of estimating a time-varying frequency with a constant ML frequency model is studied in [21].

The simple linear frequency model used in this example (Eq. (4.20)) may not be sufficient when accurate amplitude estimates are required e.g. under very low SNR conditions. In principle, the linear frequency model can be generalized to polynomials of any desired degree. This, however, may not be computationally feasible due to the increase in dimension of the joint posterior PDF. In section 6.2 is given an example that deals with this problem by using two record lengths. First, the frequency profile is estimated using short records. Second, the amplitudes are estimated using longer records.

4.5 Multiple Frequencies

If a signal contains frequencies that are close it is difficult to identify the individual frequencies. For the Fourier transform the resolution is given by the BT product and is proportional to the inverse of the record length. Thus, for a record length of $T = 250$ ms the resolution is $\Delta F = 4$ Hz, and it is independent of the sample rate. In addition the leakage effect mentioned in Sec. 3.3 is unavoidable and decreases the resolution further, e.g for the Hanning window two frequencies needs to be $2 \times \Delta F$ apart.

With the flexibility of the Bayesian framework, it is relatively easy to expand the frequency estimation model to include multiple and independent frequencies. In the following it will be shown that with the Bayesian approach it is possible to identify frequencies closer than $\Delta F = 1/T$ when a model assuming the presence of two sinusoids is used.

Example

The signal to be analyzed is defined by

$$\begin{aligned} d(t) &= \cos(2\pi f_1 t + \phi_1) + \cos(2\pi f_2 t + \phi_2) + e(t) \\ \omega_i &= 2\pi f_i, \quad f_1 = 95.5\,\text{Hz}, \quad f_2 = 98.5\,\text{Hz} \\ t &= n\Delta T, \quad \Delta T = 1/F_s, \quad F_s = 1024\,\text{Hz}, \quad 0 \le n < 256 \\ e(t) &\sim \mathcal{N}(0, 0.2), \quad \phi_1, \phi_2 \sim \mathcal{U}(0, 2\pi) \end{aligned}$$

Figure 4.2 shows two realizations of the signal. The signal is equivalent to the product of two sine wave with the frequencies $f_a = (f_1 + f_2)/2$ and $f_b = (f_1 - f_2)/2$. The segment is 1/4 second long and contains only 3/8th period of f_b. From the segment alone it is difficult to identify the beating caused by the two sinusoids.

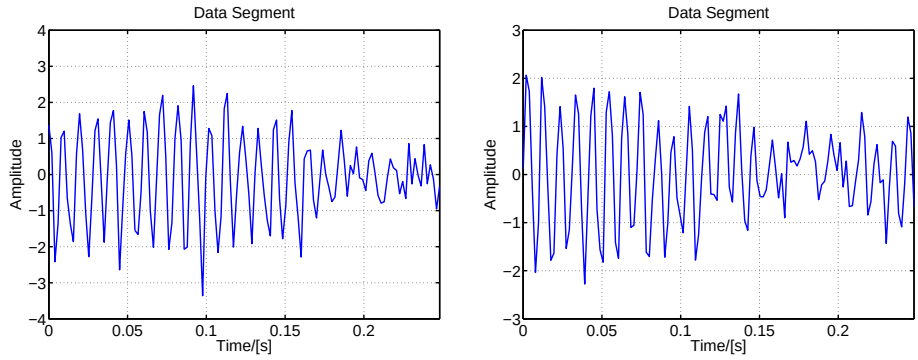

(a) (b)

Figure 4.2: Two tone signal. This graph shows two realizations of a signal with two sinusoids with unit amplitude and frequencies of 95.5 Hz and 98.5 Hz respectively. The signal is sampled at 512 samples per second and the noise variance is $\sigma^2 = 0.2$ resulting in a SNR of 7dB

One Frequency

We now try applying a single tone Bayesian model to estimate the signal and compute the ML estimate of the amplitude. The posterior distribution of $p(\omega|d)$ is computed according to Eq. (4.8) and Eq. (4.15). To reduce the amount of computations the posterior distribution is only computed in the region, $92\,\text{Hz} \leq f \leq 104\,\text{Hz}$ in increments of 0.01 Hz. In this region the Fourier transform gives four estimates of the magnitude which are also computed. The results for the two realizations are plotted in Fig. 4.3. In the first realization (Fig. 4.3(a)) the posterior, $p(\omega|d)$, is unimodal[4] and there is no indication of two sinusoids being present. The maximum *a posteriori* (MAP) estimate of ω is located between the true frequencies, giving an error of approximately 1 Hz. For the second realization (Fig. 4.3(b)) the posterior is bimodal , indicating the presence of two sinusoids. The two local MAP estimates are offset 0.5 Hz from the true frequencies.

Two Frequencies

The next step is to estimate the posterior distribution for the model containing two independent frequencies. The two-frequency linear model is

$$\begin{aligned} \mathbf{d} &= \mathbf{G}(\omega_1, \omega_2)\,\mathbf{b} + \mathbf{e} \\ \mathbf{G}(\omega_1, \omega_2) &= [\cos(\omega_1 \mathbf{t}) \quad \sin(\omega_1 \mathbf{t}) \quad \cos(\omega_2 \mathbf{t}) \quad \sin(\omega_2 \mathbf{t})] \\ \mathbf{b} &= [A_1 \quad B_1 \quad A_2 \quad B_2]^\top \\ \mathbf{t} &= [0 \quad \Delta T \quad \ldots \quad (N-1)\Delta T]^\top \end{aligned}$$

[4]The PDF only has one local maxima

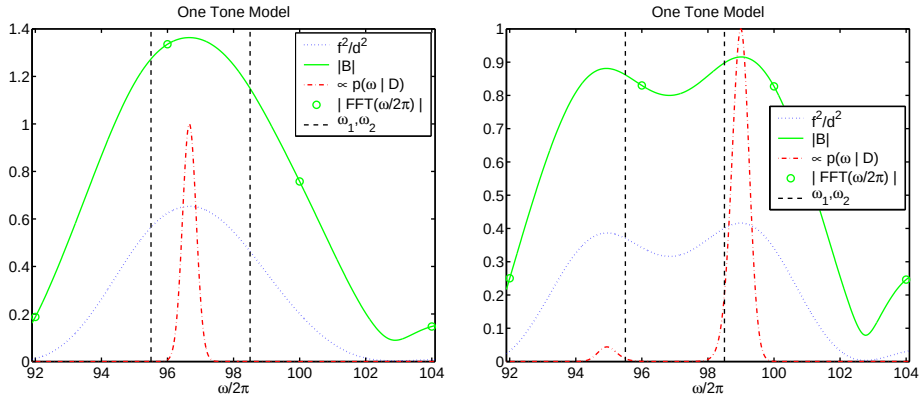

(a) (b)

Figure 4.3: Estimating Two Tone Parameter with Single Frequency Model. The vertical dashed lines indicate the position of the true frequencies in the signal. The solid line is the ML estimate of the amplitude, and the circles are Fourier estimates of the magnitude. The dotted line indicates the relative energy modeled. The posterior distribution of ω is shown with the dash-dot line. (a) corresponds to the realization shown in Fig. 4.2(a) and results in a unimodal density for $p(\omega|D)$. (b) corresponds to the realization shown in Fig. 4.2(b) and results in a bimodal density.

The joint-posterior distribution of ω_1 and ω_2 is computed by substituting $\mathbf{G}$ in Eq. (4.15) for $\mathbf{G}(\omega_1, \omega_2)$.

To reduce the amount of computations the posterior distribution is only computed in the region, $93\,\text{Hz} \leq f \leq 101\,\text{Hz}$ in increments of $0.1\,\text{Hz}$ (See Fig. 4.4). For both realizations the joint posterior have two distinct maxima at the true frequencies.

Discussion

The example has illustrated that two sinusoids with a difference $< \Delta F$, can be resolved, when the estimation method takes into account the presence of two sinusoids, and $\Delta F = 1/T$ where T is the observation time of the signal. The conditions for separating close frequencies with maximum likelihood estimation is investigated in [43, Sec.3.5].

It is seen from Fig. 4.3 that the magnitude estimates provided by the Fourier transform are identical to magnitude estimates of the Bayesian single frequency estimator. The Fourier transform only provides accurate estimates for single frequency signals - or when the sinusoids are well separated. Using an incorrect model for the estimation resulted in biased estimates.

In the context of estimating the running speed of rotating machines, it should be investigated to what extent the bias caused by an incorrect estimation model contribute to estimation error.

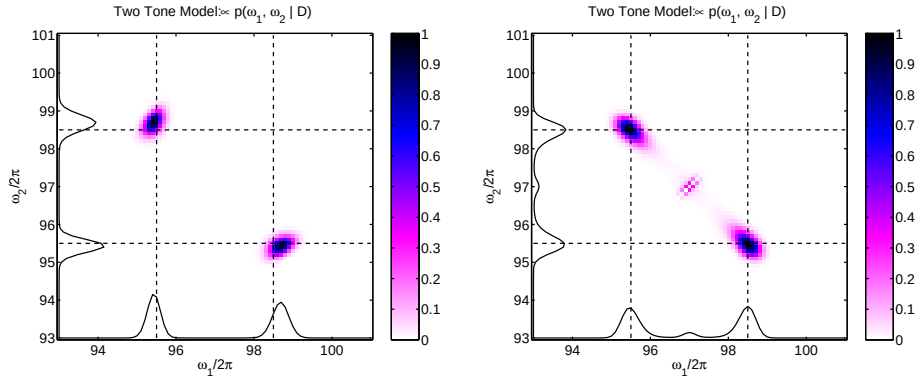

(a) (b)

Figure 4.4: Posterior Distribution for Two Independent Frequencies. For both realizations the joint posterior distribution for $p(\omega_1, \omega_2|\mathbf{d})$ show a clear peak at the true local maxima. The vertical and horizontal curves are $p(\omega_2|\mathbf{d})$ and $p(\omega_1|\mathbf{d})$ respectively. (a) corresponds to the realization shown in Fig. 4.2(a). (b) corresponds to the realization shown in Fig. 4.2(b)

For this simple example, the joint posterior was computed in a brute-force manner and only a limited part of the frequency range was explored. For real vibro-acoustic signals with many frequency components efficient methods are required. Estimation of joint posterior distribution for non-linear and multivariate problems is a topic of great attention and research. Unfortunately, there has not been time to look into that field in this study.

4.6 Multichannel Data

It is here shown that the Bayesian frequency estimator can be extended to use information in multiple data channels when estimating the fundamental frequency. It is a brief summary of the work presented in [38].

In a multichannel measurement the fundamental frequency and its higher order components are expected to be present in all channels, but with varying phases and amplitudes. With the noise in each channel also being uncorrelated, the multichannel estimation problem of Eq. (4.6) becomes the linear problem:

$$\mathbf{D} = \mathbf{G}\,\mathbf{B} + \mathbf{E} \tag{4.22}$$

The columns of the matrix $\mathbf{D}$ are the measured data channels, $\mathbf{G}$ is the matrix with basis vectors as columns (Eq. (4.5)), the columns of $\mathbf{B}$ are the amplitude parameters for each data channel, and the columns of matrix $\mathbf{E}$ are the noise contribution for

the channels:

$$\begin{aligned}
\mathbf{D}_{\mathrm{N\times M}} &= [\mathbf{d}_1 \quad \dots \quad \mathbf{d}_M] \\
\mathbf{B}_{\mathrm{2K+1\times M}} &= [\mathbf{b}_1 \quad \dots \quad \mathbf{b}_M] \\
\mathbf{E}_{\mathrm{N\times M}} &= [\mathbf{e}_1 \quad \dots \quad \mathbf{e}_M] \\
\mathbf{d}_m &= [d_m(t_0) \quad \dots \quad d_m(t_{N-1})]^\top \\
\mathbf{b}_m &= [A_{m,0} \quad \dots \quad A_{m,K} \quad B_{m,1} \quad \dots \quad B_{m,K}]^\top \\
\mathbf{e}_m &= [e_m(t_0) \quad \dots \quad e_m(t_{N-1})]^\top, \quad e_m(t) \sim \mathcal{N}(0, \sigma_m^2)
\end{aligned}$$

Using Bayes rule the posterior distribution of ω_F conditioned on the measurement channels is given by

$$p(\omega_F|\mathbf{d}_1, \dots, \mathbf{d}_M) = \frac{p(\mathbf{d}_1, \dots, \mathbf{d}_M|\omega_F)\, p(\omega_F)}{p(\mathbf{d}_1, \dots, \mathbf{d}_M)} \tag{4.23}$$

To find the distribution of the data conditioned only on ω_F, the nuisance parameters, $\{\sigma_m, \mathbf{b}_m : 1 \leq m \leq M\}$, are eliminated by integration from the likelihood in Eq. (4.24). Since the nuisance parameters conditioned on ω_F are independent the integration in Eq. (4.24) can be separated into the product of the M integrals in Eq. (4.25), each involving only the parameters of the individual channels.

$$\begin{aligned}
&p(\mathbf{d}_1, \dots, \mathbf{d}_M|\omega_F) \\
&= \int p(\mathbf{d}_1, \dots, \mathbf{d}_M|\{\sigma_m, \mathbf{b}_m : 1 \leq m \leq M\}, \omega_F) \\
&\qquad \times p(\{\sigma_m, \mathbf{b}_m : 1 \leq m \leq M\}|\omega_F) d\{\sigma_m, \mathbf{b}_m : 1 \leq m \leq M\} \qquad (4.24) \\
&= \prod_{m=1}^{M} \int p(\mathbf{d}_m|\{\sigma_m, \mathbf{b}_m\}, \omega_F) p(\{\sigma_m, \mathbf{b}_m\}|\omega_F)\, d\{\sigma_m, \mathbf{b}_m\} \qquad (4.25) \\
&= \prod_{m=1}^{M} p(\mathbf{d}_m|\omega_F) \qquad (4.26)
\end{aligned}$$

In [38] we apply the multichannel estimation scheme to the three responses of the simulated mechanical system from Sec. 2.4 and to a three channel vibration measurement from the interior of a passenger car. In both cases significant improvements are observed when the sources are combined.

4.7 Summary

This chapter has introduced the Bayesian statistical framework in the context of fundamental frequency estimation. Within the framework a new block-based frequency estimator was designed. The estimator distinguishes itself from other block based estimators by incorporating prior knowledge in the form of a harmonic sequence characterizing the periodic signal. Via simulations it was shown that the estimator was superior to any of the estimators covered in Chapter 3.

Examples were also given on how to expand the model to deal with other problems related to frequency estimation, e.g. non-stationary frequencies and identification and separation of close frequencies.

4.7.1 Relation to Recent work on Bayesian Estimation

The approach in this work to estimate the fundamental frequency is similar to that used by Walmsley [64] and Godsill [16] to estimate the pitch of musical instruments. The methods differ in the choice of priors, but all three use constant frequency sines and cosines as basis functions.

References [1] and [9] both concern the multiple frequency estimation problem addressed in Section 4.5. In [8] the parameters of generalized frequency modulated signals are estimated in a Bayesian context.

Chapter 5

Tracking

When analyzing non-stationary signals from rotating mechanical systems, it is necessary to both estimate and track the fundamental frequency.

In the previous chapter a Bayesian based frequency estimator was designed. It utilizes the harmonic structure embedded in the measured signals to enhance the frequency estimates. Theoretically, if a model of the frequency change, for the entire length of the observed signal, can be devised, then the estimator could estimate the parameters of the model. Practically, however, the length of the observed signal and the number of parameters needed will not make this approach computationally tractable.

In this chapter the tracking problem is addressed within the Bayesian framework. Section. 5.1 formulates the tracking problem in probabilistic terms and defines the *optimal track*. In Sec. 5.2 a simple tracker is devised through a conditioned prior on the fundamental frequency. In Sec. 5.3 The Viterbi algorithm [45] is used to find the optimal track assuming the track is the result of a 1st-order Markov process. Tracking examples using vibro-acoustic signals are given in Sec. 5.4.

5.1 Tracking in Probabilistic Terms

Tracking a periodic signal which changes rapidly is difficult, especially under low SNR conditions. However, if the change is slow and a simple model can be fitted to short segments of the signal, then the fundamental frequency can be tracked by observing the changes in the model parameters from one segment to another.

In this chapter the Bayesian frequency estimator from the previous chapter is used to estimate the fundamental frequency. Thus, for each segment, k, of the signal a

posterior distribution of the fundamental frequency is computed, $p(\omega_F^{(k)}|\mathbf{d}^{(k)})$, where $^{(k)}$ denotes the values related to the kth record. The data record is defined by

$$\mathbf{d}^{(k)} = [d(t_{k\Delta N}) \quad d(t_{k\Delta N+1}) \quad \dots \quad d(t_{k\Delta N+M-1})]^\top \tag{5.1}$$

where M is the number of samples in each record. The records are offset by ΔN samples from each other, thus allowing records to overlap if $\Delta N < M$.

The tracking problem can now be formulated in probabilistic terms as finding the maximum a posteriori (MAP) estimate of the joint posterior distribution of the fundamental frequencies from all records, $\Theta_L \equiv \{\omega_F^{(i)} : 0 \leq i < L\}$, conditioned on the observations, $\mathcal{D}_L \equiv \{\mathbf{d}^{(i)} : 0 \leq i < L\}$. The value of Θ_L corresponding to the MAP estimate of $p(\Theta_L|\mathcal{D}_L)$ is the *optimal track*.

Without any prior knowledge regarding $\omega_F^{(i)}$ the joint posterior is simply

$$p(\Theta_L|\mathcal{D}_L) = \prod_{i=0}^{L-1} p(\omega_F^{(i)}|\mathbf{d}^{(i)}) \tag{5.2}$$

and the MAP is the set of $\omega_F^{(i)}$ which maximizes the posterior of the individual records, $p(\omega_F^{(i)}|\mathbf{d}^{(i)})$:

$$\{\arg\max_{\omega_F^{(i)}} p(\omega_F^{(i)}|\mathbf{d}^{(i)}) : 0 \leq i < L\} \tag{5.3}$$

However, it is assumed that the frequency changes slowly. This information can be expressed as a conditioned prior distribution for $\omega_F^{(k)}$, e.g.,

$$p(\omega_F^{(k)}|\omega_F^{(k-1)}, \dots, \omega_F^{(k-P)}) \tag{5.4}$$

when $\omega_F^{(k)}$ depends on the previous P records. If ω_F obeys Eq. (5.4) it is said to be a Pth-order Markov chain process [15, 34]. Using Eq. (5.4) the joint posterior becomes[1]:

$$\begin{aligned} p(\Theta_L|\mathcal{D}_L) &= p(\omega_F^{(L-1)}|\Theta_{L-1}, \mathcal{D}_L)\, p(\Theta_{L-1}|\mathcal{D}_L) \\ &\propto p(\mathbf{d}^{(L-1)}|\omega_F^{(L-1)})\, p(\omega_F^{(L-1)}|\Theta_{L-1})\, p(\Theta_{L-1}|\mathcal{D}_{L-1}) \\ &\propto p(\mathbf{d}^{(0)}|\omega_F^{(0)})\, p(\omega_F^{(0)}) \prod_{i=1}^{P-1} p(\mathbf{d}^{(i)}|\omega_F^{(i)})\, p(\omega_F^{(i)}|\Theta_i) \\ &\quad \times \prod_{i=P}^{L-1} p(\mathbf{d}^{(i)}|\omega_F^{(i)}) p(\omega_F^{(i)}|\omega_F^{(i-1)}, \dots, \omega_F^{(i-P)}) \end{aligned} \tag{5.5}$$

The recursive nature of the equation is exploited in the next section to design a simple tracker.

[1] Follows from $p(A, B|C) = p(A|C)p(B|C)$

5.2 Tracking with Priors

The previous section showed that the tracking capabilities is linked to the PDF of the fundamental frequency estimate conditioned on the previous history of the fundamental frequency. Prior knowledge of how the fundamental frequency changes over time should therefore be used when the PDF is selected. With respect to the run-up/down example described in Section 2.2, the maximum relative change of the fundamental frequency is less than 3% from one record to the next for 250 ms long records with 75% overlap.

If we assume the frequency change is linear over the previous P records, i.e.,

$$\omega_F^{(n-k)} = \alpha\, k + \omega_F^{(n)} + \eta(n-k), \quad \eta \sim \mathcal{N}(0, \sigma_T^2), \quad 1 \le k \le P \tag{5.6}$$

then linear regression can be used to predict the location of the next observation. This is illustrated by Figure 5.1 for $P = 4$.

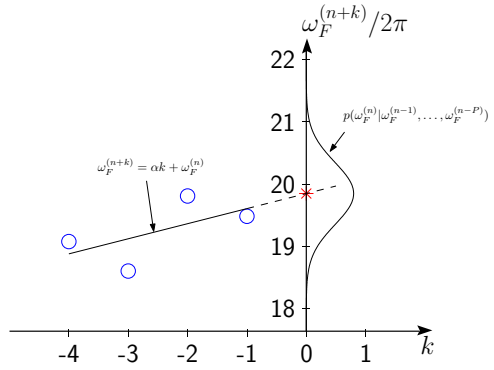

Figure 5.1: Tracking Prior from Linear Regression. The figure shows how the prior PDF of the current frequency estimate, $p(\omega_F^{(n)}|\omega_F^{(n-1)}, \ldots, \omega_F^{(n-P)})$, is determined by linear regression of the past $P = 4$ values. In the example $\sigma_T^2 = 1/4\text{Hz}^2$. The predicted value for $\omega_F^{(n)}$ is marked by the asterix (*) and the past observations by circles (o).

It is shown in Appendix A.2 that the prior PDF of $\omega_F^{(n)}$ according to Eq. (5.6) is computed by

$$\begin{aligned} &p(\omega_F^{(n)}|\omega_F^{(n-1)}, \ldots, \omega_F^{(n-P)}) = \mathcal{N}(\mu_T, \sigma_T^2), \\ &\mu_T \equiv \begin{cases} \frac{\sum_{k=1}^{P}(2(2P+1)-6k)\omega_F^{(n-k)}}{P(P-1)} & , \text{ for } P > 1 \\ \omega_F^{(n-1)} & , \text{ for } P = 1 \end{cases} \end{aligned} \tag{5.7}$$

Combining Eq. (5.7) with Eq. (5.5) a novel prior-based tracking algorithm can be devised. Using $\tilde{\omega}_F^{(k)}$ to denote the tracked frequency in record k the algorithm is

1. Initialize $p(\omega_F^{(0)})$, σ_T^2, and compute

$$\tilde{\omega}_F^{(0)} = \arg\max_{\omega_F^{(0)}} p(\mathbf{d}^{(0)}|\omega_F^{(0)})p(\omega_F^{(0)})$$

2. For $1 \leq k < P$:

$$\tilde{\omega}_F^{(k)} = \arg\max_{\omega_F^{(k)}} p(\mathbf{d}^{(k)}|\omega_F^{(k)})p(\omega_F^{(k)}|\tilde{\omega}_F^{(k-1)}, \ldots, \tilde{\omega}_F^{(0)})$$

3. For $P \leq k < L$:

$$\tilde{\omega}_F^{(k)} = \arg\max_{\omega_F^{(k)}} p(\mathbf{d}^{(k)}|\omega_F^{(k)})p(\omega_F^{(k)}|\tilde{\omega}_F^{(k-1)}, \ldots, \tilde{\omega}_F^{(k-P)})$$

In practice the algorithm has proven to be quite robust and its simplicity makes it suitable for real-time implementation. The algorithm is tested on experimental data in Section 5.4.

5.3 Tracking In Retrospect

The simple tracker is not guaranteed to give the optimal track for a given set of observations. This is illustrated with the example shown in Figure 5.2. For simplicity we assume $\omega_F^{(k)}$ is discrete, i.e., $\omega_F^{(k)} \in \{1, 2, 3, 4\}$, and there are 5 observations. The observation are shown in Fig 5.2(a), where the kth column of the table is the discrete PDF of the kth observation.

Choosing a uniform prior PDF for $\omega_F^{(k)}$ then the estimated track is simply the maxima of the individual observations as shown in Fig. 5.2(b). The encircled numbers along the track are the values of the joint PDF for $\Theta_k \equiv \{\omega_F^{(0)}, \ldots, \omega_F^{(k)}\}$. The value at the end of the track indicates how well the track matches the observed data.

The simple tracker is evaluated with the 1st-order Markov chain prior shown in Fig. 5.2(c). The track is shown in Fig. 5.2(d). Clearly, it is not the optimal track since the joint PDF ends at a lower value than in Fig. 5.2(b). The reason is, that the observation at $k = 2$ diverts the algorithm from the optimal track. Once diverted, the narrow shape of the prior prevents it from returning to the optimal track. Were the optimal track in Fig. 5.2(e) to be obtained, then at $k = 2$ the tracker should have selected $\omega_F^{(2)} = 3$ instead of $\omega_F^{(2)} = 1$. However, this choice is only obvious in retrospect.

5.3.1 The Viterbi Algorithm

To find the best single path through the sequence of observations in retrospect, the Viterbi algorithm [45] can be used. Also referred to as Viterbi Decoding, the algorithm was originally developed for use in communication systems, but it has also proved useful for frequency tracking under conditions of low SNR [4, 43, 59].

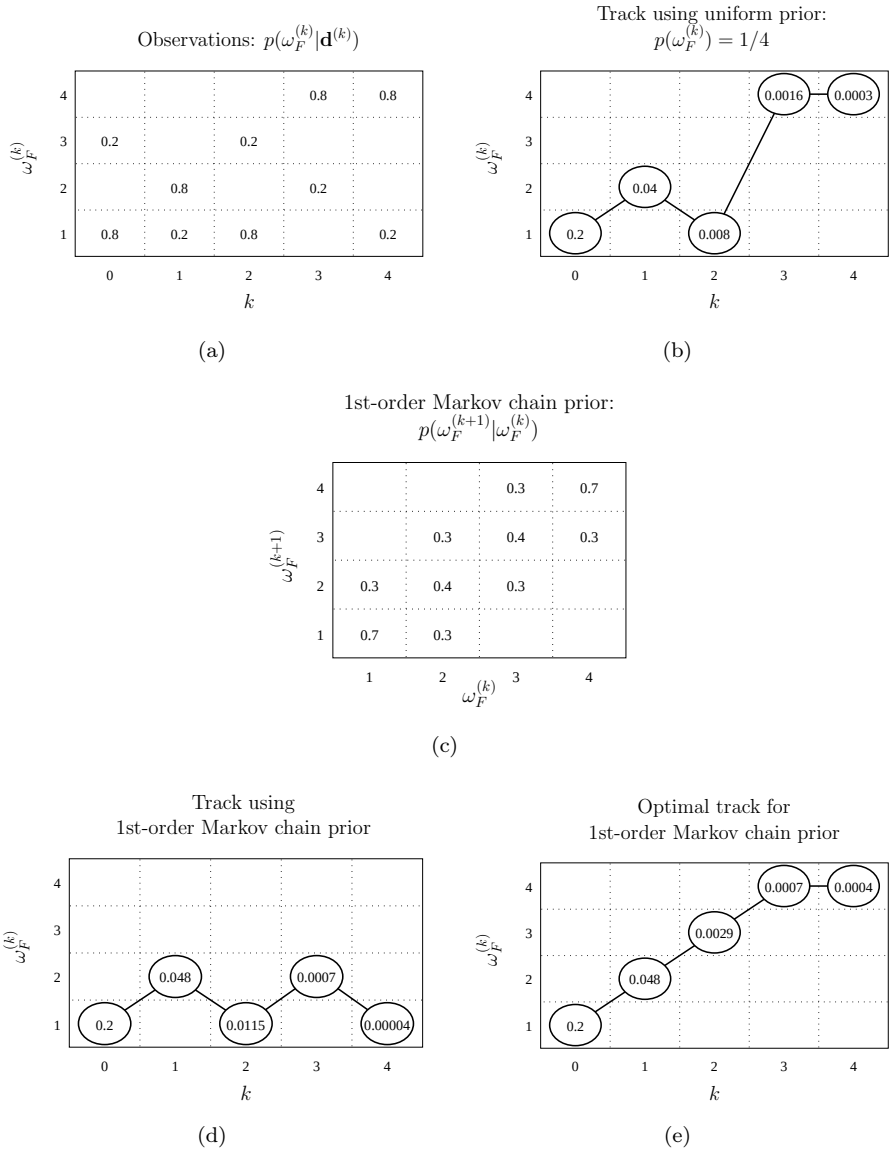

Figure 5.2: Tracking example with discrete frequencies. (a) the observations for each record. In (b) the resulting track when assigning a uniform prior PDF to the tracked frequencies. (c) shows a 1st-order Markov chain prior. (d) the obtained track using the simple algorithm (Sec. 5.2). In (e) the optimal track. All tracks are initialized identically with $p(\omega_F^{(0)}) = 1/4$. The encircled numbers along the tracks are $p(\Theta_k|\mathcal{D}_k)$ from Eq. (5.5).

The Viterbi algorithm is best explained by the *Bugs on a Grid* analogy [15]: First, a bug is placed on each of the possible frequencies of the first observation. Each bug then reproduces itself onto the frequencies of the next observation and modifies its probability accordingly (Eq. (5.5)). This continues until the final observation is reached. When there are more than one bug at a given frequency (e.g. $\omega_F^{(3)} = 2$ in Fig. 5.2(a)) then only the bug with the highest probability is allowed to reproduce. When the bugs reach the final observation, the optimal path is be found by tracing the ancestors of the bug carrying the highest probability. The tracks shown in Figures 5.2(d) and 5.2(e) can be perceived as the different paths travel by two bugs descending from the bug born in $\omega_F^{(0)} = 1$.

In this study a Viterbi tracker has been implemented. It uses the Viterbi algorithm to find the optimal track through the observations, assuming the 1st-order Markov chain prior is normally distributed Gaussian with a specified tracking variance, σ_T^2.

5.4 Experiments

The simple tracking algorithm from Section 5.2 and the Viterbi algorithm are implemented as a small Matlab™ application. The users interface is shown in Figure 5.3. To estimate the fundamental frequency, the first step is to specify the signal, the size of the records and the amount of overlap (upper left panel). The second step is to specify the parameters for the Bayesian frequency estimator, i.e., the frequency range, the resolution and the orders of the fundamental frequency (upper middle panel) of the posterior PDF estimated for each record. Figure 5.4 shows posterior PDF's for the acoustic signal described in Section 2.2. The third and last step is to set the tracking parameters. For the Viterbi tracker this amounts to selecting the variance for the normally distributed Gaussian used as prior (in Hz^2). The same variance is used by the simple tracker. In addition the linear regression length (Eq. (5.7)) and an optional starting point can be specified for the simple tracker.

The tracking results for the accelerometer signal are summarized in Figure 5.5 and Table 5.2, and in Figure 5.6 and Table 5.3 for the acoustic signal.

The parameters used for the simulations were found by systematically searching a subset of the parameter space and then selecting the combination of parameters with the lowest standard deviation of the tracking errors. For both signals the largest errors are observed during the swift deceleration. Therefore it is expected that a significant part of the standard deviation is caused by the run-down.

The subset of the parameter searched was selected primarily by inspection of the spectrograms of the signals: The Accelerometer signal (see e.g. Fig 2.3(c)) has a strong 2nd harmonic, whereas the Acoustic signal (Fig 2.3(d)) appears to have a lower SNR and dominating 2nd, 2.5th and 2.6th orders. The searched parameter subspace is listed in Table 5.1.

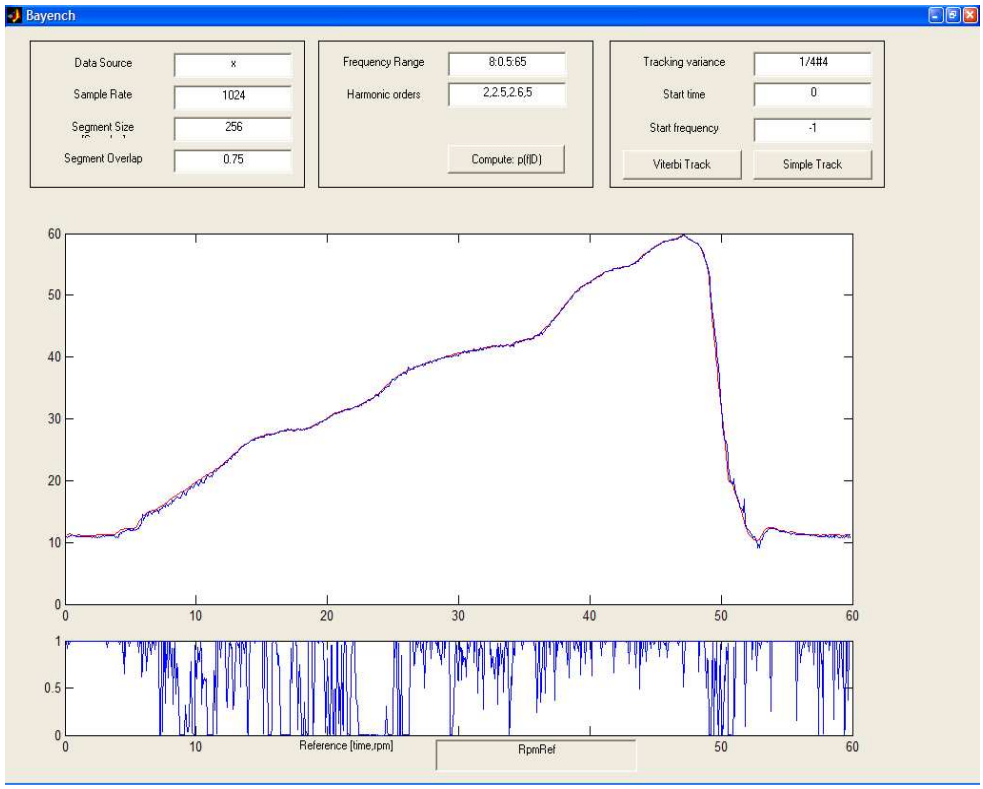

Figure 5.3: Users interface to test program. In the top panel the Bayesian frequency estimator is configured and the tracking parameters set. The frequency range is specified in Matlab™ notation, i.e., it starts at 8 Hz and increases in steps of 0.5 Hz until it ends at 65 Hz. For the simple tracker the regression length, P is specified after the $\#$ symbol following the tracking variance. A negative start frequency indicates the tracking should start at the most likely frequency in the first observation. The large graph shows the tracked frequency with a virtually overlapping reference curve. The plot in the bottom panel shows the probability of the tracked frequency in the observations, $p(\tilde{\omega}_F^{(k)}|\mathbf{d}^{(k)})$.

Tracking variance [Hz^2]	σ_T^2	$\in$	$\{4, 2, 1, 1/2, 1/4, 1/8, 1/16\}$
Regression length	P	$\in$	$\{1, 2, 3, 4, 5, 8, 16\}$ (not for Viterbi)
Record length [s]	ΔT	$\in$	$\{1/2, 1/4, 1/8\}$
Acceleration orders	H	$\in$	$\{[2], [1, 2], [1, 2, 5]\}$
Acoustic orders	H	$\in$	$\{[2, 2.5], [2, 2.5, 5], [2, 2.5, 2.6, 5]\}$

Table 5.1: Parameter subspace

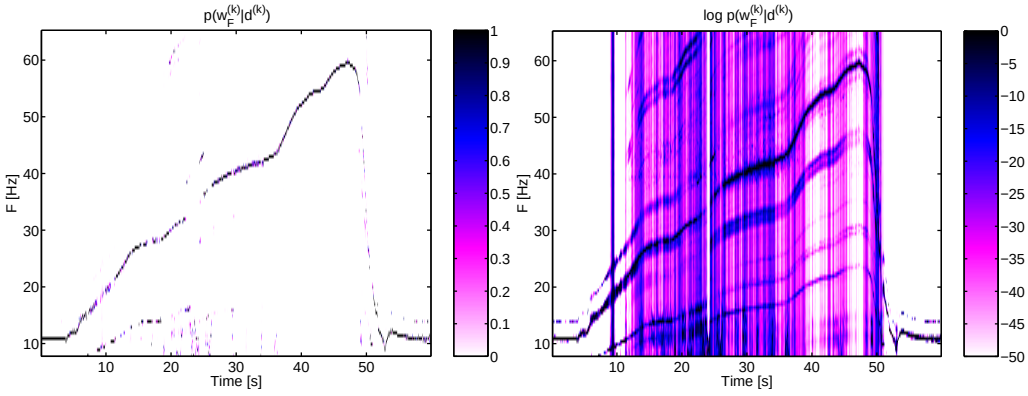

Figure 5.4: Bayesian Frequency Estimates of the Acoustic Signal. These figures show the posterior PDF's of the fundamental frequency for each of the records for the track shown in Figure 5.3. The left figure shows the posterior probability on a linear scale; the right on a logarithmic scale. The estimator has difficulties estimating the correct frequency at $t = 24s$, which shows as a gab on the left plot and bright vertical line on the right plot. This is reflected in the lower panel of Fig. 5.3 where the probability of the tracked frequency is very low in the region around $t = 24s$.

5.5 Summary and Concluding Remarks

In this chapter the Bayesian frequency estimator was extended with tracking capabilities, by using a prior for the fundamental frequency conditioned on the previous history of the fundamental frequency estimates. The result is a surprisingly simple and yet robust tracker. Tested on the experimental data the performance was comparable to the Viterbi tracker. Computationally, this tracker is much simpler than the Viterbi tracker. But, as was illustrated in Figure 5.2 it is not guaranteed to find the optimal track as opposed to the Viterbi tracker.

Another worthwhile observation from Figure 5.2 is that the shape of the prior PDF influences the accumulated probability. One could erroneously believe the uniform

Algorithm	Mean Err.	2×Std.Dev.	Max. |Err|
Simple Tracking: $H = [1, 2],\ \sigma_T^2 = 1/8,\ P = 2$	-0.0020 Hz	0.34 Hz	1.02 Hz
Viterbi Tracking: $H = [1, 2],\ \sigma_T^2 = 1/16$	-0.0017 Hz	0.34 Hz	1.02 Hz

Table 5.2: Tracking Errors from Accelerometer signal.

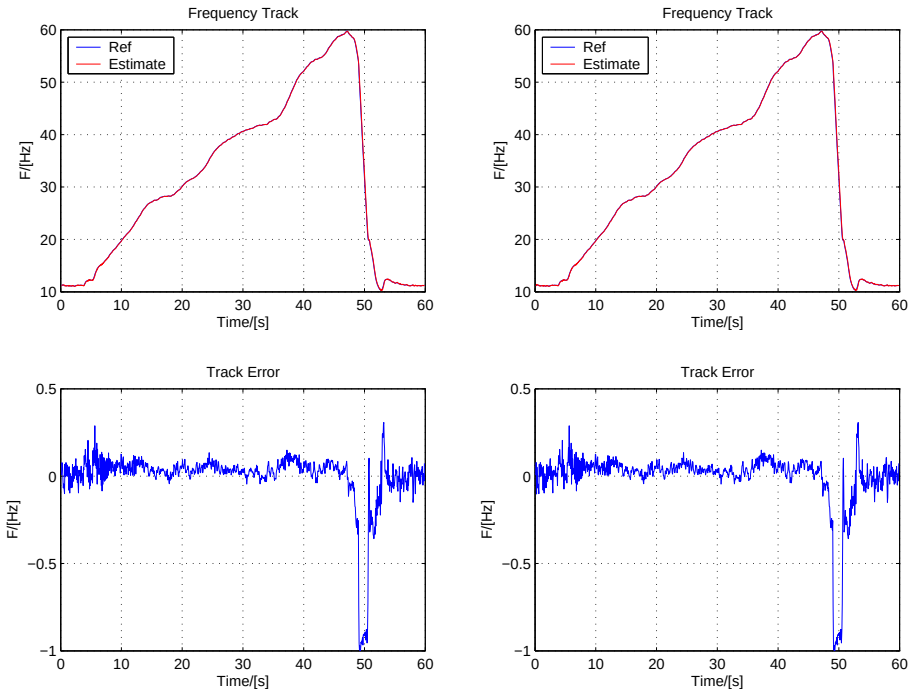

Figure 5.5: The tracking error for the accelerometer signal is measured as the difference of the estimated track to the true frequency estimated with a tacho probe. Left panel: Profile of the tracked frequency by simple tracker(top) and the error (bottom). Right panel: Similar to the left panel, but for the Viterbi tracker. Visually it is nearly impossible to distinguish the two methods.

prior would always give the highest probability for the optimal track because it always selects the maxima of all records. But, as the example shows, the optimal track with the uniform prior (Figure 5.2(b)) obtains a slightly lower probability than the optimal track with the non-uniform prior (Figure 5.2(e)).

The Viterbi algorithm is related to the theory of Hidden Markov Models (HMM) [45]. HMM's have been used with success in speech recognition applications, where the parameters for the prior PDF are estimated automatically. There has not been time to study the subject closer here, but it is believed that further improvements are possible in that direction. Regarding tracking of multiple frequencies an HMM based approach is given in [68].

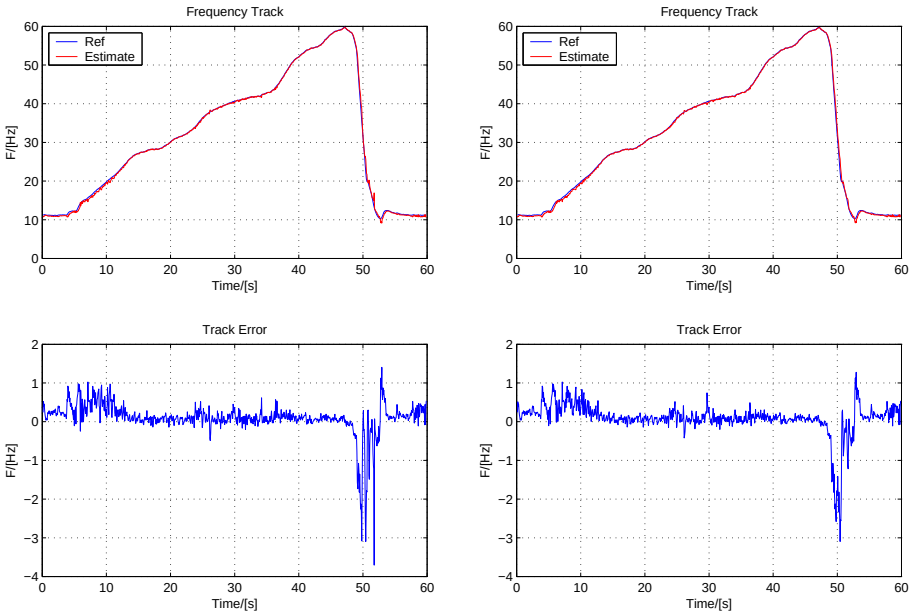

Figure 5.6: Tracking Error for Acoustic Signal. Similar to Figure 5.5

Algorithm	Mean Err.	2×Std.Dev.	Max. |Err|
Simple Tracking: $H = [2, 2.5, 2.6, 5],\ \sigma_T^2 = 1/8,\ P = 2$	0.10 Hz	0.82 Hz	3.7 Hz
Viterbi Tracking: $H = [2, 2.5, 2.6, 5],\ \sigma_T^2 = 1/16$	0.090 Hz	0.84 Hz	3.1 Hz

Table 5.3: Tracking Errors for Acoustic Signal

Chapter 6

Applications

6.1 Simulated Driveby

An application that requires frequency tracking is passive surveillance of aircrafts. The propulsion system of the aircraft radiates high levels of acoustic energy. By observing of the Doppler effect in acoustic signals from the aircraft, as it passed a stationary sensor on the ground, then information about the aircrafts flight parameters such as altitude and velocity can be estimated [12].

Similarly, we will here use the Bayesian frequency estimator to measure the Doppler shift in the sound emitted by a car driving by a microphone. From the Doppler shift, the speed and acceleration of the car is then estimated similarly to the example with aircraft. In principle, this similar to the method described in [12]. However, there are two differences: the first is that the frequency track is estimated using the Bayesian frequency estimator and the Viterbi tracker, as opposed to the interpolated maximum of the Fourier spectrum. The second difference is that model of the cars motion includes acceleration whereas it for the aircraft only includes velocity.

Two assumptions are necessary in order to determine the acceleration: first, the radiated sound is narrow banded with a fundamental frequency proportional to the velocity; second, the velocity can be approximated with a first order equation (i.e. constant acceleration).

The movement of the car relative to the microphone introduces a Doppler shift in the measured fundamental frequency. Knowing the position of the microphone it is possible to fit a model to the profile of the fundamental frequency based on the speed and acceleration of the car.

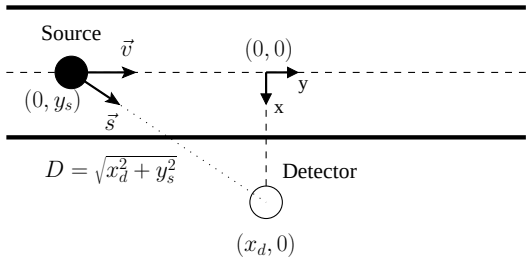

Figure 6.1: Driveby Setup. The source is moving along the y-axis with the velocity V and emits sound in direction S towards the detector located in position (Xd,0)

The Doppler shift depends on the speed of the source towards the detector.

$$\begin{aligned} \vec{v} &= (0, \dot{y_s}) \\ \vec{s} &= (x_d, -y_s) \\ v_{sd} &= \frac{\vec{v} \cdot \vec{s}}{||\vec{s}||} \\ &= \frac{-y_s \dot{y_s}}{\sqrt{x_d^2 + y_s^2}} \end{aligned}$$

The general formula for the Doppler shift from a moving source is

$$f_d = f_s \frac{1}{1 - \frac{v_{sd}}{c}} \tag{6.1}$$

where v_{sd} is the velocity of the source towards the detector, f_d is the frequency at the detector, f_s is the frequency emitted by the source, and c is the velocity of the sound. When f_s is proportional to the velocity of the source, $f_s = K\dot{y_s}$, Eq (6.1) becomes

$$f_d = \frac{K\dot{y_s}}{1 + \frac{y_s \dot{y_s}}{c\sqrt{x_d^2 + y_s^2}}} \tag{6.2}$$

The distance between the source and the detector introduces a delay before a sound emitted by the source is received at the detector. Assuming the velocity of sound is constant (c), then a sound generated by the source at time, t will be received at the detector at time t_d defined in Eq. (6.3).

$$t_d = t + \frac{1}{c}\sqrt{x_d^2 + y_s^2(t)} \tag{6.3}$$

Given the geometry in Figure 6.1 and the equations (6.2)and (6.3), the task is to fit a model for the movement of the source as it passes the detector such that the

generated Doppler frequency matches that observed at the detector. When assuming constant acceleration, the model is

$$y_s(t) = vt + \frac{1}{2}at^2 \tag{6.4}$$

$$\dot{y_s}(t) = v + at \tag{6.5}$$

6.1.1 Numerical Method

Fitting the model represented by the equations (6.4) and (6.5) is accomplished through numerical optimization. The first step in this procedure is to estimate the position of the source given the initial set of parameters: t_0, the time when the source passed the detector, i.e. $y_s(t) = 0$; x_d, the location of the detector; v_0, a_0, the velocity and acceleration at time $t = t_0$; finally the Doppler frequency at $t = t_0$ is also needed, $f_d(t_0)$. Using Eq. (6.2) and Eq. (6.3) the expected Doppler frequency is computed as a function of the *detection* time, $f_d(t_d)$. The second step involves minimizing the mean square error of the fit, e.g. using a multidimensional nonlinear minimization algorithm a la the Nelder-Mead simplex method [41, Sec.10.4].

6.1.2 Simulated Example

To illustrate the method, the detected signal is synthesized for the parameters,

$$x_d = 20\,m,\ v = 55\,ms^{-1},\ a = 4.50\,ms^{-2},\ f_d = 3\,v$$

The frequency observed at the detector is plotted in Figure 6.2(a), where the top graph shows the frequency and the lower graph shows is the amplitude when assuming it decreases with the inverse of the distance from the source.

Synthesized Signal Detection

From the frequency profile the harmonic signal $h(t_d)$ in Eq. (6.6) is created

$$h(t_d) = \sin\left(2\pi \int_0^{t_d} f_d(t)\,dt\right) \tag{6.6}$$

$$g(t_d) = \frac{1}{D(t_d)} \operatorname{sgn} h(t_d) |h(t_d)|^2 + \mathcal{N}(0, \sigma) \tag{6.7}$$

Squaring $h(t_d)$ and keeping the sign is a nonlinear operation that introduces higher overtones. Equation (6.7) is the final expression for the simulated signal. The term $1/D(t_d)$ is identical to the amplitude graph in Figure 6.2(a). The variance of additive Gaussian noise is adjusted to give an average signal to noise ratio of 12 dB. Figure 6.2(b) shows the time signal and Figure 6.2(c) shows the spectrogram of the same signal.

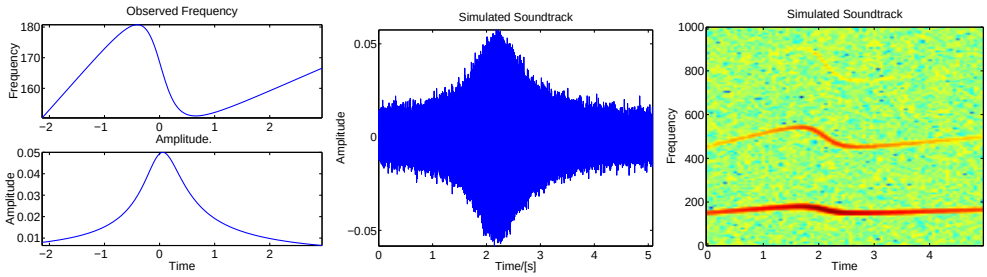

(a) (b) (c)

Figure 6.2: Simulated Soundtrack

Model Fitting

The Bayesian frequency tracker is configured to search for a track in the range from $140 - 200$Hz in increments of $1/4$Hz. The posterior of the fundamental frequency is shown in Figure 6.3(a) along with the estimated track. The track is used in the numerical optimization process which results in the final parameter estimates shown in Table 6.1 and the fit is plotted in Figure 6.3(b).

	t_0/s	f_d/Hz	v/ms^{-1}	a/ms^{-2}	x/m
Initial	1.90	120.0	20	2.0	10
Final	2.13	165.0	54.95	4.49	19.99
True	–	165.0	55.00	4.50	20.00

Table 6.1: Parameters for Simulation

6.1.3 Racecar Example

Figure 6.4(a) shows a soundtrack from a racecar driveby recorded at the Daytona International Raceway [36, Track 1]. Unfortunately only few facts are known about the recording, hence there are no results to compare the estimates with.

The spectrogram (Figure 6.4(b)) indicates that the fundamental frequency is in the range 150-200 Hz and that higher harmonics are present. Hence, the Bayesian tracker is configured to search for the track in the range $150 - 200$ Hz, using the first and second harmonics of the fundamental frequency.

Once the track is estimated, the model is fitted using the initial parameters listed in Table 6.2.

The detected track along with the fitted curve is shown in Figure 6.4(c). The model parameters are listed in Table 6.2.

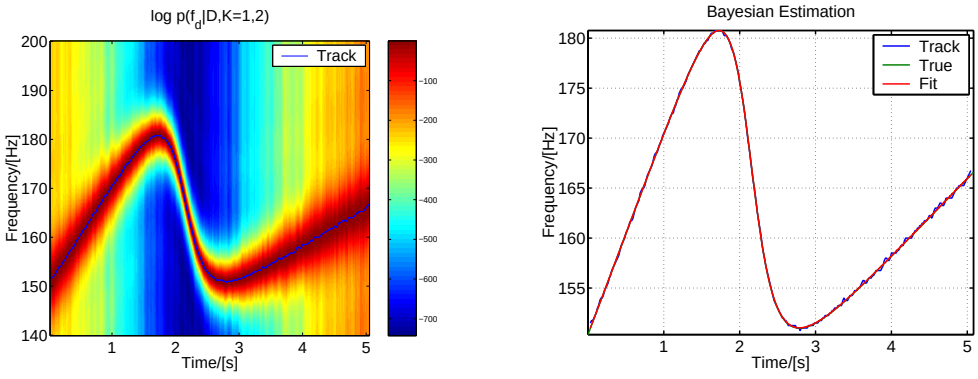

(a) (b)

Figure 6.3: Fitted Track

	t_0/s	f_d/Hz	v/ms^{-1}	a/ms^{-2}	x/m
Initial	1.50	170.0	20	2.0	15
Final	1.48	167.9	54.6	4.5	19.8

Table 6.2: Parameters for Racecar

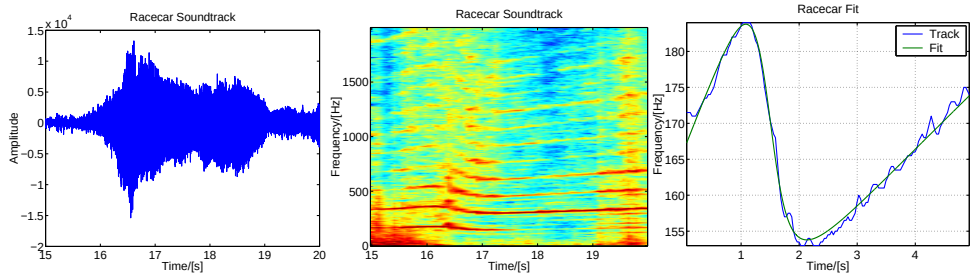

(a) (b) (c)

Figure 6.4: Soundtrack from race car driveby. (a) soundtrack of a Nissan GTP Racecar recorded 15.2 meters from the roadway on the back straight away of the Daytona International Raceway [36, Track 1]. (b) Frequency contents of sound track. (c) Measured and fitted frequency track. See Table 6.2 for the parameters.

6.1.4 Discussion

In this section the Bayesian frequency estimator and tracker was used to estimate the fundamental frequency of a moving source as it passes by a microphone. Based on this frequency estimate a nonlinear numerical optimization method was used to fit a model of motion to the source from which the velocity and acceleration of source was determined.

The spectrograms of the real data from the Daytona racing track showed the presence of a large number overtones. With its ability to track harmonic sequences, the Bayesian tracker is expected to provide optimal estimates of the fundamental frequency for this type of signals, and thus provide the best input for the numerical optimization procedure.

To keep the entire problem within the Bayesian framework, it would be obvious to replace the Nelder-Mead simplex method, with a Bayesian sampling method to find the maximum a posteriori estimate for the model parameters. Two different directions can be taken: The first is to keep the two-step approach used here, where the frequency track is estimated as the first step and the model is fitted in the second step. When dealing with long sequences where the Doppler shift is relatively slow, the approach works quite well as demonstrated here. But when dealing with fast Doppler shifts or short sequences, it becomes difficult to divide the signal into segments from which accurate frequency estimates can be made. In this case a second direction should be investigated. Namely, the possibility of synthesizing the basis functions in the Bayesian Estimator directly from the model parameters as in Eq. (6.6), possibly combined with the amplitude correction used in Eq. (6.7).

6.2 Order Tracking

When analyzing vibrations from rotating machines, it is of interest to estimate and track the amplitudes and phases of different orders of the fundamental frequency. Unless the fundamental frequency is stationary, traditional spectral estimation techniques (e.g. Fourier analysis) can give inaccurate amplitude estimates for the orders due to the non-stationarity which causes *smearing* of the amplitude estimates of the orders. The smearing can be avoided by resampling the vibration signal from having a constant time increment to a constant angular increment in-between samples. Figure 6.5 shows a simplified block diagram of an order tracker based on resampling. The Tacho Analyzer measures the delays between the tacho pulses and computes the times at which the resampler should resample the vibration signal to ensure an equidistant vibration signal in the angular domain.

Here it will be shown that comparable order tracks are obtainable using the Bayesian frequency tracker without resampling the vibration signal. The resampling is avoided by incorporating the non-stationarity of the fundamental frequency into the basis vectors of the linear model as discussed in Sec. 4.4.

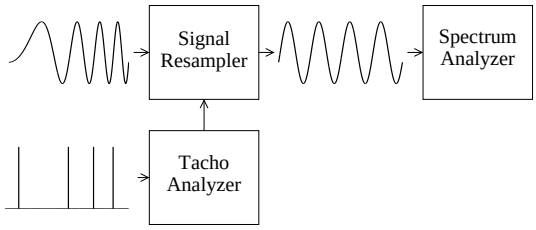

Figure 6.5: Ordertracking by Resampling

6.2.1 Resampling Setup

The vibration signal described in Chapter 2 is chosen as the source signal for which the amplitudes of the orders $1, 2, 2.5$ and 5 of the fundamental frequency are to be estimated. The measurement bandwidth of the vibration signal is reduced to 800 Hz and sampled at a rate of 2048 samples per second.

For reference, the signal is processed by a B&K Pulse order tracking analyzer. The analyzer is configured to compute 10 orders with a resolution of 0.05 order, hence each record must contain 20 periods of the fundamental frequency since the equivalent of the BT product in the angular domain is

$$\Delta \mathrm{F} \cdot \mathrm{T}_{\mathrm{Rec}} = 1 \quad \sim \quad \Delta \mathrm{Order} \cdot \mathrm{Rev}_{\mathrm{Rec}} = 1$$

where ΔF and $\mathrm{T}_{\mathrm{Rec}}$ are the frequency resolution and record length in the time domain, ΔOrder is the order resolution and $\mathrm{Rev}_{\mathrm{Rec}}$ is the record length in periods of the fundamental frequency in the angular domain. The amplitude of the selected orders are computed as the power in the order bands listed in Table 6.3. The bandwidth

Order	Width
1.0	0.3
2.0	0.3
2.5	0.1
5.0	0.1

Table 6.3: Definition of Order slices. *Order* specifies the center of the order band and *Width* specifies the width of the slice (in orders).

of orders 2.5 and 5 is set to 0.1 orders so that orders 2.6 and 5.2 do not interfere. The interfering orders can be identified on the spectrogram in Figure 2.3.

6.2.2 Estimating the Fundamental Frequency

The fundamental frequency must first be estimated. This is accomplished using the Bayesian frequency estimator and the Viterbi tracker described in Section 5.3.1. The parameters for the frequency estimator and tracker are listed in Table 6.4. Figure 6.6

Parameter	Value
Harmonic Sequence	1, 2, 2.5, 5
Frequency Range	8, 8.5, ..., 80 Hz
Record Length	250 ms
Record Overlap	75%
Tracking Variance ($\sigma_T{}^2$)	1/16

Table 6.4: Frequency Tracker Configuration

shows the tracked profile and the tracking error. The maximum frequency error is 0.22 Hz and standard deviation is 0.077 Hz for the track in full.

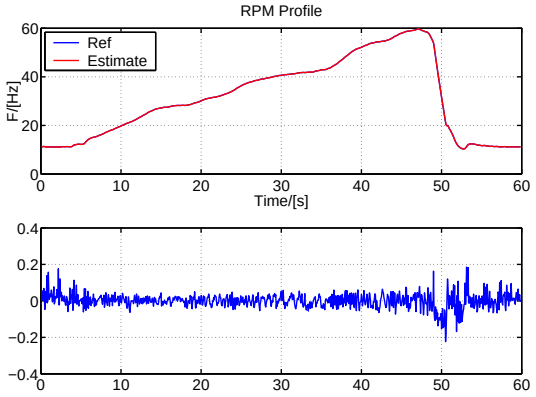

Figure 6.6: Tracking Error. The top graph shows the profile of the estimated fundamental frequency for the Bayesian order tracking example. The bottom graph shows the estimation error in Hz as a function of time.

6.2.3 Estimating the Amplitudes

The primary focus until now has been on estimating the fundamental frequency in the signal, but in the process the amplitude and phase of the harmonics in the signal model are also estimated as the coefficient vector in the linear problem (Eq. (4.6)). Knowing the fundamental frequency for each data record, the amplitudes and phases of the harmonic orders can easily be computed by recomputing the basis vectors using the estimate of the fundamental frequency and using the maximum likelihood estimator given by Eq. (4.8). For the vibration signal segmented into 250 ms records this gives the order tracks shown in Figure 6.7. The figure shows that the estimated order tracks are noisier than the resampled order tracks. The explanation for this is found in the CRLB for the amplitude estimates; it is shown in [31] that

$$\mathrm{Var}(\hat{C}_k) \geq \frac{2\sigma^2}{N}$$

where $\hat{C}_k$ is the amplitude of the k'th harmonic, σ^2 is the noise variance, and N is the number of samples used in the estimate. The record length of the resampled order-tracks is 20 periods of the fundamental frequency, this gives effective record lengths ranging from $2.0s$ at the low frequencies (10 Hz) to $1/3$ s at the high frequencies (60 Hz).

To be able to compare the two methods, the record length of the Bayesian estimator is also adapted to 20 periods of the fundamental frequency. Unfortunately, as has been shown by example in Sec. 4.4 the amplitude estimates becomes inaccurate when the basis functions start deviating from the true frequency profile, which is likely to occur when record lengths are increased. A remedy to this problem is to model the frequency change in the basis functions which was also discussed.

The approach taken here models the frequency changes as polynomials up to degree 10 and estimates the order from records equivalent to 20 periods of the fundamental frequency as in the resampled order tracker. To find the center of the records, the fundamental frequency is integrated,

$$Rev(t) = \int_0^t F_f(t)\, dt \tag{6.8}$$

which gives the revolution number as a function of time. Since $Rev(t)$ is a monotous rising function it is possible to find the values of t_n corresponding to a specified number of cycles of the fundamental frequency. When using 20 periods per record, then selecting every $5th$ period corresponds to a 75% overlap. This is similar to the setup of the resampled order tracker. To get a good polynomial fit to the frequency profile, the polynomial is fitted to a record of twice the length ($t_n \pm 20$ rev) of the segment for the amplitude estimate ($t_n \pm 10$ rev). The order tracks resulting from this procedure are shown in Figure 6.8 and reveals very close resemblance to the resampled order tracks.

6.2.4 Discussion

This example has shown that the Bayesian estimator is capable of both estimating the fundamental frequency and the amplitudes of the orders. The results were found to be comparable to the resampled order tracks. The resampled order tracks are computed by resampling the source signals from the time domain to angular domain, opposed to the Bayesian estimator which resamples its basis functions instead. If the order tracks are to be computed for many signals, then there is a computationally advantage of resampling the basis functions instead of the individual signals. Another advantage doing order tracking in the time domain, is that it becomes possible with simple means to remove, extract or edit the orders in individual signals.

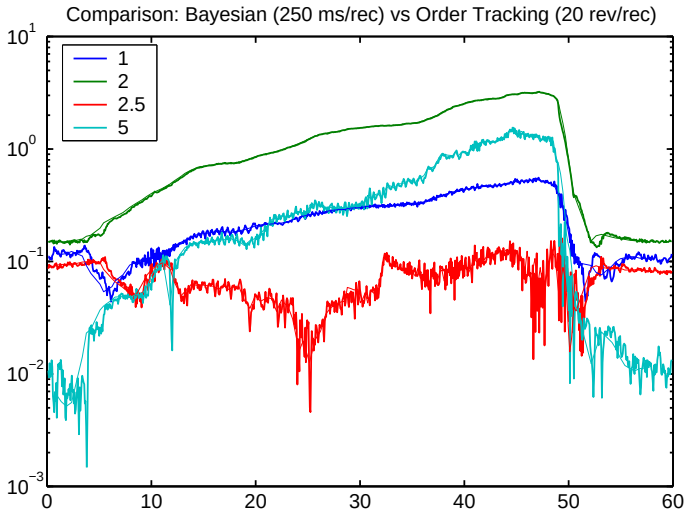

Figure 6.7: Order Estimation with fixed record length. This figure shows with thick lines the estimated amplitude order tracks for the Bayesian order tracking example. The amplitudes are measured in RMS ms^{-2} and the time in seconds. The record length is fixed in time to 250 ms. The thin lines are the resampled order tracks computed in records of a fixed length of 20 revolutions.

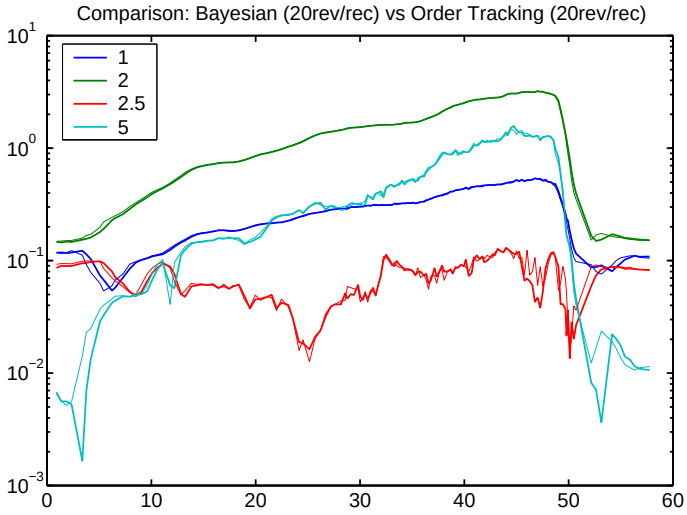

Figure 6.8: Order Estimation with varying record length. This figure is similar to Figure 6.7, except the Bayesian amplitudes are now computed in records of a fixed length of 20 revolutions, identically to the resampled order tracks. Very little difference between the two estimates are observed.

Chapter 7

Conclusion

The original motivation behind this study was to solve the practical problem of estimating the fundamental frequency of rotating machine parts without the need of dedicated tacho probes. Instead, the fundamental frequency was to be estimated from other sources such as the emitted sound pressure or the vibrations of the machine measured with microphones and accelerometers respectively.

In Chapter 2 the characteristics of a microphone and an accelerometer signal were examined. The signals were from a run-up/down experiment with a 5 cylinder engine in a passenger car. Numerous orders of the fundamental frequency were observed in both signals. This poses a problem for the estimation algorithms, namely to choose the fundamental frequency for these orders order. For the purpose of evaluating different frequency estimation algorithms, a simple signal model was devised based on the observations. The synthesized signals were modeled as a sequence of harmonics of the fundamental frequency, where the relative amplitudes and phases are made dependent on the fundamental frequency.

Different frequency estimation algorithms and methods were examined in Chapter 3 and evaluated against the simulated signals. Special attention was paid to the Adaptive Comb Filter (ACF), being the only method using a harmonic sequence for the estimate. A minor contribution of this work is the new and efficient version of the ACF which was derived for estimating non-stationary signals. The simplicity and efficiency of the ACF makes it suitable for implementations where limited computational resources are available. Of the evaluated methods the interpolated FFT and the ACF were found to perform best.

The main contribution of this work is the Bayesian frequency estimator described in Chapter 4 and its extension to tracking described in Chapter 5. The Bayesian sta-

tistical framework has proven itself a powerful tool for incorporating prior knowledge into the estimation procedure. For the Bayesian frequency estimator the prior knowledge concerns the sequence of the known orders of the fundamental frequency, and knowledge about how the fundamental frequency evolves to enable tracking across overlapping records of the signal. Examples were given for other possible extensions, e.g., modeling close frequencies, modeling known non-stationary frequency changes, and merging data channels. The fact that the Bayesian estimator does not require equidistant sampled observations, makes it possible to exclude e.g. overloaded or missing data values from a record in order to prevent them from corrupting the estimates. This is not possible with any of the other frequency estimation algorithms examined.

Applications

The applicability of Bayesian frequency estimator was demonstrated in Chapter 6, where it was applied successfully on two practical problems.

In the first problem, the Bayesian estimator determined the Doppler shifted frequency in the sound from a race car passing by a microphone. With a nonlinear optimization method, the Doppler shifted frequency track was fitted to a model of the cars motion, and the race car's speed, acceleration, and distance to the microphone was determined.

The second problem concerned amplitude order tracking, i.e., estimating the amplitudes of orders of the fundamental frequency. This was accomplished in two steps. First, the Bayesian frequency estimator was used to obtain the track of the fundamental frequency. Second, the amplitudes were estimated over longer segments equivalent to a fixed number of cycles of the fundamental frequency. For each segment the fundamental frequency was approximated by a polynomial. The resulting amplitude order tracks were found to be comparable to those computed using conventional order tracking. In conventional Ordertracking the signals are resampled against a tacho reference, prior to using the Fast Fourier Transform (FFT) for the amplitude estimation. The resampling is necessary because the FFT has fixed frequencies as basis functions. The Bayesian approach allows frequency variation in the basis functions. The conceptual difference of the two methods is that the conventional method resamples the signals to match the basis functions, whereas the Bayesian approach resamples the basis functions to match the signals. In a scenario with many channels there will be computationally advantages in only resampling the basis functions.

Further Work

The Bayesian framework is appealing in the way it includes prior knowledge in the modeling process. When we measure signals, e.g., from mechanical systems or structures, it is often to gain insight into the systems or structures. Often we do possess prior knowledge of the system which could be useful in the measurement process, e.g. for validating the results.

In this work only relatively simple models with few parameters have been considered. The maximum a posteriori (MAP) estimates were found using an exhaustive search over a limited region of the parameter space. For vibro-acoustic signals there are many other parameters that would be interesting to estimate, e.g., which orders of the fundamental frequency to include in the harmonic sequence, or to include frequency change in the basis functions. Unfortunately, additional parameters increase the dimensionality of the problem. Locating the MAP estimate via exhaustive search quickly becomes impractical for a multi-dimensional parameter space. However, the recent literature on Bayesian Estimation is rich on examples addressing these problems, e.g., sampling techniques for computing the MAP estimate for multi-dimensional densities, or *Reversible jump Markov chain Monte Carlo methods* [1] for exploring different sizes of the parameter subspaces (i.e. allowing comparison of different model sizes).

Specifically concerning the tracking capabilities, it is believed that improvements are possible using techniques from Hidden Markov Models (HMM).

Appendix A

Probability Densities

A.1 Probability Density Function for a Harmonic Signal

A harmonic signal is deterministic and not stochastic, but therefore it is still possible to compute the probability density function for a randomly sampled sinusoid. Assuming that the harmonic signal is given by

$$y = A\sin(x) \tag{A.1}$$

we first note that y is symmetric around $x = 0$ and periodic in 2π. It therefore suffices to compute the PDF for only half a period, $x \in]-\pi/2; +\pi/2[$. In this interval y is rising monotonously and it is found that

$$\Pr\{Y \leq y\} = \frac{1}{2} + \frac{\sin^{-1}(y/A)}{\pi} \tag{A.2}$$

The PDF of Y is found by differentiation of Eq. (A.2) with respect to y which gives,

$$\mathrm{p}(y) = \frac{1}{\pi\sqrt{A^2 - y^2}}, \quad |y| < A \tag{A.3}$$

The PDF has discontinuities for $|y| = A$. Figure A.1 shows the PDF for a sine wave with unit amplitude.

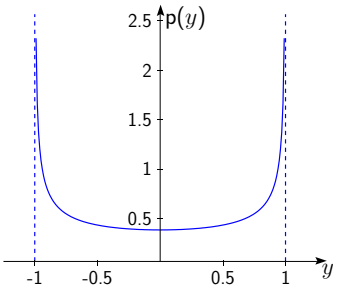

Figure A.1: PDF for sine wave with unit amplitude

A.2 Probability Density Function for a Linear Regression Tracking Prior

For tracking a slowly changing frequency, a normally distributed Gaussian can be chosen. The width of the PDF is specified by the tracking variance, σ_T^2, and the mean, μ_T, is predicted from a linear regression over the previous P estimates of the fundamental frequency. The linear regression problem is defined by:

$$\omega_F^{(n-k)} = \alpha\, k + \omega_F^{(n)} + e(n-k), \quad e \sim \mathcal{N}(0, \sigma_T^2), \quad 1 \leq k \leq P \tag{A.4}$$

Written in matrix notation and assuming the estimates are given in equidistant time steps, then the predicted mean value of $\omega_F^{(n)}$ is is derived as follows.

$$\mathbf{W} = \left[\omega_F^{(n-1)} \quad \cdots \quad \omega_F^{(n-P)}\right]^\top \tag{A.5}$$

$$\mathbf{X} = \begin{bmatrix} -1 & -2 & \cdots & -P \\ 1 & 1 & \cdots & 1 \end{bmatrix}^\top \tag{A.6}$$

$$\mathbf{u} = [\alpha \quad \mu_T]^\top \tag{A.7}$$

$$\mathbf{e} = [e(n-1) \quad e(n-P)]^\top, \quad e \sim \mathcal{N}(0, \sigma_T^2 \tag{A.8}$$

$$\mathbf{W} = \mathbf{X}\,\mathbf{u} + \mathbf{e} \tag{A.9}$$

Eq. (A.9) corresponds to Eq. (A.4). α is the slope and μ_T is the bias of the line fitted through the previous estimates. Since time n is chosen as the reference point then $\mu_T \equiv \omega_F^{(n)}$. Minimizing the least square error, $\mathbf{e}^\top\mathbf{e}$, results in

$$\mathbf{X}^\top\mathbf{W} = \mathbf{X}^\top\mathbf{X}\,\mathbf{u} \tag{A.10}$$

where

$$\mathbf{X}^\top \mathbf{W} = \begin{bmatrix} -\sum_{k=1}^{P} k\,\omega_F^{(n-k)} \\ \sum_{k=1}^{P} \omega_F^{(n-k)} \end{bmatrix} \tag{A.11}$$

$$\mathbf{X}^\top \mathbf{X} = \begin{bmatrix} \sum_{k=1}^{P} k^2 & \sum_{k=1}^{P} -k \\ \sum_{k=1}^{P} -k & P \end{bmatrix} = \frac{P(P+1)}{2} \begin{bmatrix} \frac{2P+1}{3} & -1 \\ -1 & \frac{2}{P+1} \end{bmatrix} \tag{A.12}$$

From this, the mean of the prior distribution, μ_T, is found to be

$$\begin{aligned} \mu_T &= \frac{\frac{2}{P(P+1)} \begin{vmatrix} \frac{2P+1}{3} & -\sum_{k=1}^{P} k\,\omega_F^{(n-k)} \\ -1 & \sum_{k=1}^{P} \omega_F^{(n-k)} \end{vmatrix}}{\begin{vmatrix} \frac{2P+1}{3} & -1 \\ -1 & \frac{2}{P+1} \end{vmatrix}} \\ &= \frac{\sum_{k=1}^{P} (2(2P+1) - 6k)\omega_F^{(n-k)}}{P(P-1)} \end{aligned} \tag{A.13}$$

Appendix B

Frequency Estimation Formulas

In this appendix some of the formulas for frequency estimation are derived.

B.1 Hanning Window Fourier Interpolation

Here the equations for fourier interpolation using the Hanning window are derived. First, recalling the definition of the rectangular window, $W_R(f)$ and the Hanning window, $W_H(f)$:

$$W_R(f) = \frac{\sin(\pi f T)}{\pi f T} \tag{B.1}$$

$$W_H(f) = \frac{1}{2}W_R(f) + \frac{1}{4}\left[W_R(f - 1/T) + W_R(f + 1/T)\right] \tag{B.2}$$

Writing out eq. (B.2) using eq. (B.1) gives

$$W_H(f) = W_R(f)\frac{1}{1 - (fT)^2} \tag{B.3}$$

For a Hanning weighted sinusoid with the frequency, $F_0 = (\hat{m} + \delta)\Delta F = (\hat{m} + \delta)/T$, the Fourier coefficients thus becomes

$$G_m = \frac{A}{2}\frac{\sin(\pi(m - \hat{m} - \delta))}{\pi(m - \hat{m} - \delta)}\frac{1}{1 - (m - \hat{m} - \delta)^2} \tag{B.4}$$

Evaluating Eq. (B.4) for the two values of m surrounding the peak, $m = \hat{m}$ and $m = \hat{m} + 1$ gives

$$G_{\hat{m}} = \frac{A}{2}\frac{\sin(\pi\delta)}{\pi}\frac{1}{\delta(1-\delta)(1+\delta)} \tag{B.5}$$

$$G_{\hat{m}+1} = \frac{A}{2}\frac{\sin(\pi\delta)}{\pi}\frac{1}{\delta(1-\delta)(2-\delta)} \tag{B.6}$$

The fractional part of the interpolated value of the true frequency, δ, is easily obtained from the ratio of the two equations,

$$\alpha = \frac{G_{\hat{m}+1}}{G_{\hat{m}}} = \frac{1+\delta}{2-\delta} \iff \delta = \frac{2\alpha - 1}{\alpha + 1} \tag{B.7}$$

B.2 Prony Method

Considering a noise-free signal being a summation of sinusoids,

$$y(t) = \sum_{m=1}^{M} A_m \cos(\omega_m t + \phi_m)$$

The one-sides Z transform is defined by

$$X^+(z) \equiv \sum_{n=0}^{\infty} x(n) z^{-n}$$

Using X^+ on $y(t)$,

$$y(t) \overset{X^+}{\longleftrightarrow} Y(z)$$

gives

$$\begin{aligned} Y(z) &= \sum_{m=1}^{M} \frac{A_m \left[\cos(\phi_m) - \cos(\omega_m - \phi_m) z^{-1}\right]}{1 - 2\cos(\omega_m) z^{-1} + z^{-2}} \\ &= \frac{1}{\prod_{m=1}^{M} (1 - 2\cos(\omega_m) z^{-1} + z^{-2})} \times \\ &\quad \sum_{m=1}^{M} \left(A_m \left[\cos(\phi_m) - \cos(\omega_m - \phi_m) z^{-1}\right] \prod_{l \neq m}^{M} (1 - 2\cos(\omega_l) z^{-1} + z^{-2}) \right) \end{aligned} \tag{B.8}$$

Defing the polynomail $c(z)$ by

$$c(z) = \prod_{m=1}^{M} (1 - 2\cos(\omega_m) z^{-1} + z^{-2}) = \sum_{k=0}^{2M} c_k z^{-k} \tag{B.9}$$

and mutiplying it onto both sides of eq. (B.8) gives

$$\begin{aligned} c(z)Y(z) &= \sum_{m=1}^{M} \left(A_m \left[\cos(\phi_m) - \cos(\omega_m - \phi_m) z^{-1} \right] \prod_{l \neq m} (1 - 2\cos(\omega_l) z^{-1} + z^{-2}) \right) \\ &= \sum_{k=0}^{2M-1} d_k z^{-k} \end{aligned} \tag{B.10}$$

Since both $c(z)$ and $Y(z)$ are polynomials in z, then their product is the convolution of the two,

$$c(z)Y(z) = \sum_{t}^{\infty} d_t z^{-t}$$

where

$$d_t = \sum_{k=0}^{2M} c_k y(t-k)$$

From eq. (B.10) we find that $d_t = 0$ for $t \geq 2M$, I.e.

$$\sum_{k=0}^{2M} c_k y_{t-k} = 0, \; t \geq 2M$$

The one-sided z-transform allows arbitrary starting points, t_0 therefore $t \geq 2M + t_0$ and the expression is valid for all t. Finally, with the coefficient in $c(z)$ defined in eq. (B.9), we find

$$\sum_{k=0}^{2M} c_k y_{t-k} = 0 \quad \Rightarrow y(t) = -\sum_{k=1}^{2M} c_k y(t-k)$$

which proves that a sum of M sinusoids can be written as a diffence equation of order $2M$.

B.3 Quinn & Fernandez

The derivation given here is similar to that of Quinn [43]. The Q&F algorithm is a simple iterative procedure to fit an ARMA(2,2) model to the signal

$$d(t) = A\cos(\omega t + \phi) + e(t) \tag{B.11}$$

where $e(t)$ is additive white Gaussian noise.

Writing out the cosine expression in Eq. (B.11) for $t-1$ and $t+1$ using the addition formulas gives,

$$\begin{aligned} u(t) &= \cos(\omega t + \phi) \\ u(t+1) &= \cos(\omega t + \phi + \omega) = u(t)\cos(\omega) - \sin(\omega t + \phi)\sin(\omega) \\ u(t-1) &= \cos(\omega t + \phi - \omega) = u(t)\cos(\omega) + \sin(\omega t + \phi)\sin(\omega) \end{aligned} \tag{B.12}$$

Adding them results in

$$u(t+1) + u(t-1) = 2\cos(\omega)u(t)$$

This shows that Eq. (B.12) is a 2nd order difference equation:

$$u(t) = 2\cos(\omega)u(t-1) - u(t-2) \tag{B.13}$$

First by substituting Eq. (B.12) into Eq. (B.11) we find,

$$u(t) = \frac{1}{A}(d(t) - e(t))$$

From the difference equation, Eq. (B.13), the ARMA(2,2) model is derived,

$$d(t) - \beta d(t-1) + d(t-2) = e(t) - \alpha e(t-1) + e(t-2) \tag{B.14}$$

with the constraint $\alpha = \beta$, and $\beta = 2\cos(\omega)$.

The objective is to determine β from a sequence of observations $d(t), t = 0, 1, \ldots, N-1$. The motivation behind the QF algorithm is best explained by transforming Eq. (B.14) into the Z-domain.

$$D(z) = \frac{1 - \alpha z^{-1} + z^{-2}}{1 - \beta z^{-1} + z^{-2}} E(z)$$

$D(z)$ is the Z-tranformation of the observed noisy sinusoid and $E(z)$ is the Z-transform of the noise. Assuming we have a qualified estimate for α, then applying the transfer function

$$H_\xi(z) = \frac{1}{1 - \alpha z^{-1} + z^{-2}}$$

gives

$$\begin{aligned} D_\xi(z) &= H_\xi(z)D(z) = \frac{1}{1 - \beta z^{-1} + z^{-2}} E(z) \\ \xi(t) &= d(t) + \alpha\xi(t-1) - \xi(t-2) \end{aligned}$$

where $D_\xi(z)$ and $\xi(t)$ are the filtered sinusoid in the Z-domain and sample domain respectively. The problem is now reduced to an AR(2) problem. This is illustrated

below where applying the FIR filter represented by the transfer function, $H_{\hat{e}}(z)$, restores the original noise.

$$\begin{aligned} H_{\hat{e}}(z) &= 1 - \beta z^1 + z^2 \\ \hat{E}(z) &= H_{\hat{e}}(z) D_\xi(z) = E(z) \\ \hat{e}(t) &= \xi(t) - \beta\xi(t-1) + \xi(t-2) = d(t) + (\alpha - \beta)\xi(t-1) \end{aligned}$$

Finding β is equivalent to minimizing the sum of squared errors on $n(t)$ with respect to β, which is a simple regression problem.

$$\min_\beta \sum_{t=0}^{N-1} \hat{e}(t)^2 \Rightarrow \frac{d}{d\beta} \sum_{t=0}^{N-1} \hat{e}(t)^2 = 0 \Rightarrow \beta = \alpha + \frac{\sum_{t=0}^{N-1} d(t)\xi(t-1)}{\sum_{t=0}^{N-1} \xi(t-1)^2}$$

The procedure is repeated with $\alpha = \beta$, until the newly found value of β is sufficiently close to α.

B.4 Adaptive Comb Filter

The adaptive comb filter with zeros constrained to the unit circle and the poles inside is defined by

$$e_t = \frac{A(q^{-1})}{A(\rho q^{-1})} d_t \quad \Leftrightarrow \quad A(\rho q^{-1}) e_t = A(q^{-1}) d_t \tag{B.15}$$

where q^{-1} is the unit delay operator and the polynomial $A(q)$ is defined by

$$A(q) = \prod_{i=1}^{M} \left(1 + b_i q^{-1} + q^{-2}\right) \tag{B.16}$$

$$= \sum_{i=0}^{2M} a_i q^{-i}, \quad a_0 = 1 \tag{B.17}$$

and the coefficients, $b_i = -2\cos(k_i\omega)$. When the orders of the harmonic frequencies, k_i, are all integer multiplicands of the frequency ω, the cosine expressions in the b_i coefficients can be expressed as a polynomials of $\cos(\omega)$ using the general trigonometric formula,

$$\begin{aligned} \cos(k_i\,\omega) = \frac{1}{2}\Bigg\{ &(2\cos(\omega))^{k_i} - \frac{k_i}{1}(2\cos(\omega))^{k_i-2} + \\ &\frac{k_i}{2}\binom{k_i-3}{1}(2\cos(\omega))^{k_i-4} - \frac{k_i}{3}\binom{k_i-4}{2}(2\cos(\omega))^{k_i-6} + \cdots \Bigg\}. \end{aligned}$$

The M products in Eq. (B.16) of the polynomials in q, thus involves multiplication of the polynomials in $b = 2\cos(\omega)$ corresponding to b_i coefficients. Polynomial multiplication is accomplished by convolution of the coefficients. Each of the a_i coefficients

will therefore also be polynomials in b and as a result the a_i coefficient in $A(q)$ can be expressed as a matrix multiplication of a constant matrix, $\mathbf{K}$, with the vector $\mathbf{b}$ containing the powers of b:

$$\begin{aligned} b &= -2\cos(\omega) \\ \mathbf{a} &= [a_1\ a_2\ \cdots\ a_m\ \cdots\ a_1\ 1]^\top \\ \mathbf{a} &= \mathbf{K}\mathbf{b} \qquad \text{(B.18)} \\ \mathbf{b} &= [1\ b\ b^2\ \cdots b^k]^\top \qquad \text{(B.19)} \end{aligned}$$

$\mathbf{K}$ solely depends on the harmonic sequence and need only be computed once for each configuration. It is noted that all the polynomials in q are symmetric, why their product, $A(q)$ is also symmetric. Therefore, only the M first a_i coefficients need to be computed. Matlab™ scripts to compute $\mathbf{K}$ for a given harmonic sequence are listed in Section B.4.1.

Introducing the matrix notation:

$$\begin{aligned} A(q^{-1}) &= 1 + [q^{-1}\cdots q^{-2m}]\mathbf{a} \\ A(\rho q^{-1}) &= 1 + [q^{-1}\cdots q^{-2m}]\mathbf{\Pi}\mathbf{a} \\ \mathbf{\Pi} &= \text{diag}[\rho\ \rho^2\ \cdots\ \rho^{2m}] \\ \mathbf{d}_t &= [d_{t-1}\ d_{t-2}\ \cdots\ d_{t-2m}]^\top \\ \mathbf{e}_t &= [e_{t-1}\ e_{t-2}\ \cdots\ e_{t-2m}]^\top \end{aligned}$$

and inserting into Eq. (B.15) gives,

$$\begin{aligned} e_t + \mathbf{a}^\top\mathbf{\Pi}\mathbf{e}_t &= d_t + \mathbf{a}^\top\mathbf{d}_t. \\ &\Updownarrow \\ e_t &= d_t + \mathbf{a}^\top\mathbf{d}_t - \mathbf{a}^\top\mathbf{\Pi}\mathbf{e}_t \\ &= d_t + \mathbf{a}^\top(\mathbf{d}_t - \mathbf{\Pi}\mathbf{e}_t) \end{aligned}$$

The gradient is computed by taking $\frac{\partial}{\partial b}$ on both sides (d_t independent of b):

$$\frac{\partial e_t}{\partial b} = \frac{\partial \mathbf{a}}{\partial b}^\top(\mathbf{d}_t - \mathbf{\Pi}\mathbf{e}_t) - \mathbf{a}^\top\mathbf{\Pi}\frac{\partial \mathbf{e}_t}{\partial b} \qquad \text{(B.20)}$$

where

$$\frac{\partial \mathbf{e}_t}{\partial b} = \left[\frac{\partial e_{t-1}}{\partial b}\quad \frac{\partial e_{t-2}}{\partial b}\quad \cdots\quad \frac{\partial e_{t-2m}}{\partial b}\right]^\top$$

From Eqs. (B.18,B.19), the derivative of $\mathbf{a}$ is found:

$$\begin{aligned} \frac{\partial \mathbf{a}}{\partial b} &= \mathbf{K}\frac{\partial \mathbf{b}}{\partial b} \\ \frac{\partial \mathbf{b}}{\partial b} &= \frac{1}{b}\mathbf{D}_k\mathbf{b} \\ \mathbf{D}_k &= \text{diag}\,[0\ 1\ \cdots\ k] \end{aligned}$$

Inserting it all into Eq. (B.20) gives the gradient,

$$\frac{\partial}{\partial b}e_t \quad = \quad \frac{1}{b}\mathbf{b}^\top \mathbf{D}_k \mathbf{K}^\top \left(\mathbf{d}_t - \mathbf{\Pi}\mathbf{e}_t\right) - \mathbf{b}^\top \mathbf{K}^\top \mathbf{\Pi}\frac{\partial \mathbf{e}_t}{\partial b}$$

and the rest of the algorithm follows Eqs. (3.47-3.49) and the update step in Eq. (3.52).

B.4.1 Matlab Code

The following two Matlab functions compute the constant matrix $\mathbf{K}$ for a given harmonic sequence. The example below shows how to invoke the scripts to compute $\mathbf{K}$ for the harmonic sequence, [1, 2, 2.5], with the common frequency 0.5.

```
>> K=harmcoef(harmpoly(.5,[1,2,2.5]))

K =

     0     5     3    -5    -1     1     0     0     0     0     0     0
    -1     0    10    15    -6   -20     1     8     0    -1     0     0
     0   -10     6    60    -2   -82     0    45     0   -11     0     1


>>
```

```
function B=harmpoly(n0, k)
% Synopsis:
%       B=harmpoly(n0, k)
% Description:
%       Generates the polynomial coefficients for computing the
%       harmonic components specified in 'k'. The polynomials are a
%       function of b=-2*cos(w*n0) where 'n0' is the greatest
%       common divisor of the orders in 'k', I.e for the harmonic
%       sequence
%               k = [1, 2, 2.5]
%       then
%               n0= 0.5
% Input:
%       n0 - Order of the fundamental frequency tracked.
%       k  - [Mx1] Vector with orders of notches in filter.
% Output:
%       B  - [MxN] Polynomial coefficients for computing the
%            harmonic orders in k. Each row corresponds to a
%             value in k.
% TFP 2003-2-16
K=max(k)/n0; % Max power of b=2cos(w_0)
```

```
B=zeros(K,K+1);
B(1,end-1)     = 1;
if K>1,
  B(2,end-2:end) = [-1 0 2];
  for i=3:K,
    p      = -conv([1 0],B(i-1,:));
    B(i,:) = p(end-K:end) - B(i-2,:);
  end
end
% Only keep harmonic polynomials used:
B = B(k/n0,:);



function K=harmcoef(B)
% Synopsis:
%       K = harmcoef(B)
% Description:
%       Computes the coefficients for the polynomial,
%               A(q) = Prod(m=1,M)[1 + b_i*q^-1 + q^-2]
%                    = Sum(i=0,2M)[a_i*q^-i], a_0=1
%       where the coefficents
%               b_i = -2*cos(w_i)
%       are specified by rows of B(i,:) as polynomials of
%               b_0 = -2*cos(w_0)
%       A(q) is symmetric, hence only the M  coefficients, b_1 ... b_M
%       are computed.
% Input:
%       B  - [MxN] b_i coefficients on polynomial form.
%            M: number of harmonics.
%            N: maximum polynomial degree.
% Output:
%       K  - [M,Mx(M*(N-1)+1)]
%            Matrix where each row, K(i,:), corresponds to the
%            polynomial in b=-2*cos(w) for the coefficient, a_i.
% TFP 2003-2-16

% M - number of harmonics
% N - polynomial degree
[M,N]   = size(B);
D       = M*(N-1);
K       = zeros(M,D+1);
K(1,:)  = poln(B(1,:),D);
```

```
for m=2:M,
  q     = poln(B(m,:));
  p3    = poln(0,D);
  p2    = poln(1,D);
  p1    = K(1,:);
  for i=1:m-1,
    p1    = K(i,:);
    K(i,:)= p3 + poln(conv(q,p2),D) + p1;
    p3    = p2;
    p2    = p1;
  end;
  K(m,:)= 2*p3 + poln(conv(q,p2),D);
end;

% Reduce K by removing 'empty' columns:
i    = find(K(:)~=0);
if length(i)
  c1 = fix(i(1)/M); % Column of first non-zero value
  K  = K(:,c1:end);
end
K = fliplr(K);


function P = poln(p,n)
% Adjust polynomial to fixed length
 i  =find(p~=0);
 if length(i)>0
   dp   = length(p)-i(1); % Degree of 'p'
   P    = p(end-dp:end);
 else
   P    = 0;
   dp   = 0;
 end
 if exist('n') & n>=dp
   P    = [zeros(1,n-dp),P];
 end
```

Appendix C

Simulation Results

The figures in this appendix supplement the simulation results in Section 3.5 and Section 4.3.1.

In general only little difference is observed in the simulation results for the average SNR levels of 30 dB and 0 dB. At the low level, SNR = 0 dB, only the ACF and the Bayesian estimator have estimates with less than 1 Hz RMS for larger parts of the signal.

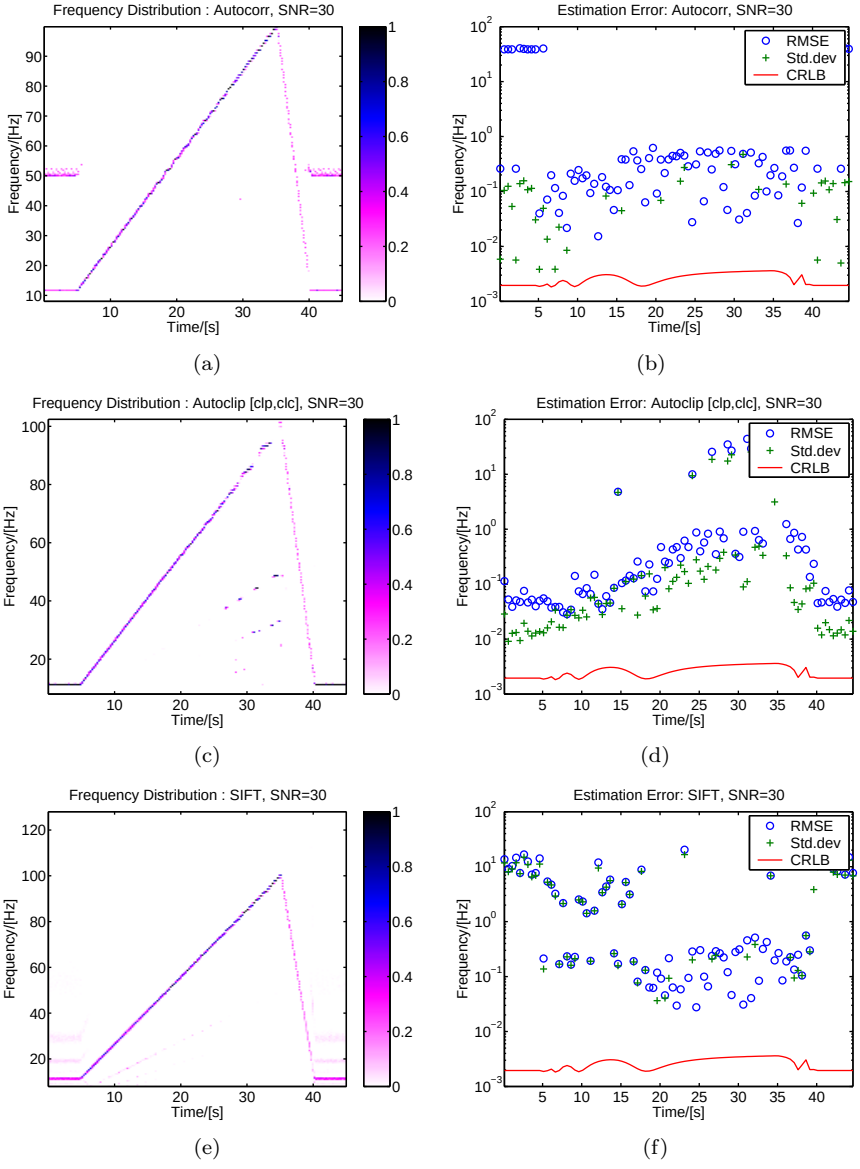

Figure C.1: Simulation Results for Correlation Methods, SNR=30dB

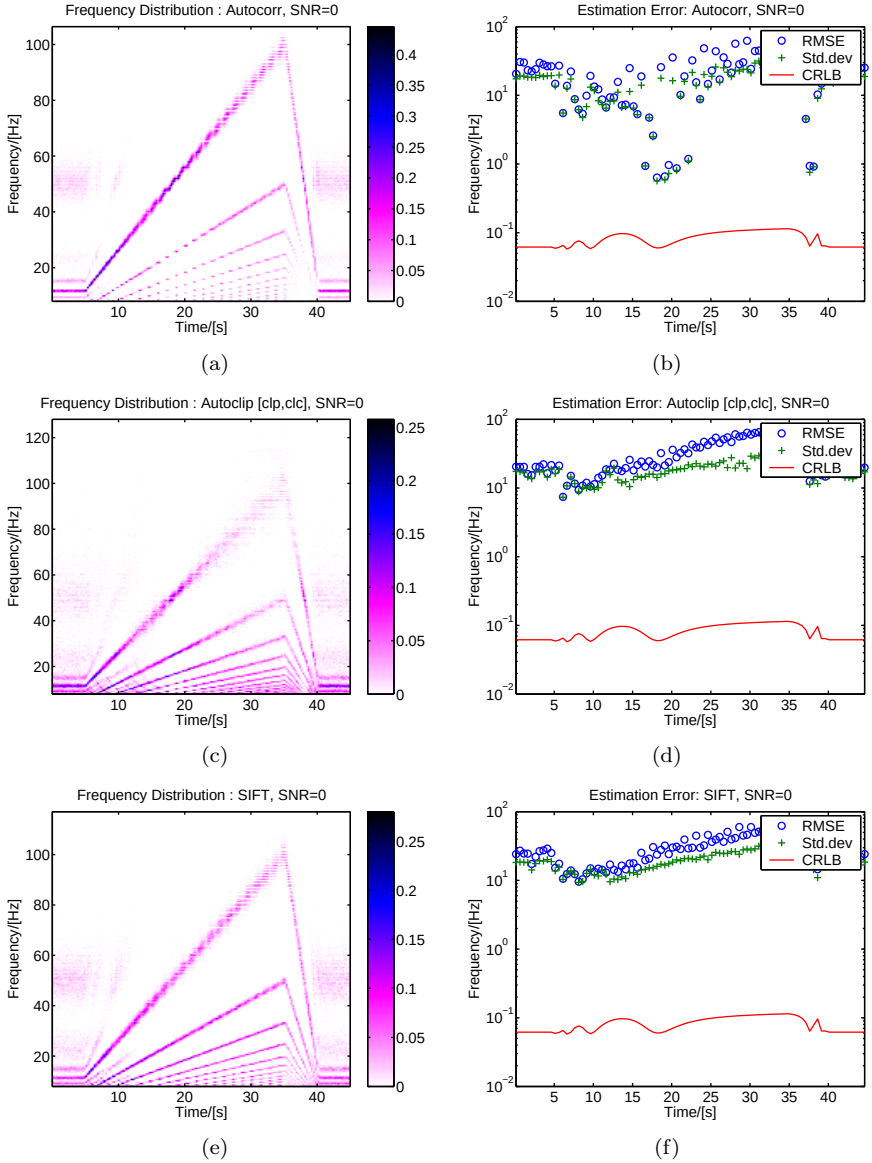

Figure C.2: Simulation Results for Correlation Methods, SNR=0dB

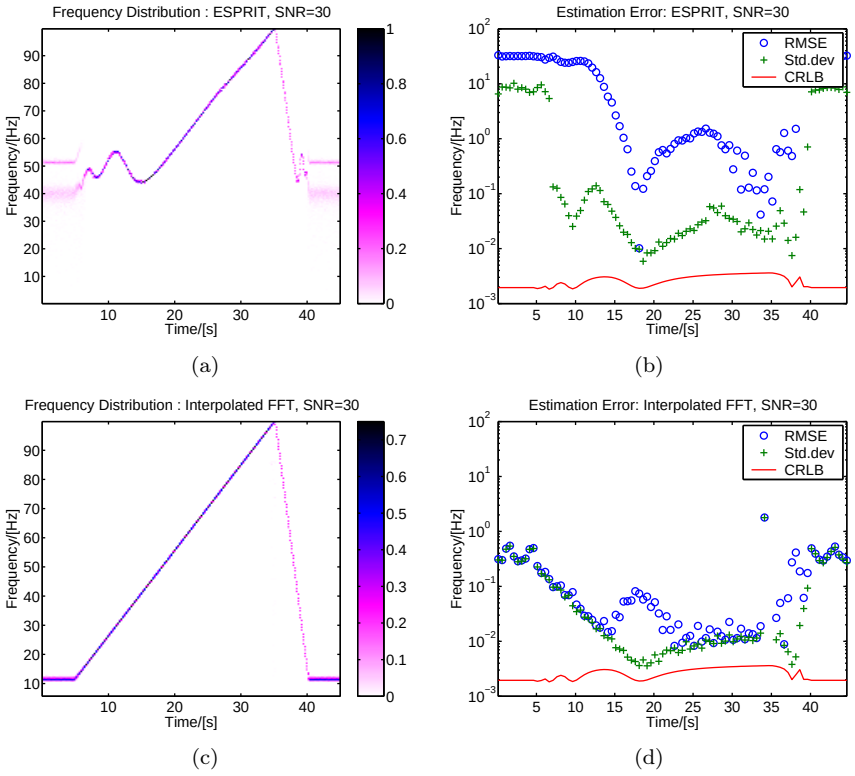

Figure C.3: Simulation Results for ESPRIT and FFT Methods, SNR=30dB

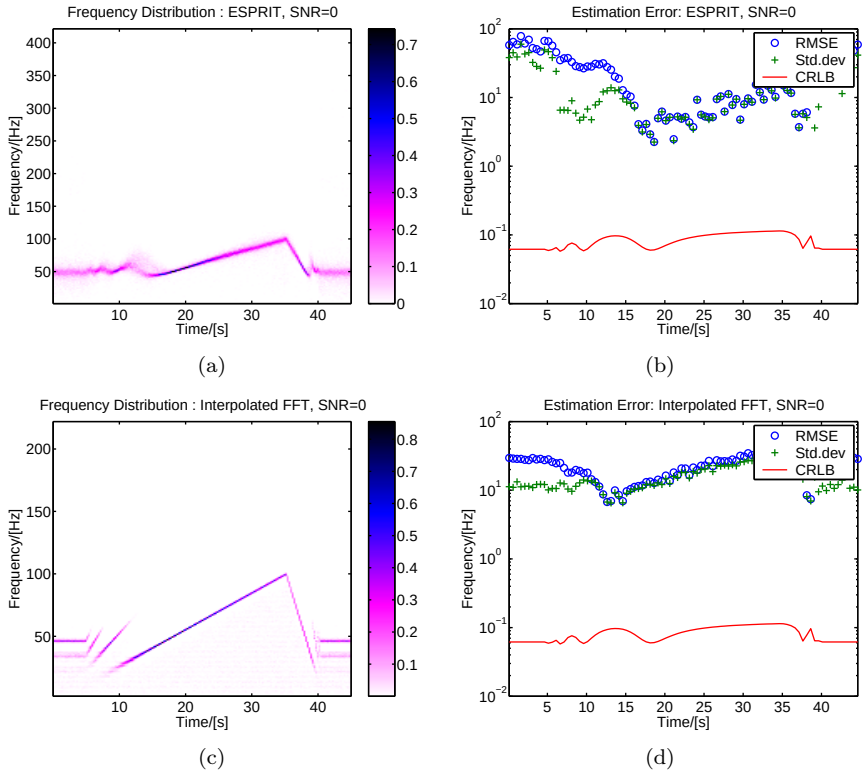

Figure C.4: Simulation Results for ESPRIT and FFT Methods, SNR=0dB

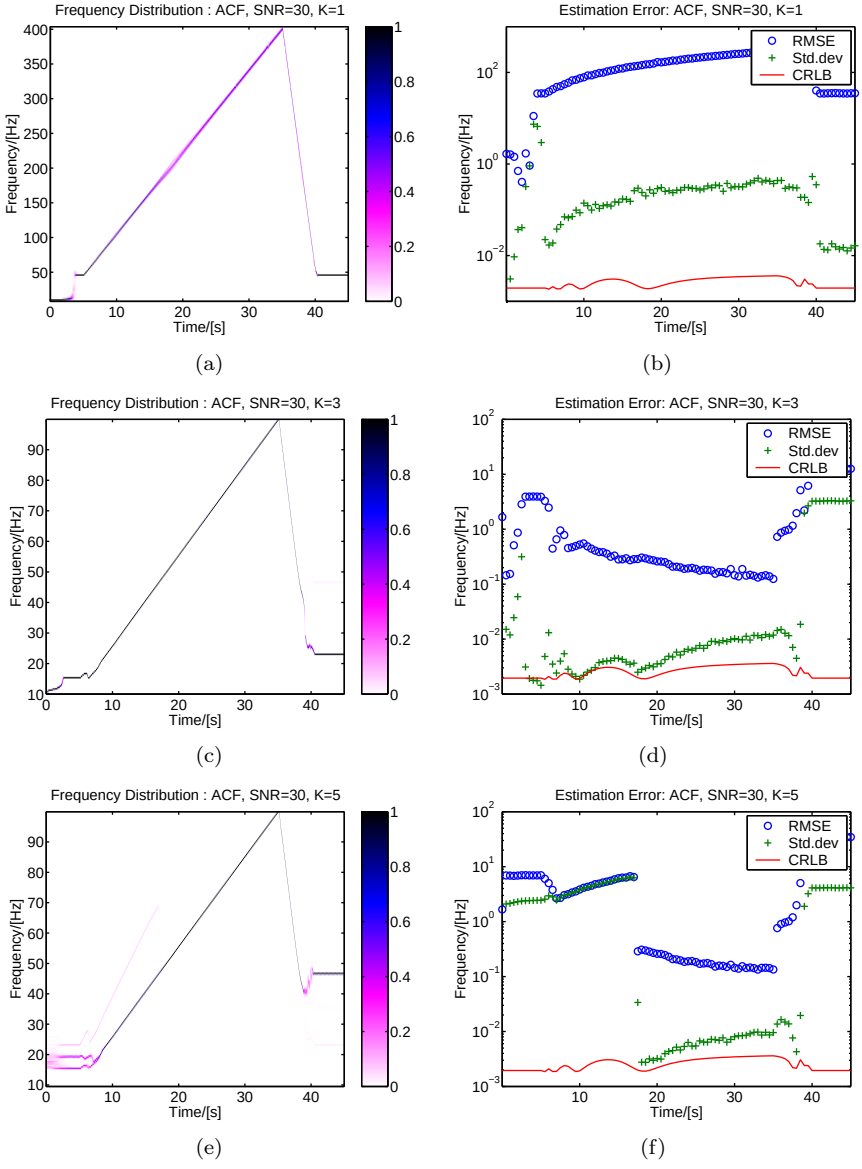

Figure C.5: Simulation Results for ACF, SNR=30dB

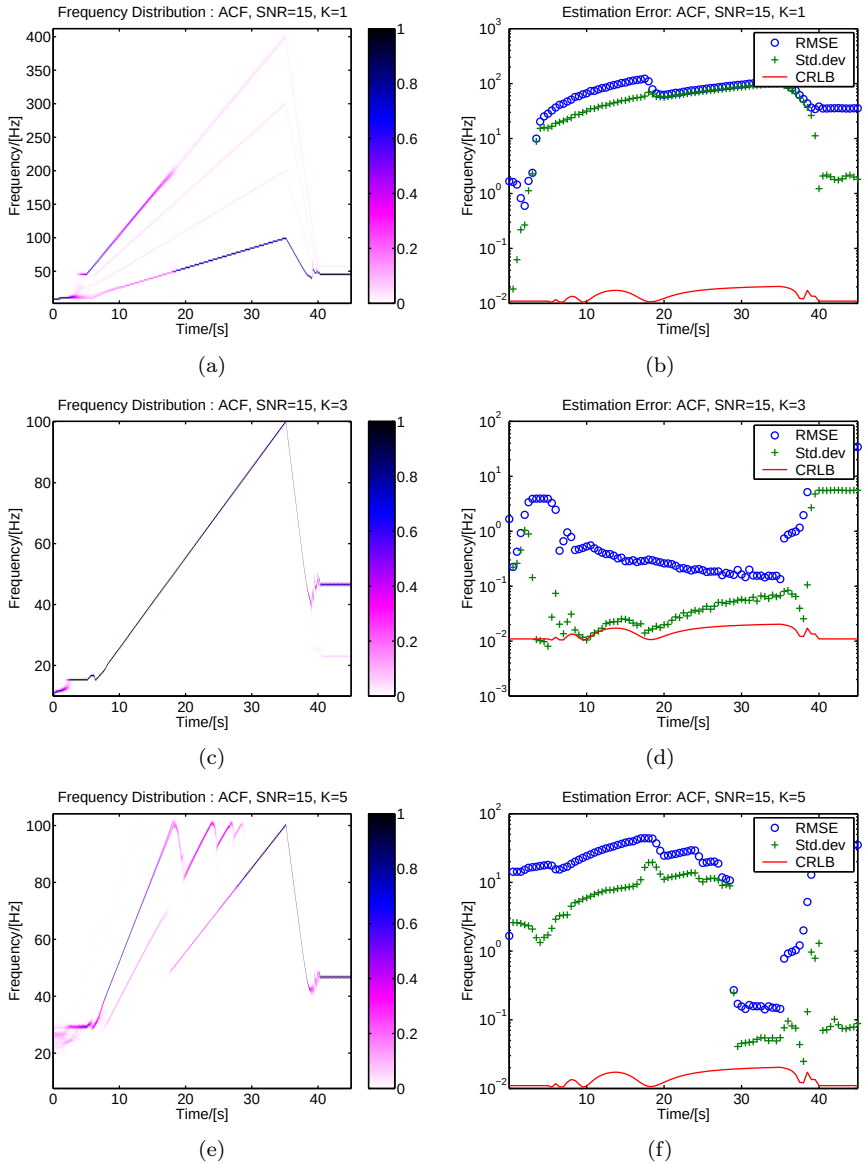

Figure C.6: Simulation Results for ACF, SNR=15dB

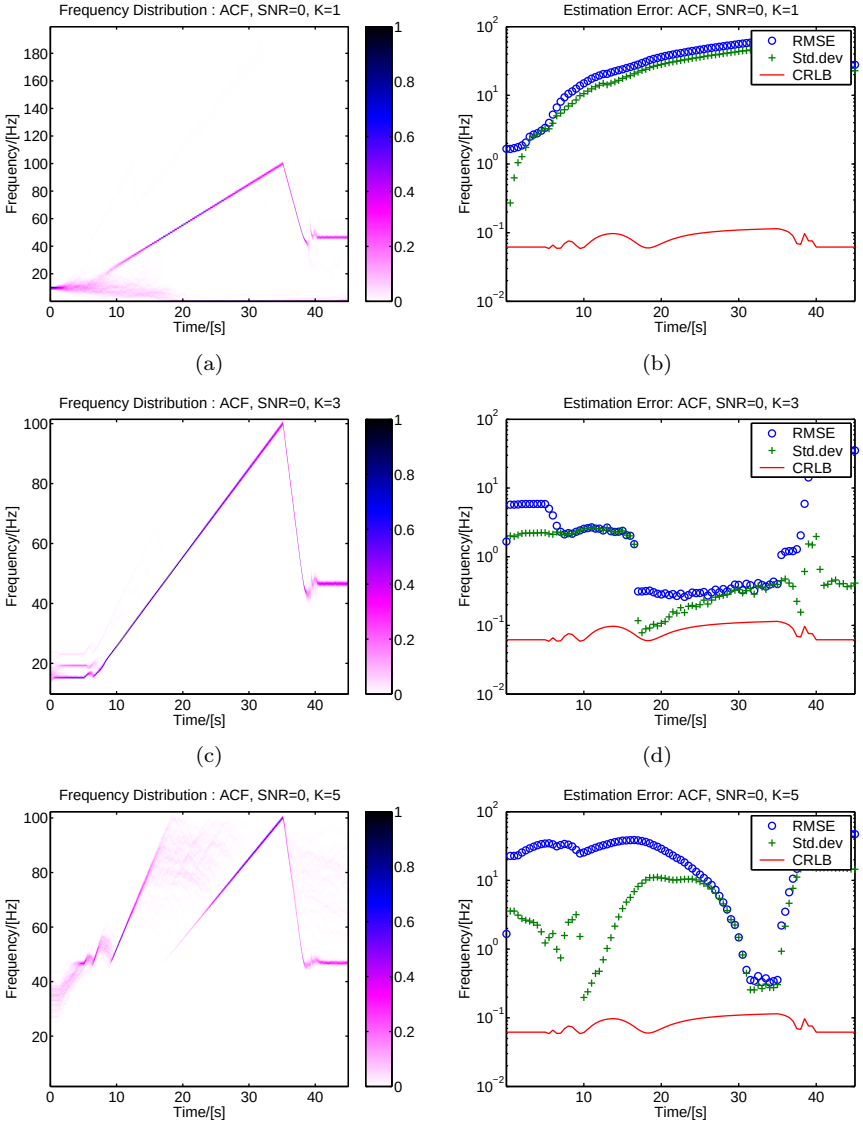

Figure C.7: Simulation Results for ACF, SNR=0dB

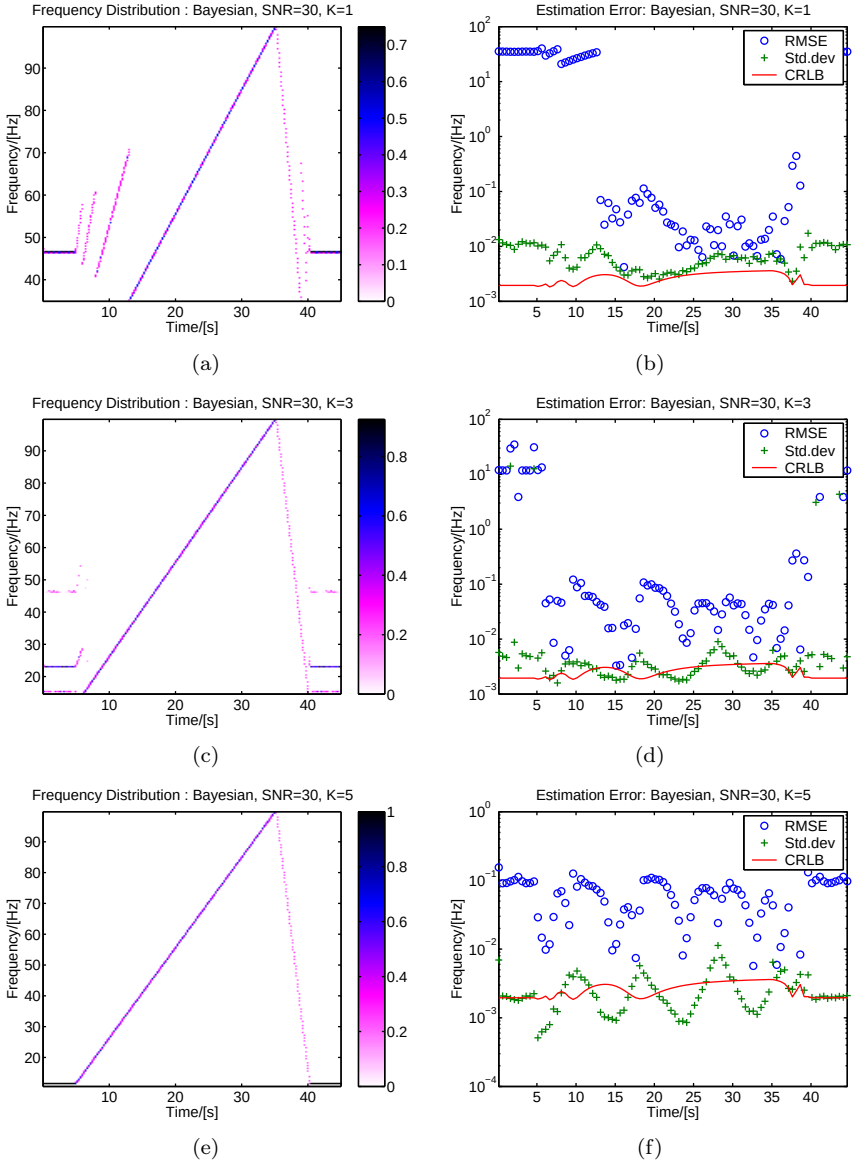

Figure C.8: Simulation Results for Bayesian estimation, SNR=30dB

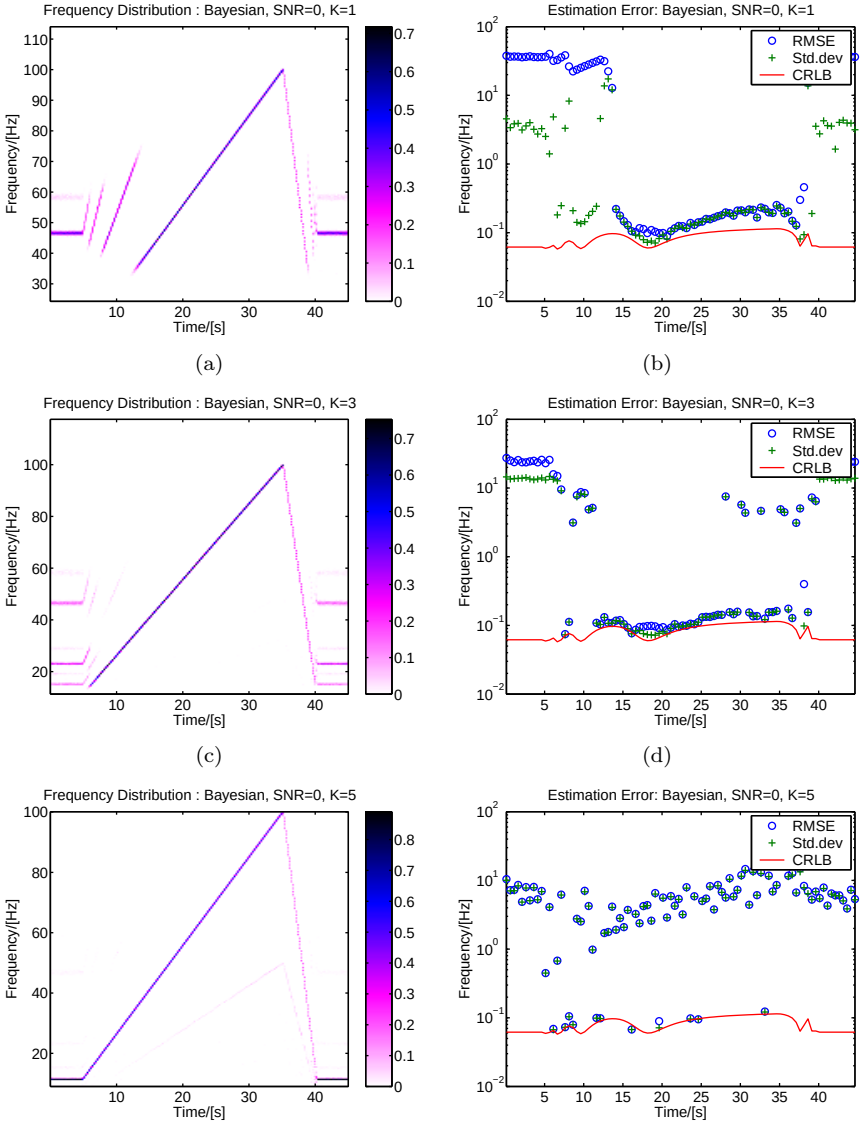

Figure C.9: Simulation Results for Bayesian estimation, SNR=0dB

List of Figures

List of Tables

Bibliography

[1] C. Andrieu and A. Doucet. Joint bayesian model selection and estimation of noisy sinusoids via reversible jump mcmc. *Signal Processing, IEEE Transactions on*, 47(10):2667 –2676, 1999.

[2] M. Angelo. Vibration monitoring of machines. Technical Review No.1-1987, Brüel & Kjær, 1987.

[3] Yaakov Bar-Shalom and Thomas E. Fortmann. *Tracking and Data Association*, volume 179 of *Mathematics in science and engineering*. Academic Press, Inc., 1988.

[4] R.F. Barrett and D.A. Holdsworth. Frequency tracking using hidden markov models with amplitude and phase information. *Signal Processing, IEEE Transactions on*, 41(10):2965 –2976, 1993.

[5] Niclas Bergman. *Recursive Bayesian Estimation. Navigation and Tracking Applications*. PhD thesis, Department of Electrical Engineering. Linköping University, Sweden, 1999.

[6] G. L. Bretthorst. *Bayesian Spectrum Analysis and Parameter Estimation*, volume 48 of *Lecture Notes in Statistics*. Springer-Verlag, 1988.

[7] P. Comon and G.H. Golub. Tracking a few extreme singular values and vectors in signal processing. *Proceedings of the IEEE*, 78(8), August 1990.

[8] K. Copsey, N. Gordon, and A. Marrs. Bayesian analysis of generalized frequency-modulated signals. *Signal Processing, IEEE Transactions on*, 50(3):725–735, 2002.

[9] P.M. Djuric and Hsiang-Tsun Li. Bayesian spectrum estimation of harmonic signals. *IEEE Signal Processing Letters*, 2(11):213 –215, 1995.

[10] Lixin Dou and R.J.W. Hodgson. Bayesian inference and gibbs sampling in spectral analysis and parameter estimation. i. *Inverse Problems*, 11(5):1069–85, 1995.

[11] E.M. Dowling, L.P. Ammann, and R.D. DeGroat. A tqr-iteration based adaptive svd for real time angle and frequency tracking. *IEEE Transactions on Signal Processing*, 42(4), April 1994.

[12] B.G. Ferguson and K.W. Lo. Turboprop and rotary-wing aircraft flight parameter estimation using narrow-band and broadband passive acoustic signal-processing methods. *J. Acoust. Soc. Am.*, 108(4):1763, 2000.

[13] K. R. Fyfe and E. D. S. Munck. Analysis of computed order tracking. *Mechanical Systems & Signal Processing*, 11(2):187–205, 1997.

[14] S. Gade and K Gram-Hansen. Non-stationary signal analysis using wavelet transform, short-time fourier transfom and wigner-ville distribution. Technical Review No.2-1996, Brüel & Kjær, 1996.

[15] Z. Ghahramani and C. E. Rasmussen. Unsupervised learning 2001. lecture 4: Latent variable time series models. Lecture notes, http://www.gatsby.ucl.ac.uk/ zoubin/imm/.

[16] S. Godsill and M. Davy. Bayesian harmonic models for musical pitch estimation and analysis. In *ICASSP 2002*, number II, pages 1769–1772. IEEE, 2002.

[17] Yun-Sik Han and Chong-Won Lee. Directional wigner distribution for order analysis in rotating/reciprocating machines. *Mechanical Systems and Signal Processing*, 13(5):723–37, 1999.

[18] C. Hue, J. Le Cadre, and P. Peréz. Sequential monte carlo methods for multiple target tracking and data fusion. *IEEE Transactions on Signal Processing*, 50(2), February 2002.

[19] E.T. Jaynes. Bayesian spectrum and chirp analysis. In C.R. Smith and G.J. Erickson, editors, *Maximum-Entropy and Bayesian Spectral Analysis and Estimation Problems*. D. Reidel Publishing Co., 1987.

[20] O.G. Jørsboe. *Sandsynlighedsregning*. Matematisk Institut, DTU, 1990.

[21] M. Karan, R.C. Williamson, and B.D.O. Anderson. Performance of the maximum likelihood constant frequency estimator for frequency tracking. *Signal Processing, IEEE Transactions on*, 42(10):2749 –2757, 1994.

[22] S.M. Kay and S.L. Marple Jr. Spectrum analysis - a modern perspective. *Proceedings of the IEEE*, 69(11):1380–1419, November 1981.

[23] Ioannis A. Koutrouvelis. An iterative procedure for the estimation of the parameters of stable laws. *Commun. Statist.-Simla. Computa.*, (10):17–28, 1981.

[24] E.E. Kuruoglu. Signal processing with heavy-tailed distributions. *Signal Processing*, 82(12):1805–1806, December 2002. Special Section on Signal processing with Heavy-tailed Models.

[25] T.I. Laakso, V. Valimaki, M. Karjalainen, and U.K. Laine. Splitting the unit delay [fir/all pass filters design]. *IEEE Signal Processing Magazine*, 13(1):30–60, 1996.

[26] S.K Lee and P. R. White. The enhancement of impulsive noise and vibration signals for fault detection in rotating and reciprocating machinery. *Journal of Sound and Vibration*, 217(3):485–505, 1998.

[27] Sun Ung Lee, David Robb, and Colin Besant. The directional choi-williams distribution for the analysis of rotar-vibration signals. *Mechanical Systems and Signal Processing*, 15(4):789–811, 2001.

[28] L. Ljung. *System Identification, Theory For the User*. Prentice Hall PTR, 2nd edition, 1999.

[29] M.D. Macleod. Fast nearly ml estimation of the parameters of real or complex single tones or resolved multiple tones. *Signal Processing, IEEE Transactions on*, 46(1):141 –148, 1998.

[30] Y Medan, E Yair, and D Chazan. Super resolution pitch determination of speech signals. *IEEE Transactions on Signal Processing*, 39(1):40–48, January 1991.

[31] A. Nehorai and B. Porat. Adaptive comb filtering for harmonic signal enhancement. *IEEE Transactions on Acoustics, Speech and Signal Processing*, ASSP-34(5):1124–38, 1986.

[32] C.L. Nikias and Petropopulu. *Higher-Order Spectra Analysis: A nonlinear signal processing framework*. Prentice Hall, 1993.

[33] C.L. Nikias and M. Shao. *Signal Processing with Alpha-Stable Distributions and Applications*. John Wiley & Sons, 1995.

[34] Joseph J.K. Ó Ruanaidh and William J. Fitzgerald. *Numerical Bayesian Methods Applied to Signal Processing*. Statistics and Computing. Springer-Verlag, 1998.

[35] M. Orton and W. Fitzgerald. A bayesian approach to tracking multiple targets using sensor arrays and particle filters. *IEEE Transactions on Signal Processing*, 50(2), February 2002.

[36] Hewlett Packard. Dynamic signals cd, volume two, 1992.

[37] P.J. Parker and B.D.O. Anderson. Frequency tracking of nonsinusoidal periodic signals in noise. *Signal Processing*, 20(2):127–52, 1990.

[38] T.F. Pedersen and L.K. Hansen. Bayesian multichannel tracking of periodic signals: A new way to determine the running speed of mechanical systems. In *ISSPA 2003 (submitted)*.

[39] F Plante, W.A. Ainsworth, and G. Meyer. A pitch extraction reference database. In *Proc Eurospeech Madrid*, pages 837–840, 1995.

[40] Boaz Porat. *Digital processing of random signals: Theory and methods*. Prentice-Hall information and system sciences series. Prentice-Hall, 1993.

[41] W.H. Press, B. P. Flannery, S. A. Teukolsky, and W. T. Vetterling. *Numerical Recipes in C The Art of Scientific Computing*. Cambridge University Press, 1988.

[42] J.G. Proakis and D.G. Manolakis. *Digital Signal Processing. Principles, Algorithms, and Applications*. Prentice-Hall International, Inc, 3rd edition, 1996.

[43] B. G. Quinn and E. J. Hannah. *The Estimation and Tracking of Frequency*. Cambridge series in statistical and probabilistic mathematics. Cambrigde University Press, 2001.

[44] L.R. Rabiner. On the use of autocorrelation analysis for pitch detection. *IEEE Transactions on Acoustics, Speech and Signal Processing*, ASSP-25(1):24–33, 1977.

[45] L.R. Rabiner. A tutorial on hidden markov models and selected applications in speech recognition. *Proceedings of the IEEE*, 77(2):257–286, February 1989.

[46] L.R. Rabiner, M.J. Cheng, A.E. Rosenberg, and C.A. McGonegal. A comparative performance study of several pitch detection algorithms. *IEEE Transactions on Acoustics, Speech and Signal Processing*, ASSP-24(5):399–418, 1976.

[47] R. B. Randall. *Frequency Analysis*. Brüel & Kjær, third edition, 1987.

[48] B.D. Rao and K.V.S. Hari. Performance analysis of root-music. *IEEE Transactions on Acoustics, Speech and Signal Processing*, 37(12), 1989.

[49] H. Renders, J. Schoukens, and G. Vilain. High-accuracy spectrum analysis of sampled discrete frequency signals by analytical leakage compensation. *IEEE Transactions on Instrumentation and Measurement*, IM-33(4):287–292, December 1984.

[50] D.C. Rife and R.R Boorstyn. Single-tone parameter estimation from discrete-time observations. *IEEE Tranactions on Information Theory*, IT-20(5):591–598, September 1974.

[51] D.C. Rife and R.R Boorstyn. Multiple-tone parameter estimation from discrete-time observations. *The Bell System Technical Journal*, 55(9):1389–1410, November 1976.

[52] D.C. Rife and G.A. Vincent. Use of the discrete fourier transform in the measurement of frequencies and levels of tones. *Bell Syst. Tech. J.*, 49:197–228, 1970.

[53] R. Roy and T. Kailath. Esprit - estimation of signal parameters via rotational invariance techniques. *IEEE Transactions on Acoustics, Speech and Signal Processing*, 37(7), July 1989.

[54] R.O. Schmidt. Multiple emitter location and signal parameter estimation. *IEEE Transactions on Antennas and Propagation*, AP-34(3), March 1986.

[55] J. Schoukens, R. Pintelon, and H. Van Hamme. The interpolated fast fourier transform: a comparative study. *Instrumentation and Measurement, IEEE Transactions on*, 41(2):226–232, 1992.

[56] P. Stoica, R.L. Moses, B. Friedlander, and T. Söderström. Maximum likelihood estimation of the parameters of multiple sinusoids from noisy measurements. *IEEE Transactions on Acoustics, Speech, and Signal Processing*, 37(3):378–392, March 1989.

[57] P. Stoica and T. Söderström. Statistical analysis of music and subspace rotation estimates of sinusoidal frequencies. *IEEE Transactions on Signal Processing*, 39(8), August 1991.

[58] L.D. Stone, C.A. Barlow, and T.L. Corwin. *Bayesian Multiple Target Tracking.* Artec House, Inc., 1999.

[59] R.L. Streit and R.F. Barrett. Frequency line tracking using hidden markov models. *Acoustics, Speech and Signal Processing*, 38(4):586 –598, 1990.

[60] R.L. Streit and T.E. Luginbuhl. Maximum likelihood method for probabilistic multi-hypothsis tracking. *Proc. SPIE*, 2235, 1994.

[61] P. Strobach. Bi-iteration recursive instrumental variable subspace tracking and adaptive filtering. *IEEE Transactions on Signal Processing*, 46(10), 1998.

[62] P. Strobach. Fast recursive subspace adaptive esprit algorithms. *IEEE Transactions on Signal Processing*, 46(9), 1998.

[63] T Takagi, N Seiyama, and E Miyasaka. A method for pitch extraction of speech signals using autocorrelation functions through multiple window lengths. *Electronics and Communications in Japan*, Part 3, Vol. 83:No. 2, 2000.

[64] P.J. Walmsley, S.J. Godsill, and P.J.W. Rayner. Polyphonic pitch tracking using joint bayesian estimation of multiple frame parameters. *Applications of Signal Processing to Audio and Acoustics, 1999 IEEE Workshop on*, pages 119 –122, 1999.

[65] L.B. White. A fast recursive algorihtm for the maximum likelihood estimation of the parameters of a periodic signal. *IEEE Transactions on Signal Processing*, 41(11):3199–3202, November 1993.

[66] L.B. White. An iterative method for exact maximum likelihood estimation of the parameters of a harmonic series. *IEEE Transactions on Automatic Control*, 38(2):367–370, February 1993.

[67] P. Willett, R. Niu, and Y. Bar-Shalom. Integration of bayes detection with target tracking. *IEEE Transactions on Signal Processing*, 49(1), January 2001.

[68] X. Xie and R.J. Evans. Multiple target tracking and multiple frequency line tracking using hidden markov models. *Signal Processing, IEEE Transactions on*, 39(12):2659 –2676, 1991.

[69] Alexander Ypma. *Learning methods for machine vibration analysis and health monitoring*. PhD thesis, Technische Universiteit Delft, 2001.